R-7720-4514

AN EVALUATION OF THE EFFECTS OF TRAVELING SEISMIC WAVES ON THE THREE-DIMENSIONAL RESPONSE OF STRUCTURES

by

S.D. Werner
L.C. Lee
H.L. Wong
M.D. Trifunac

October 1977

Prepared Under
National Science Foundation Grant No. ENV75-02473

AGBABIAN ASSOCIATES
El Segundo, California

BIBLIOGRAPHIC DATA SHEET	1. Report No. NSF/RA-770310	2.	3. Recipient's Accession No. PB275869
4. Title and Subtitle Evaluation of the Effects of Traveling Seismic Waves on the Three-Dimensional Response of Structures			5. Report Date October 1977 6.
7. Author(s) S.D. Werner, L.C. Lee, H.L. Wong, M.D. Trifunac			8. Performing Organization Rept. No. R-7720-4514
9. Performing Organization Name and Address Agbabian Associates El Segundo, California 90245			10. Project/Task/Work Unit No. 11. Contract/Grant No. ENV7502473
12. Sponsoring Organization Name and Address Research Applied to National Needs (RANN) National Science Foundation Washington, D.C. 20550			13. Type of Report & Period Covered 14.

15. Supplementary Notes

16. Abstracts Although usually not considered in design applications, the spatial variations of incident seismic wave motions may, under certain conditions, have a profound influence on the response of structures. To investigate these effects, a new methodology has been developed for analyzing the fully three-dimensional dynamic response of structures that: (1) are above the ground, elastic, and have an arbitrary configuration; (2) are supported on any number of rigid foundations of arbitrary shape that rest on the surface of an elastic half-space; and (3) are subjected to input motions from body or surface waves with arbitrary excitation frequencies and angles of incidence. The superstructure is represented using a finite element model; foundation/soil interaction effects are analyzed using a continuum method. This report describes the general methodology and presents an example of its application to the analysis of a simple single-span bridge/soil system subjected to incident SH-waves. The analysis results clearly demonstrate the importance of traveling wave effects and the influence of different angles of incidence on the three-dimensional bridge response characteristics.

17. Key Words and Document Analysis. 17a. Descriptors

Earthquakes
Buildings
Architecture
Design
Earth movements
Seismic waves
Earthquake resistant structures

17b. Identifiers/Open-Ended Terms

17c. COSATI Field/Group

18. Availability Statement NTIS	19. Security Class (This Report) UNCLASSIFIED	22. Price A08-A01
	20. Security Class (This Page) UNCLASSIFIED	

FORM NTIS-35 (REV. 10-73) ENDORSED BY ANSI AND UNESCO. THIS FORM MAY BE REPRODUCED USCOMM-DC 8265-P74

ABSTRACT

Although usually not considered in design applications, the spatial variations of incident seismic wave motions may, under certain conditions, have a profound influence on the response of structures. To investigate these effects, a new methodology has been developed for analyzing the fully three-dimensional dynamic response of structures that: (1) are above the ground, elastic, and have an arbitrary configuration; (2) are supported on any number of rigid foundations of arbitrary shape that rest on the surface of an elastic half-space; and (3) are subjected to input motions from body or surface waves with arbitrary excitation frequencies and angles of incidence. The superstructure is represented using a finite element model; foundation/soil interaction effects are analyzed using a continuum method.

This report describes the general methodology and presents an example of its application to the analysis of a simple single-span bridge/soil system subjected to incident SH-waves. The analysis results clearly demonstrate the importance of traveling wave effects and the influence of different angles of incidence on the three-dimensional bridge response characteristics.

ACKNOWLEDGEMENTS

This research effort has been supported by the National Science Foundation under Grant No. ENV-02473. The support is gratefully acknowledged.

Primary contributors to this work were S.D. Werner (principal investigator) and L.C. Lee of Agbabian Associates, and M.D. Trifunac and H.L. Wong, special consultants from the University of Southern California. Staff members from Agbabian Associates who also supported the work were J.M. Clark, who carried out much of the required programming effort; J.D. Radler, who edited the final report; and M.S. Agbabian, who contributed suggestions throughout the program and reviewed the final report.

Any opinions, findings, conclusions or recommendations expressed in this publication are those of the author(s) and do not necessarily reflect the views of the National Science Foundation.

CONTENTS

Chapter			Page
1	INTRODUCTION AND SUMMARY		1-1
	1.1	Statement of the Problem	1-1
	1.2	Purpose and Scope of Research Program	1-2
	1.3	Summary of Results	1-2
	1.4	Report Organization	1-4
2	PRIOR STUDIES OF TRAVELING WAVE EFFECTS ON STRUCTURE RESPONSE		2-1
	2.1	Definition of Spatially Varying Input Motions	2-1
	2.2	Studies of Structure Response	2-4
3	DESCRIPTION OF THE CAST1 METHODOLOGY		3-1
	3.1	Overview of the Methodology	3-1
	3.2	Assumptions	3-3
	3.3	Analysis Procedure	3-6
	3.4	Possible Extensions of CAST1 Methodology	3-27
4	AN EXAMPLE ANALYSIS OF A SINGLE-SPAN BRIDGE ON A SOFT SOIL MEDIUM SUBJECTED TO INCIDENT SH-WAVES		4-1
	4.1	System Description	4-1
	4.2	Form of Results	4-6
	4.3	Results for Incident SH-Waves with θ_H = 0 Deg	4-9
	4.4	Results for Incident SH-Waves with θ_H = 90 Deg	4-32
	4.5	Results for Incident SH-Waves with θ_H = 45 Deg	4-42
5	REFERENCES		5-1

Appendix		
A	COMPUTATION OF GREEN'S FUNCTIONS FOR AN ELASTIC HALF-SPACE--SUBPROGRAM *GREEN*	A-1
B	COMPUTATION OF FOUNDATION/SOIL INTERACTION EFFECTS--SUBPROGRAM *FOUND*	B-1

TABLES

Table		Page
3-1	Superstructure Element Library in Subprogram SAP	3-14
4-1	Section Properties and Material Properties Considered in Example Analysis	4-3
4-2	Dependence of Dimensionless Frequency on θ_H . .	4-8
4-3	Amplitudes and Phase Angles of Bridge Response to Incident SH-Waves with θ_H = 0 Deg	4-11
4-4	Amplitudes and Phase Angles of Bridge Response to Incident SH-Waves with θ_H = 90 Deg	4-36
4-5	Amplitudes and Phase Angles of Bridge Response to Incident SH-Waves with θ_H = 45 Deg	4-44

ILLUSTRATIONS

Figure		Page
3-1	Soil/Structure System Considered by CAST1 Methodology	3-2
3-2	CAST1 Analysis Procedure	3-7
3-3	Development of Foundation/Soil Driving Forces and Impedance Matrix--Subprogram FOUND	3-11
3-4	Frequency-Dependent Amplitude and Phase Angle Plots	3-22
3-5	Displacement Time-Histories Used to Construct Deformed-Shape Plot	3-25
3-6	Deformed-Shape Plots	3-26
4-1	Soil/Structure System Configuration and Model Considered in Example Analysis	4-2
4-2	Fixed-Base Mode Shapes and Frequencies of Superstructure	4-4
4-3	Frequency-Dependent Response Amplitudes of Bridge Subjected to Incident SH-Waves with θ_H = 0 Deg, θ_V = 90 Deg	4-10
4-4	Deformed Shapes of Bridge Subjected to Incident SH-Waves with θ_H = 0 Deg, θ_V = 90 Deg	4-12
4-5	Frequency-Dependent Response Amplitudes of Bridge Subjected to Incident SH-Waves with θ_H = 0 Deg, θ_V = 0 Deg	4-16
4-6	Influence of Wavelength of Incident Waves on Structure Response Characteristics -- θ_H = 0 Deg, θ_V = 0 Deg	4-17
4-7	Deformed Shapes of Bridge Subjected to Incident SH-Waves with θ_H = 0 Deg, θ_V = 0 Deg (Antisymmetric Response)	4-18
4-8	Deformed Shapes of Bridge Subjected to Incident SH-Waves with θ_H = 0 Deg, θ_V = 0 Deg (Symmetric Response)	4-21

ILLUSTRATIONS (CONTINUED)

Figure		Page
4-9	Deformed Shapes of Bridge Subjected to Incident SH-Waves with θ_H = 0 Deg, θ_V = 0 Deg (Whipping Response)	4-24
4-10	Frequency-Dependent Response Amplitudes of Bridge Subjected to Incident SH-Waves with θ_H = 0 Deg, θ_V = 45 Deg	4-28
4-11	Deformed Shapes of Bridge Subjected to Incident SH-Waves with θ_H = 0 Deg, θ_V = 45 Deg	4-29
4-12	Decomposition of Nonuniform Load Distribution into Symmetric and Antisymmetric Components . . .	4-33
4-13	Frequency-Dependent Response Amplitudes of Bridge Subjected to Incident SH-Waves with θ_H = 90 Deg, θ_V = 0 Deg	4-37
4-14	Frequency-Dependent Response Amplitudes of Bridge Subjected to Incident SH-Waves with θ_H = 90 Deg, θ_V = 45 Deg	4-38
4-15	Frequency-Dependent Response Amplitudes of Bridge Subjected to Incident SH-Waves with θ_H = 90 Deg, θ_V = 90 Deg	4-39
4-16	Deformed Shapes of Bridge Subjected to Incident SH-Waves with θ_H = 90 Deg, θ_V = 0 Deg and 90 Deg (R_{L_y} = 0.412)	4-40
4-17	Frequency-Dependent Response Amplitudes of Bridge Subjected to Incident SH-Waves with θ_H = 45 Deg, θ_V = 90 Deg	4-45
4-18	Deformed Shapes of Bridge Subjected to Incident SH-Waves with θ_H = 45 Deg, θ_V = 90 Deg (R_{L_x} = 0.423)	4-47
4-19	Frequency-Dependent Response Amplitudes of Bridge Subjected to Incident SH-Waves with θ_H = 45 Deg, θ_V = 0 Deg	4-50
4-20	Deformed Shapes of Bridge Subjected to Incident SH-Waves with θ_H = 45 Deg, θ_V = 0 Deg (R_{L_x} = 0.401)	4-52

ILLUSTRATIONS (CONTINUED)

Figure		Page
4-21	Frequency-Dependent Response Amplitudes of Bridge Subjected to Incident SH-Waves with θ_H = 45 Deg, θ_V = 45 Deg	4-57
4-22	Deformed Shapes of Bridge Subjected to Incident SH-Waves with θ_H = 45 Deg, θ_V = 45 Deg	4-59

CHAPTER 1

INTRODUCTION AND SUMMARY

1.1 STATEMENT OF THE PROBLEM

In most analyses of the response of complex structures to earthquake ground motions, the seismic input is defined either from a family of damped response spectra or as one or more time histories of ground acceleration. This input is usually applied simultaneously along the entire base of the structure, regardless of its dimensions and dynamic characteristics, the properties of the underlying soil material, or the nature of the ground motions themselves.

The above assumption only approximates the input motions actually applied to the structure, since it does not account for spatial variations of the traveling seismic waves that lead to the ground shaking. These spatial variations cause different locations along the structure foundation to be subjected to excitations that differ in both amplitude and phase. Their effect on the structure response is dependent on the type and angles of incidence of the seismic waves; the frequency content of the incident wave motions; the topography and subsurface soil conditions in the vicinity of the structure; and the material properties, length, and configuration of the structure and its foundation.

Several investigators, recognizing the potential importance of traveling wave effects, have studied these effects for a variety of particular structure types. These studies have provided some important insights into traveling wave effects (see Chap. 2); nevertheless, two main deficiencies still preclude the practical assessment of such effects. The first is a lack of closely spaced free-field ground motion measurements, which are necessary to guide the specification of spatially varying input motions for seismic response analyses. A limited number of such measurements have been obtained from the 1971 San Fernando earthquake and from several earthquakes in Japan, but considerably more are required.

The second deficiency is the lack of definitive design guidelines necessary to assess structure response to traveling seismic waves. A possible source of data for such guidelines is simultaneous response measurements taken during actual earthquakes at several locations along the length of several types of structures. However, relatively few data have been collected to date; and even if the networks for such structure-response measurements were expanded immediately, an adequate ensemble of measured data would not be obtained for many years. Therefore, an approach that is more feasible for use in the near future, is through the development and application of new state-of-the-art computational methodologies that (1) can compute the fully three-dimensional response of soil/structure systems to traveling seismic waves, and (2) are practical and cost effective to apply to engineering analysis and design. It is toward this end that this research program is directed.

1.2 PURPOSE AND SCOPE OF RESEARCH PROGRAM

In October 1976, Agbabian Associates (AA) was awarded a grant by the National Science Foundation to carry out the first year's effort in a multiyear research program for studying traveling wave effects on the response of structures. The overall objectives of this multiyear program are (1) to develop a new methodology that is appropriate for use in this research program as well as in actual engineering design and analysis applications; and (2) to apply this methodology to develop engineering guidelines for assessing the potential importance of traveling wave effects on the response of structures. This report describes the past year's work under the program.

1.3 SUMMARY OF RESULTS

During the past year, the research effort has been primarily directed toward Objective 1 above, for which the first step (now completed) was to develop CAST1*. CAST1 is a new, state-of-the-art methodology for

*The acronym CAST1 corresponds to "Continuum and Arbitrary Structures Subjected to Traveling Waves." The number "1" indicates that this is the first version of this methodology, which will be extended in the future.

analyzing the three-dimensional dynamic response of arbitrary structures founded on an elastic half-space and subjected to traveling seismic waves. The structure is represented by a finite element model; interaction between the foundations (assumed rigid and of arbitrary shape) and the soil medium is computed by a continuum method. Input motions correspond to plane harmonic body or surface waves with arbitrary excitation frequencies and angles of horizontal and vertical incidence. The CAST1 analysis procedure is described in detail in Chapter 3.

CAST1 has now been formulated, programmed, and verified. It has also been used to study the response of a single-span bridge subjected to incident SH-waves. This example analysis demonstrates CAST1's applicability and strongly indicates the potential importance of traveling wave effects, even for this simple structure. Results from the analysis, detailed in Chapter 4, show two particularly important trends. First, the phasing of the input motions applied by nonvertically incident waves has significant effects on the bridge response that are not induced when the input motions are not phased (i.e., when vertically incident waves are applied). This demonstrates the importance of considering such traveling-wave effects when designing earthquake-resistant structures of this type. Second, the nature of these traveling wave effects is strongly dependent on the angles of incidence as well as the excitation frequency of the incident waves. Therefore, it is not sufficient to consider only a single direction of propagation when evaluating traveling wave effects on the response of bridge-type structures.

CAST1 represents only the first step in the development of a general methodology for carrying out three-dimensional analyses that include traveling wave effects. For subsequent steps, possible extensions of CAST1 include (1) consideration of arbitrary transient excitations using Fast-Fourier Transform techniques, (2) computation of moments and stresses as well as displacements, (3) representation of the soil as a viscoelastic, layered medium, and (4) consideration of foundations that are partially embedded within the soil medium.

1.4 REPORT ORGANIZATION

This report is organized into four chapters and two appendices. Chapter 2 summarizes significant results from previous studies of traveling wave effects. The CAST1 methodology is described in Chapter 3, and the example application is described in Chapter 4. The theory behind the computation of Green's functions for an elastic half-space is contained in Appendix A, and the continuum method used in CAST1 for representing foundation/soil interaction effects is provided in Appendix B.

CHAPTER 2

PRIOR STUDIES OF TRAVELING WAVE EFFECTS ON STRUCTURE RESPONSE

During early phases of this program, a review of prior studies of traveling wave effects on the response of structures was conducted to (1) define the current state of knowledge in this area; and (2) use this information in the planning and development of the present research program. Procedures and results from these studies are summarized in this chapter. The chapter is divided into two main sections. The first describes prior studies of spatially varying free-field input motions and the second describes structure-response results.

2.1 DEFINITION OF SPATIALLY VARYING INPUT MOTIONS

2.1.1 GENERAL DISCUSSION

The analysis of any structure subjected to traveling seismic waves requires (1) a definition of spatially varying input motions, and (2) the implementation of an appropriate analysis technique. Some analysis techniques that include traveling wave effects, as required for Item 2, are described in several current structural dynamics textbooks (e.g., Clough and Penzien, 1975), and are being improved by the methodology being developed under this research program. However, the current state of knowledge regarding Item 1 is not nearly as well developed. This is discussed below.

Spatially varying ground motions are caused (1) by different types of direct incident seismic waves that are associated with a range of frequencies and different angles of incidence, (e.g., Bullen, 1963; Johnson, 1977); and (2) by reflections, refractions, scattering, and diffraction that are induced by variations in topography and subsurface conditions along the travel path of the seismic waves. Because of these phenomena, two stations a given distance apart receive motions whose differences in amplitude and phase are dependent on the ratio between the wavelength of the incident wave and the

distance between the stations. When this ratio is large (i.e., for long wavelengths) the motions at the two stations will be nearly equal in amplitude and phase. However, when the ratio is smaller (i.e., for wavelengths comparable to or less than the station-to-station distance) the motions at the two stations may have markedly different amplitudes and phase angles (Udwadia and Trifunac, 1974; Jennings, 1976; Wong and Trifunac, 1974 and 1977).

A potential vehicle for gaining further insight regarding spatially varying motions is closely spaced ground-motion records measured during an actual earthquake. However, such records are currently quite scarce; among the only arrays of closely spaced records obtained to date are those summarized in Section 2.1.2. More closely spaced records may eventually be obtained from the expanding network of strong motion accelerographs in the United States (Matthiesen, 1975). However, for the present, the data are far from sufficient--a factor that has hampered understanding of spatially varying ground motions.

Because of the complex phenomena that affect spatially varying ground motions and the scarcity of closely spaced strong-motion records that could provide insight into these phenomena, there is considerable uncertainty involved in defining spatially varying input motions for structure-response computations. Because of these uncertainties, traveling wave excitations have often been neglected, even in analyses where their effects may be important (Tseng and Penzien, 1975). When considered, spatially varying input motions have typically been represented either as a single motion time history that propagates at a constant horizontal velocity along the base of the structure or, in several recent studies, as an incident plane wave. For either of these simplified representations, the difference in excitation at any two points on the ground surface is limited to differences in phase; i.e., differences in amplitude are not represented.

2.1.2 SOME PAST STUDIES OF SPATIALLY VARYING GROUND-MOTION MEASUREMENTS

Very few sets of closely spaced ground-motion records have been obtained that are appropriate for investigating the nature of spatially varying motions. In the United States, only the 1971 San Fernando earthquake has provided such records whereas earthquakes in Japan have produced a somewhat larger array. The paragraphs that follow briefly summarize studies based on these various measurements.

Accelerograms measured during the 1971 San Fernando earthquake have been investigated by Toki (1976, 1977) to deduce phase velocities for frequencies ranging from 0.2 Hz to 2 Hz. The resulting dispersion curves showed strong frequency dependence. These curves were also used to confirm the existence of surface wave contributions to the records and to show that strain levels induced near the ground surface by these waves are comparable to those attributed to vertically propagating SH-waves.

In Japan, one of the first arrays of closely spaced accelerometers was deployed during the Matsushiro earthquake swarm of 1965-1967. During this time, five accelerometers were placed at equal intervals along a 120-m base line at which subsurface soil property measurements and layer thicknesses were measured. Numerous accelerograms were thereby obtained during this earthquake swarm. Subsequent studies of these records indicated that spatial variations of the ground motions could be attributed to the presence of surface waves and to the nonuniformity of the ground structure along the base line (Okamoto, 1973).

There are several other examples of accelerograms obtained in Japan from arrays of closely spaced instruments. From January through June 1968, measurements of small-to-moderate ground motions were obtained along two orthogonal base lines of accelerometers on reclaimed ground at Koto-ku, Tokyo. These measurements indicated the predominance of components with vibration characteristics of the surface layer, and were used to measure phase velocities (Tamura et al., 1977). In another instance, measured records

from more than 35 small earthquakes were obtained by six sets of equally spaced accelerometers located along a line 2500-m long at the Tokyo International Airport. Wave propagation characteristics of acceleration and displacement histories from these instruments are now being studied (Tsuchida and Kurata, 1976; Tsuchida et al., 1977).

2.2 STUDIES OF STRUCTURE RESPONSE

2.2.1 SIMPLE STRUCTURES AND FOUNDATION ELEMENTS

A number of investigators have considered simple structures and foundation elements subjected to traveling seismic waves. Despite the simplicity of the elements considered, such studies have provided valuable insights into the potential effects of the spatial variations of the ground motions. For example, Masri (1976) described an exact solution for the transient response of viscously damped Bernoulli-Euler beams with arbitrary boundary conditions when subjected to propagating boundary excitation. He showed that the beam dimensions and the propagation times of the traveling excitation can have a pronounced influence on the response. For certain combinations of the system parameters and support motion, Masri showed that the beam response to propagating support motion can be significantly higher than when uniform (nonpropagating) support motions are applied.

Examples of studies of the effects of traveling seismic waves on the response of rigid footing elements are those of Scanlan (1976), Wong and Luco (1977); and Luco and Wong (1977). The first two studies considered traveling P- and S-waves, whereas the third considered horizontally propagating Rayleigh waves. The results showed that traveling wave effects are most pronounced when wavelengths of the incident waves are comparable to or less than the footing length, and become negligible when the ratio of the wavelength to the footing length is large. Other traveling wave effects indicated by the studies are these: (1) the net translational excitation caused by nonvertically incident P- and S-waves can be reduced relative to the excitations caused by

vertically-incident waves; (2) nonvertically incident SH-waves generate torsional response, whereas nonvertically incident P- and SV-waves cause rocking of the rigid footing (these responses are not generated by vertically-incident waves); (3) horizontally propagating Rayleigh waves whose angles of incidence is normal to one of the sides of the foundation can induce significant rocking motions and cause translational motions that decrease in amplitude with increasing excitation frequency; and (4) obliquely incident, horizontally propagating Rayleigh waves excite all six components of motion.

A study of traveling wave effects on the response of footing elements that are flexible rather than rigid was carried out by Iguchi (1977). This study considered the vertical response of a long, slender base plate on an elastic half-space subjected to obliquely incident SV-waves that propagate along the long dimension of the plate. Iguchi used Green's functions for an elastic half-space to define incident and scattered wave displacements that were, in turn, incorporated into the differential equation of motion of the plate. The resulting dual integral equations were solved by Galerkin's method. Example calculations showed that when the incident waves are propagating parallel to the ground surface, effects of elastic deformations on the plate response are small; however, for other directions of propagation, such effects may be more significant.

2.2.2 BUILDINGS

Newmark et al. (1977) studied the ground motions measured in the Hollywood Storage Building (Los Angeles) basement and in its nearby parking lot during the Kern County (1952) and San Fernando (1971) earthquakes in California. They suggested that the input base motions applied to this building could be estimated by an averaging of the free-field excitation as measured in the parking lot. This averaging is performed over a transit time that is related to the size of the building and the velocity of the incident waves. On this basis, simplified techniques for estimating average translational and torsional base input motions induced by traveling seismic waves were described.

Other investigations of the effects of traveling seismic waves on the response of buildings were carried out by Matsushima (1977) and Veletsos et al. (1975). Matsushima studied the influence of traveling waves on the stochastic response of single-story buildings consisting of a slab supported by multiple discrete columns; input motions to each column support were considered to be stationary and interrelated through an assumed cross-spectral density function that is distance dependent. His results for several different foundation conditions showed that the influence of spatial variations of the earthquake excitations on the building response can be significant. Veletsos et al. carried out a deterministic analysis of a single-story building composed of a rigid deck and a series of columns supported on individual rigid spread footings. This system was subjected to input in the form of shear waves that propagate horizontally, at constant speed and without change in the incident wave form, along the principal axes of the building. Results developed from this study showed that the traveling waves had the following effects on the building response: (1) they modified the effective translational response of the structure, reducing the peak value of excitation; and (2) they induced a torsional or rotational component of response.

2.2.3 BRIDGES

One of the first studies of the response of bridges to traveling seismic waves was carried out by Bogdanoff et al. (1965), who developed an analysis technique for a simplified model of a suspension bridge and concluded that traveling seismic waves should be considered when analyzing long structures of this type. Johnson and Galletley (1972) used a three-dimensional mathematical model to investigate the response of a highway bridge to combined horizontal and vertical shaking. Their study found that the bridge had responses to traveling ground motions which were noticeably different from the responses induced when the same input motions were uniformly applied. They concluded that out-of-phase ground motions should be considered in the seismic design of bridges on multiple supports.

A study of the influence of various parameters on the response of elastic, two-dimensional, single- and multispan bridges on an elastic half-space was carried out by Abdel-Ghaffar and Trifunac (1977a, b) for the case of incident plane SH-waves. Their bridge model consisted of an elastic shear girder supported by two rigid abutments and rigid foundations that had a circular cross section and were bonded to the half-space. The analyses showed the dynamic response to be dependent on the angle of incidence of the plane SH-waves; the ratio of the rigidities of the girder and soil; the ratio of the girder mass to the mass of the rigid abutment/foundation system; and the span of the bridge. The simplest response modes (symmetric vibration of the girders) occurred for a symmetric bridge/abutment/foundation system and for vertically incident SH-waves. When the angles of incidence was not vertical, or when the bridge/abutment/foundation system was not symmetric, more complicated response occurred. Nonsymmetry of the abutments was shown to enhance the overall torsional response and to accentuate other phenomena such as shielding, scattering, and diffraction effects.

A recent study by Goto et al. (1976) considered in-plane rocking and swaying motions of a simple single-span bridge model comprised of a rigid pin-ended girder on rigid piers that, in turn, were founded on soil springs. Input motions consisted of SV-waves that propagated along the length of the bridge and had an arbitrary angle of vertical incidence. Elastic analyses of this system indicated that when the delay time between the input motions applied at each end of the bridge was equal to half the natural period of the pier/spring system, the dynamic response of the two piers was out of phase; for this case the relative displacement between the two piers was maximized. Goto et al. also carried out nonlinear analyses that incorporated friction along one of the girder supports and bilinear hysteretic soil springs; however, these analyses did not lead to conclusive trends that could be related to traveling wave effects. It is noted that a number of comprehensive nonlinear bridge analyses, including detailed models of nonlinearities in the expansion joints, have been conducted but typically have not incorporated spatially varying input motions (Tseng and Penzien, 1975; AA, 1972).

2.2.4 BURIED PIPELINES AND TUNNELS

Evaluation of traveling-wave effects on the response of buried tunnels and pipelines has been based on observed damage or measurements from actual earthquakes, on laboratory tests, and on analytical studies. For example, Sakurai and Takahashi (1969) evaluated pipeline and adjacent soil motions measured during the Matsushiro, Japan, earthquake swarm of 1965-1967. The results indicated the following: (1) pipeline deformations were quite similar to the deformations in the adjacent soil medium; (2) axial strain components in the straight portion of the pipe were significantly greater than bending strains, which were most notable at pipe bends; (3) pipe strains were directly proportional to acceleration and inversely proportional to wavelength; and (4) surface waves were judged to have had an important influence on the behavior of pipelines during these earthquakes. Also, Sakurai and Takahashi suggested that during larger earthquakes, ground and pipe deformations may not be similar, i.e., that a relative displacement between the pipe and soil may occur. In such a case, the strains in the pipe could be limited by frictional characteristics along the pipeline/soil interface.

Experimental studies of traveling-wave effects on the response of buried pipelines and tunnels were reported by Kubo (1973) and by Goto et al. (1973). Kubo reported tests of the response of embedded steel pipe subjected to waves generated by three methods--a dynamic explosion, an S-wave generator, and an air gun. Goto el al, described a model test in which a rubber rod representing a tunnel was embedded in a gelatin-like material; the enclosure for these materials was then subjected to random shaking. In both sets of tests, the deformations of the buried structure closely followed the deformations in the surrounding medium.

Procedures for analyzing and designing buried pipelines and tunnels to resist traveling seismic waves are typically based on an approach in which deformations are imposed by the traveling waves, rather than by inertia

loading. This approach is consistent with observations from field measurements and laboratory tests, as summarized above, and has been described in work by Kubo (1973), Miyajima et al. (1976), Jennings (1976), and Hall and Newmark (1977).

2.2.5 OTHER STRUCTURE TYPES

Studies of traveling seismic wave effects on structure response have been carried out for certain other structure types as well. For example, Masri and Weingarten (1977) studied the response of cooling towers to traveling waves. Their analysis included the shell modes of response as well as the more typically-considered beam modes. They showed that traveling seismic waves can excite shell modes as well as beam modes of the tower and can therefore produce a decidedly different structure response than does uniform excitation, which would only excite beam modes.

There have been several studies of the response of earth dams to traveling seismic waves, but most have been based on the simplified assumption that the ground motion propagates without any modification across the base of the dam (see Sec. 2.1). Chopra et al. (1969), Dibaj and Penzien (1969), and Kaldjian (1973) all used this assumption in finite element analyses of earth dams. Their results all led to the same trends: the slower the velocity of propagation of the ground motions, the more the response differed from the case where all base points were excited in phase.

A limited number of analyses of the response of nuclear plant structures to traveling seismic waves have also been carried out. One of the more recent studies of this type, by Wolf (1977), included base mat uplift in an analysis of the response of a nuclear plant structure subjected to horizontally propagating shear waves. Isenberg (1970) carried out a finite element analysis of a nuclear plant structure partially embedded in a soil island that was modeled using a nonlinear material representation. Input motions applied along the left boundary of the soil island were allowed to propagate within the island in a manner dependent on its node point spacing and element properties.

Other structures may also be susceptible to traveling wave effects. For example, Foss (1977) has stated that traveling wave effects may be important for buried communication cables and for tall radio and television towers that are guyed and supported on the ground by widely spaced anchor blocks. Still other structure types for which traveling wave effects could be significant are long harbor structures such as piers, dry docks, and moorings; long warehouses; airport facilities such as large terminal buildings and hangers; and concrete spillways in the vicinity of dam structures, to name only a few.

CHAPTER 3

DESCRIPTION OF THE CAST1 METHODOLOGY

3.1 OVERVIEW OF THE METHODOLOGY

As noted in Chapter 1, much of this research program has been directed toward improving the current technology for analyzing how three-dimensional soil/structure systems respond to traveling seismic waves. The result has been the development of CAST1*--a new methodology that has the following features (see Fig. 3-1):

- It computes the three-dimensional dynamic response of an arbitrarily-configured, elastic, aboveground structure. It can also consider two or more closely spaced structures.
- It assumes each structure to be supported on any number of rigid foundations of arbitrary shape that rest on the surface of an elastic half-space.
- It represents input motions as any desired combination of planar harmonic body and/or surface waves with arbitrary excitation frequencies, amplitudes, and angles of incidence.

The methodology uses a three-dimensional finite element model to represent the superstructure and a continuum method to analyze foundation/soil interaction effects. The finite element model defines the stiffness and mass matrices of the superstructure, together with its fixed-base mode shapes and frequencies. The continuum method characterizes the foundation/soil system and the incident wave motions in terms of complex frequency-dependent impedance matrices and driving force vectors. Compatibility and equilibrium requirements at the superstructure/foundation interface are

*The acronym CAST1 is defined in Section 1.3 of Chapter 1.

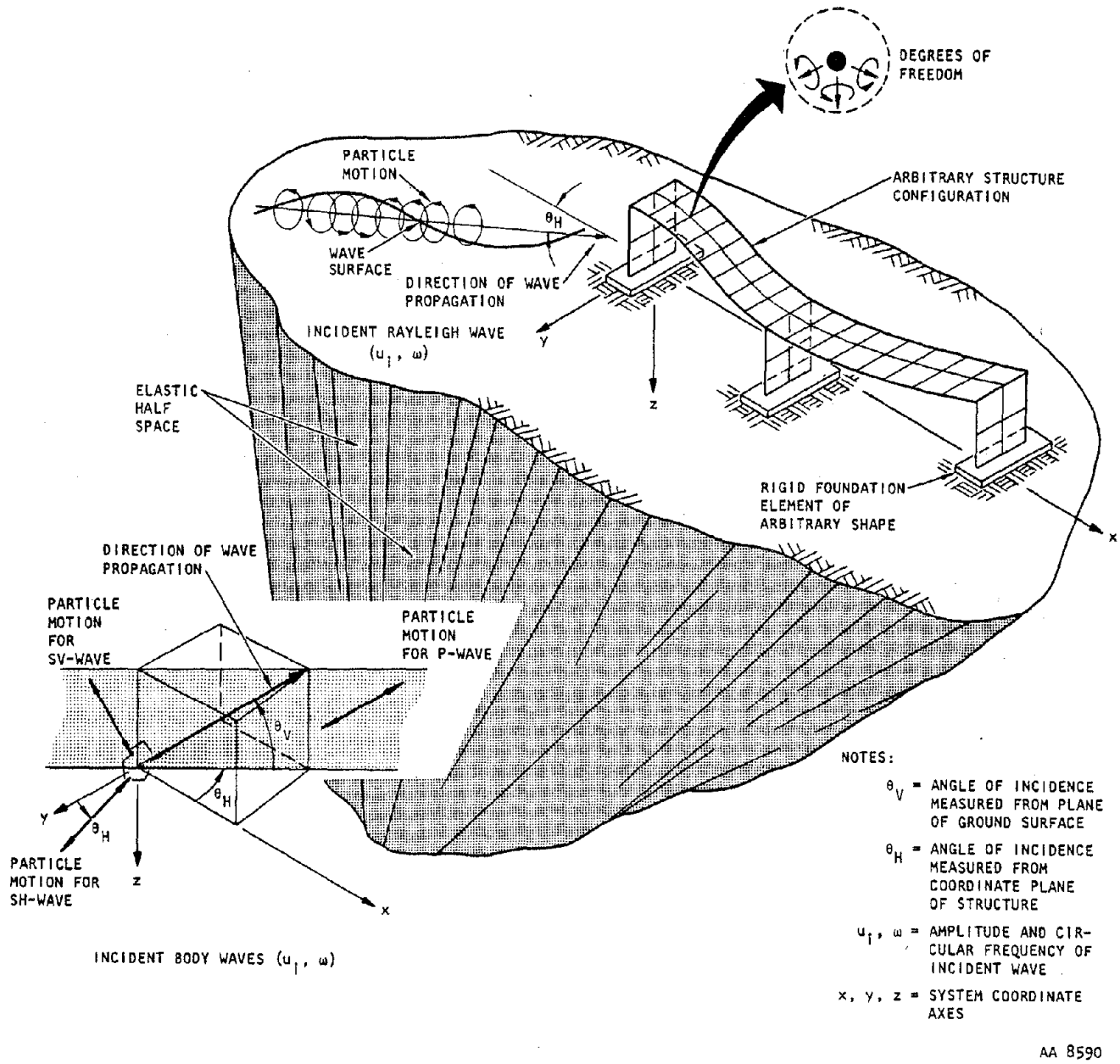

FIGURE 3-1. SOIL/STRUCTURE SYSTEM CONSIDERED BY CAST1 METHODOLOGY

used to combine these two sets of results and to thereby characterize the complete superstructure/foundation/soil/incident-wave system. The steady-state response of the system is then computed and provided to the user in various printed and plotted forms.

The remainder of this chapter provides more detailed information regarding the features of CAST1. The sections that follow deal specifically with the assumptions, the analysis procedures, and the possible future extensions of this methodology.

3.2 ASSUMPTIONS

The CAST1 methodology is based on various assumptions that fall under the following categories: (1) representation of the superstructure; (2) representation of the foundation/soil system; (3) representation of the input motions; and (4) computation of foundation/soil interaction effects.

3.2.1 REPRESENTATION OF SUPERSTRUCTURE

Each structure to be analyzed is assumed to be three-dimensional, linear elastic, and arbitrarily-configured. It is represented by a general finite element model that comprises any combination of the several element types described in Section 3.3.2.2. Each node point in the model can have as many as six degrees of freedom, depending on the particular element types used. The node point spacing and the element sizes depend on the structure geometry and the highest frequency of response pertinent to the calculations.

3.2.2 REPRESENTATION OF FOUNDATION/SOIL SYSTEM

Each structure in the system can be supported on any number of foundation elements, each of which can have an arbitrary shape. The foundations are assumed rigid and fully bonded to the surface of the soil medium. Therefore, the methodology is strictly valid only for those cases where such conditions are reasonably well satisfied, i.e., where effects of foundation flexibility, separation along the foundation/soil interface, or embedment of the foundation are unimportant.

The soil medium is represented as an elastic half-space. Because of this assumption, the CAST1 dynamic analysis cannot include such effects as soil layering and strain-dependent stiffness and damping characteristics. Nevertheless, the methodology in its present form is a valuable tool for studying the basic phenomena associated with traveling wave effects on the three-dimensional response of one or more structures. Furthermore, procedures for representing a viscoelastic-layered soil medium in CAST1 have been developed and can be easily incorporated with the methodology (see Sec. 3.4).

3.2.3 REPRESENTATION OF INPUT MOTIONS

The input motions specified in the present CAST1 methodology correspond to incident wave motions induced by planar, harmonic P-, SV-, SH-, and Rayleigh waves. The angles of incidence, excitation frequency, and complex amplitude of these wave motions are arbitrary.

Although only harmonic input motions have been considered in this methodology, the results can be readily extended to apply to cases where the most general transient excitations are considered (see Sec. 3.4). This is because any transient input can be expressed as the superposition of a series of harmonic excitations--a fact that forms the basis for the widely used Fourier transform techniques for analyzing soil/structure systems (Liu and Fagel, 1971; Lysmer et al., 1975). In such an approach, the system response in the frequency domain is computed as the product of the Fourier transform of the transient input motions and the system transfer function; the inverse Fourier transform of this product then defines the corresponding system response in the time domain.

3.2.4 COMPUTATION OF FOUNDATION/SOIL INTERACTION EFFECTS

Usually, two analysis techniques are employed to represent the soil/foundation system under the action of traveling waves. These techniques--continuum methods and finite element methods--have been extensively described in the technical literature (e.g., Werner, 1976a). Continuum methods represent

the soil and foundation by a simplified idealized system for which analytical solutions are feasible in terms of elastic wave theory. For example, the theory of a rigid disk on an elastic half-space has been widely used in past analyses, although more general continuum methods have been developed in recent years. Finite element methods represent the soil and structure as a network of discrete elements interconnected at their node points. This network satisfies force-equilibrium at the node points, stress/strain material properties within each element, and usually (but not always) the compatibility of strains along adjacent element interfaces. With increasing refinement of the network, finite element methods may produce excellent solutions; however, computer costs, storage requirements, and finite model boundaries place practical limits on the degree of refinement that can be attained. Especially in wave-propagation applications, finite element methods are limited by the lack of a general procedure for absorbing signals reflected at the artificial boundaries of the network.

In general, the selection of one of the above techniques over the other should be based on an assessment of which technique is most suitable for the particular soil/structure system being investigated. For those systems that are the basis for the development of CAST1, continuum methods are judged to be most suitable since they offer the following advantages:

- With an elastic half-space representation of the soil medium, solutions for foundation/soil impedance functions and driving forces can be developed for any arbitrary foundation shape.

- Continuum methods represent radiation damping and wave propagation whereas the finite element method must simulate these effects by using approximate, energy-absorbing boundary conditions.

- Continuum methods are considerably less expensive to use than are finite element methods.

3.3 ANALYSIS PROCEDURE

The analysis procedure associated with the CAST1 methodology is outlined in the flowchart given in Figure 3-2. It consists of five different subprograms that are organized into three different phases: the input phase, the response analysis phase, and the output phase.

3.3.1 INPUT PHASE

This phase of the methodology provides all basic input data required for the calculation of the soil/structure system response. The data required for each of the various components in the system--the superstructure, foundation, soil medium, and incident wave--are described in the paragraphs that follow.

3.3.1.1 Superstructure

Three sets of input parameters are required to represent the superstructure in the subsequent response analyses--these are (1) the geometric configuration, (2) the material properties, and (3) the number of normal modes. The geometric configuration is represented from an appropriate combination of the various structure element types that are available in Subprogram SAP (see Sec. 3.3.2.2). The sizes of these elements and the spacing of the node points are dependent on the highest frequency of response to be considered in the calculations. Material properties are defined separately for each element in terms of its Young's modulus, Poisson's ratio, and mass density. In addition, Rayleigh damping coefficients are specified for the overall superstructure/foundation system (Eq. 3-2, Sec. 3.3.2.3).

The number of normal modes is selected according to the convergence requirements for the system response computations carried out in Subprogram COMBINE. These requirements depend on the highest excitation frequency to be considered in the calculations, the type and angles of incidence of the input waves being considered, the structure configuration, and the specification of an acceptable level of accuracy of the response computations. The assessment

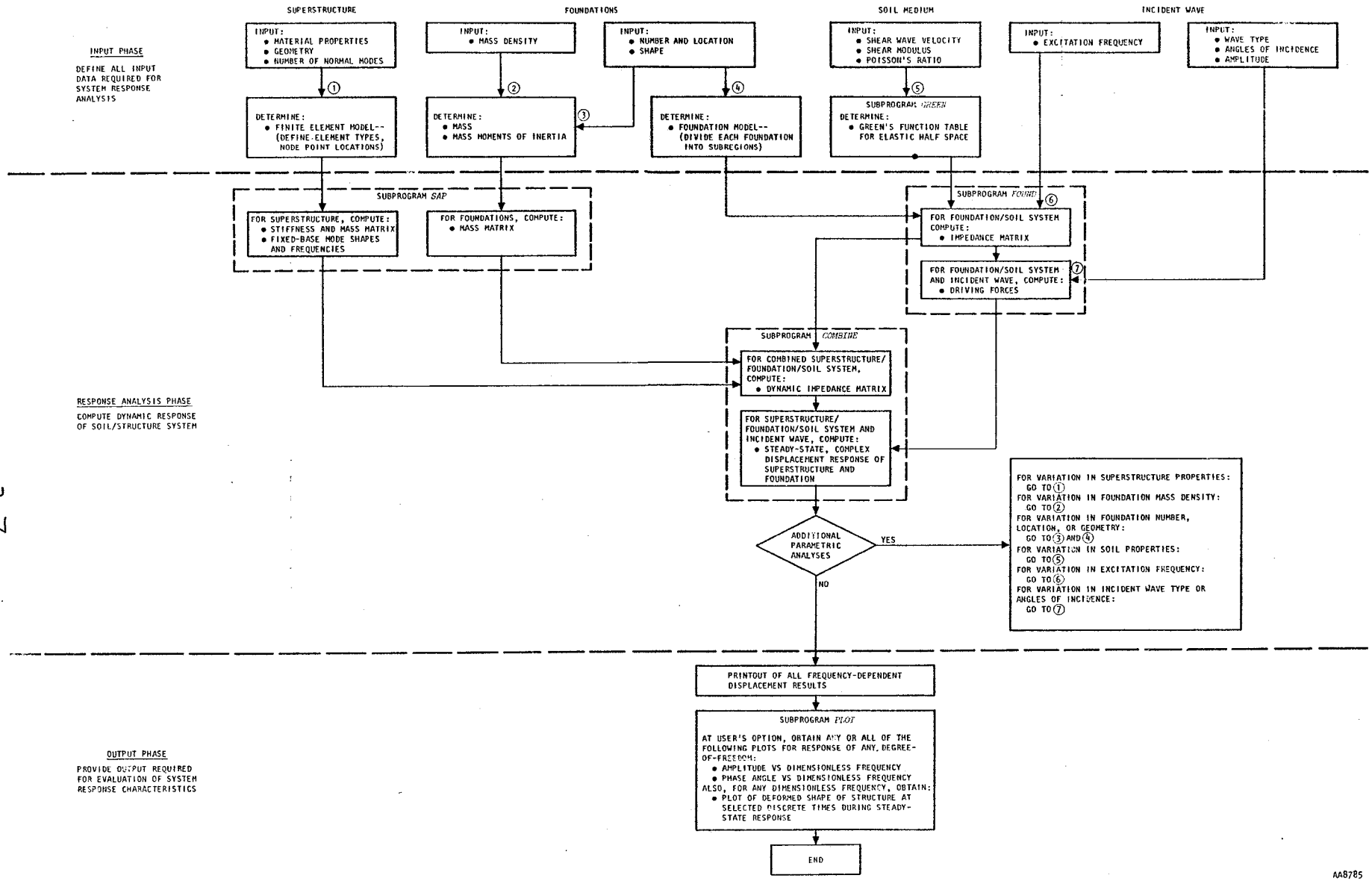

FIGURE 3-2. CAST1 ANALYSIS PROCEDURE

of an adequate number of modes for a specific problem may entail a trial-and-error procedure since a suitably simple convergence criterion that includes all of the above variables is difficult to develop. For the bridge analysis described in Chapter 4, 29 modes were used to represent the structure response with sufficient accuracy for excitation frequencies up to 25 Hz.

3.3.1.2 Foundations

The superstructure is assumed to be supported on an arbitrary number of rigid foundations that rest on the surface of the soil medium. To define this system of foundations for the response analyses requires specification of the total number of foundations and the location, shape, and mass density of each individual foundation. The geometry of each foundation is specified by subdividing its shape into a given number of rectangular subregions within which the contact stresses along the foundation/soil interface are assumed constant (see App. B). To simplify the formation of the foundation impedance matrix, the degree of symmetry of the shape of each foundation about its local coordinate axes is also specified. The mass density is used to compute the total mass and mass moments of inertia of each foundation.

3.3.1.3 Soil Medium--Subprogram GREEN

The soil medium is represented in CAST1 as an elastic half-space with input properties consisting of its shear wave velocity, shear modulus, and Poisson's ratio. These properties are then used as input to Subprogram GREEN, a program that computes an array of four Green's function parameters at N equally spaced steps in the frequency domain, as described in Appendix A. This 4 x N array of parameters contains the data required to represent the soil medium in the subsequent system response analyses. It is input directly into Subprogram FOUND to form the Green's function matrix used in computing the foundation/soil impedance matrices and driving force vectors (Sec. 3.3.2.1).

3.3.1.4 Incident Wave

The input data required to define the incident wave in the response analysis calculations consist of the excitation frequency, angles of incidence, amplitude, and wave type. The excitation frequency is expressed as a non-dimensional parameter $\frac{\omega \ell}{2\pi V_s}$, where ω is the circular frequency, ℓ is a reference characteristic length, and V_s is the shear wave velocity (see Sec. 4.2). The angles of horizontal and vertical incidence, θ_H and θ_V, are defined in Figure 3-1. The amplitude of the incident wave motion is defined as a 3 x 1 complex vector whose terms correspond to the longitudinal, transverse, and vertical components of motion. From this, the wave type--i.e., whether the incident wave is a P, SV, SH, or Rayleigh wave--is specified by an appropriate definition of the various components of the amplitude vector. For example, a P-wave is specified by defining real and imaginary values for the longitudinal component and zero values for the transverse and vertical components.

3.3.2 RESPONSE ANALYSIS PHASE

This phase of the methodology performs the computations that lead directly to the response of the soil/structure system to the traveling seismic waves. The phase involves three main steps:

- Compute a soil/foundation impedance matrix and driving force vector that together characterize the soil/foundation system subjected to the incident waves (Subprogram FOUND)
- Represent the superstructure in terms of its stiffness and mass matrices and its fixed-base mode shapes and frequencies. Also compute the foundation mass matrix (Subprogram SAP).
- Combine the results from the above two steps to form an overall soil/foundation/superstructure impedance matrix, and use this matrix together with the soil/foundation driving forces to obtain the system response (Subprogram COMBINE)

The three subprograms that carry out these steps--FOUND, SAP, and COMBINE--are described in the remainder of this section.

3.3.2.1 Subprogram FOUND

To represent foundation/soil interaction effects in the response analysis phase, a continuum method that follows the work by Wong (1975) has been programmed as Subprogram FOUND. The method is described in detail in Appendix B and is briefly summarized in terms of the following steps:

- Provide the following input: (1) the frequency-dependent Green's functions for the elastic half-space, as developed from Subprogram GREEN; (2) the angles of incidence, wave type, excitation frequency and complex amplitude of the incident wave; and (3) the geometry and location of each of the foundations, which are assumed massless as well as rigid in the Subprogram FOUND calculations.*

- Compute foundation driving forces by fixing each discrete foundation and calculating frequency-dependent reaction forces induced by the waves transmitted through the soil medium (Fig. 3-3a). These forces depend on the properties of the foundation and soil and on the type of the incident wave and its angles of incidence, complex amplitude, and frequency.

- Determine the soil/foundation impedance matrix. The elements in the jth column of this matrix are computed as the foundation reaction forces caused by a unit harmonic displacement of the jth foundation degree of freedom when all other degrees of freedom are fixed (Fig. 3-3b). This impedance matrix is dependent on the characteristics of the foundation and soil, and on the excitation frequency of the incident wave.

The soil/foundation driving force vector and impedance matrix completely characterize the interaction between the rigid foundation and the underlying elastic half-space. The computation of these quantities for one

*Although not required in Subprogram FOUND, the foundation mass and associated inertia forces are fully represented in the overall solution technique for CAST1 and in the derivation of the superstructure/foundation/soil impedance matrix (see Sec. 3.3.2.3).

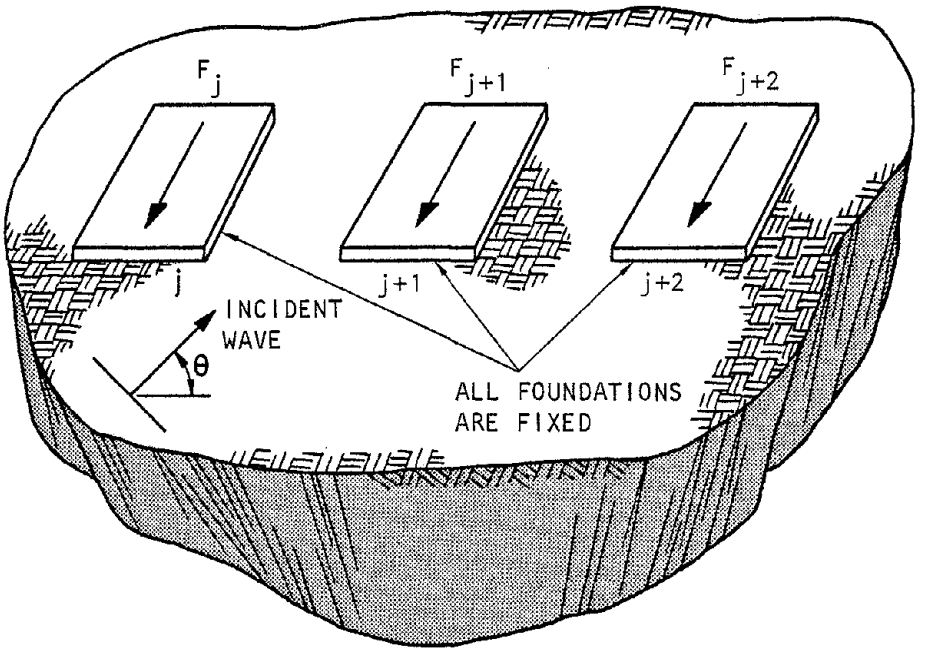

(a) Development of foundation driving forces (only longitudinal forces shown)

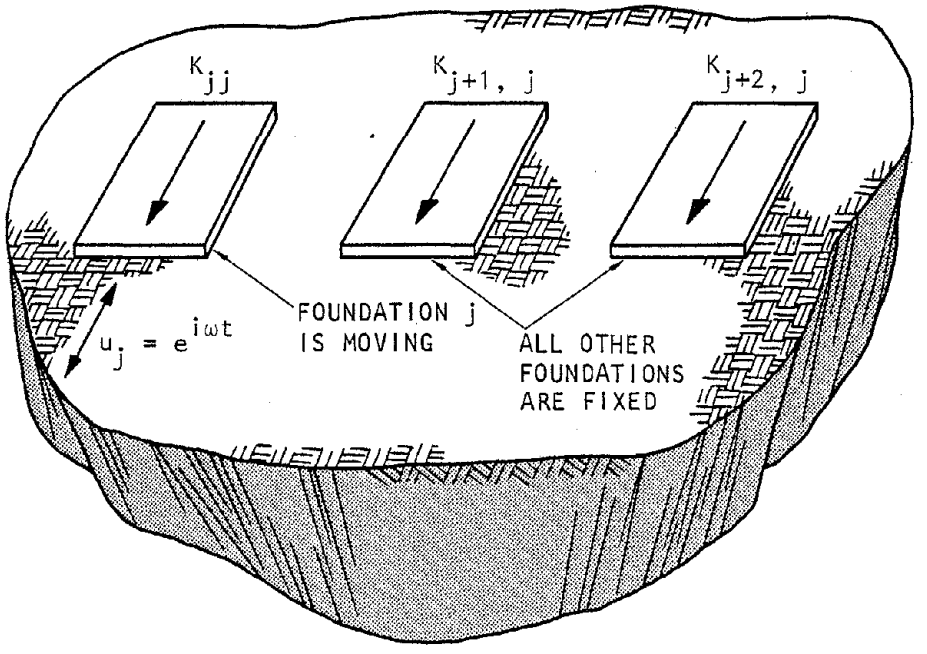

(b) Development of jth column of soil/foundation impedance matrix (only longitudinal forces shown)

FIGURE 3-3. DEVELOPMENT OF FOUNDATION/SOIL DRIVING FORCES AND IMPEDANCE MATRIX--SUBPROGRAM FOUND

or more foundations of arbitrary shape is based on a division of the contact area between each foundation and the soil into a number of subregions, within which the contact stresses are uniform but of unknown magnitude. The displacements within the contact areas are expressed in terms of the contact stresses, using the Green's functions for a point source on an elastic half-space. Displacement boundary conditions are then imposed to develop a system of linear algebraic equations that relate the stresses to the rigid body translational and rotational components of motion of each foundation. Once the contact stresses are known, the total forces and moments acting on each foundation can be determined. This leads to a force-displacement relationship for the overall foundation/soil system from which its impedance matrix and driving force vector can be readily obtained.

3.3.2.2 Subprogram SAP

The response analysis phase of CAST1 requires the representation of the superstructure in terms of its stiffness and mass matrices, and its fixed-base mode shapes and frequencies. Although there are several currently available programs that can carry out this function, the SAP code has been used in the CAST1 methodology for this purpose.*

The SAP code is a three-dimensional finite element computer program that is especially well suited to the analysis of large structural systems. It was originally developed by Wilson (1970) and has since been updated several times to include such features as dynamic storage allocation and new element types and numerical integration procedures. The code can carry out static response analyses, the computation of mode shapes and frequencies, and dynamic response analyses using the normal mode, direct integration, or response spectrum methods.

---

*Although the primary function of the SAP code is to represent the superstructure as indicated above, SAP is also used in CAST1 to form the foundation mass matrix (Fig. 3-2).

The SAP IV version of the program, as described by Bathé et al. (1974) has been incorporated into CAST1. This version features a library of the following element types: (1) three-dimensional truss elements; (2) three-dimensional beam elements; (3) plane stress, plane strain, and axisymmetric elements; (4) three-dimensional solid element; (5) variable-number-nodes thick shell and three-dimensional element; (6) thin plate and shell element; (7) boundary element; and (8) pipe element. This variety of element types provides a capability for representing nearly any arbitrary superstructure configuration. The features of each element are summarized in Table 3-1.

SAP IV uses two different procedures to compute mode shapes and frequencies--a subspace iteration technique and a determinant search solution. The subspace-iteration technique is particularly useful when applied to systems whose stiffness and mass matrices have large bandwidths (Bathé and Wilson, 1972). It consists of a repeated application of the Rayleigh-Ritz method in which the computed mode shapes from one step are used as trial-basis vectors for the next iteration; this process continues until convergence is obtained for each of the required number of mode shapes and frequencies. The technique is initiated by specifying a number of static load cases equal to or greater than the desired number of mode shapes. The load cases are selected so that the resulting structure displacements contain the lower mode shapes. These displacements define a transformation matrix that transforms the nodal coordinates of the finite element model to a smaller number of generalized coordinates. This transformation results in an equivalent mass and stiffness matrix for the structure, and a Jacobi diagonalization procedure is used to solve the resulting eigenvalue problem and to obtain modal frequencies and generalized mode shapes. The generalized mode shapes are then used as trial values for the iterative process described above, which continues until the trial and computed generalized mode shape amplitudes are sufficiently close. The generalized mode shapes are finally transformed to the mode shapes of the structure by the transformation matrix discussed above.

TABLE 3-1. SUPERSTRUCTURE ELEMENT LIBRARY IN SUBPROGRAM SAP (Bathé et al., 1974)

ELEMENT TYPE	DESCRIPTION	DEGREES OF FREEDOM PER NODE POINT	USE	FORCES OR STRESSES COMPUTED
3-D TRUSS 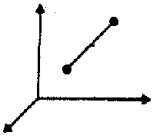	Straight, prismatic, elastic element; stiffness matrix computed from standard theory for truss members.	Three translations.	Represents one-dimensional members that transmit axial forces only.	Axial force.
3-D BEAM	Straight, prismatic, elastic element; stiffness matrix computed from classical beam theory.	Three translations and three rotations.	Represents beams that transmit axial and shear forces, bending moments, and torsional moments.	Three forces and three moments at each end of element.
PLANE STRESS, PLANE STRAIN, OR AXISYMMETRIC 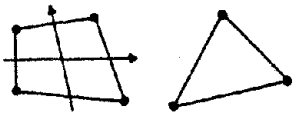	Quadrilateral or triangular elastic element. Stiffness matrix formulation based on assumed parabolic variation of displacements within element.	Two in-plane translations.	Plane stress or plane strain: Represents elastic continuum with known state of lateral constraint. Axisymmetric: Represents elastic body symmetrical about one of the coordinate axes.	Normal and shear stresses at center of element.
3-D SOLID 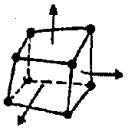	Eight-node, solid brick elastic element. Stiffness matrix formulation based on assumed cubic variation of displacements within element.	Three translations.	Represents any 3-D, elastic, isotropic continuum.	Six stress components at center of element and at center of each side.
VARIABLE-NUMBER-NODES THICK SHELL AND 3-D 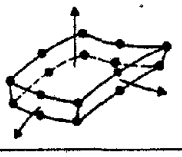	3-D isoparametric or subparametric element with isotropic or orthotropic elastic material properties. Has minimum of 8 node points and maximum of 21.	Three translations.	3-D or thick-shell analyses. Represents bending moments, shear deformations, and normal deformations better than does standard 3-D element.	Six global stress components at up to seven locations within element.
THIN PLATE AND SHELL 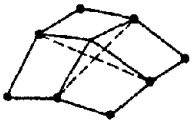	Flat, elastic, quadrilateral or triangular element. Uses constant-strain triangle and LCCT9 element* to represent membrane and bending behavior, respectively.	Three translations and three rotations.	Models thin-shell or plate structures that transmit in-plane and out-of-plane forces and moments.	Three normal stresses and three moments at center of element.
BOUNDARY 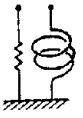	Elastic spring element.	One axial translation and one rotation about element axis.	Imposes displacement boundary conditions and defines support reactions.	Axial force and torsional moment.
PIPE 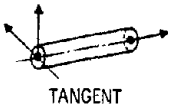 TANGENT 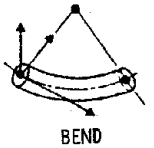 BEND	Prismatic; uniform elastic material properties. Stiffness matrix based on classical theory for straight and curved beams. Includes effect of internal pressure on stiffness of curved pipe elements.	Three translations and three rotations.	Represents straight segment (tangent) or circularly curved segment (bend) in a pipe.	Three forces and three moments at each end and at center of each bend.

AA8777

*Linear Curvature Compatible Triangular plate-bending element developed by Clough and Felippa (1968).

The second procedure for computing mode shapes and frequencies--the determinant-search solution--is best suited to the analysis of large systems whose stiffness and mass matrices have small bandwidths. The solution algorithm, as described by Bathé and Wilson (1973), combines triangular factorization and vector inverse iteration to calculate the required mode shapes and frequencies. These are obtained in sequence, starting with the first mode of the system. A secant iteration procedure, which operates on the characteristic polynomial

$$p(\omega^2) = \det\left|[K] - \omega^2[M]\right|$$

(where [K] and [M] are the system stiffness and mass matrices and ω^2 is an eigenvalue), is used to obtain a shift near the next unknown eigenvalue. Each determinant evaluation requires a triangular factorization of the matrix $\left|[K] - \omega^2[M]\right|$. Once a shift near the unknown eigenvalue is obtained, inverse iteration is used to calculate the mode shape; the frequency is obtained by adding the Rayleigh quotient correction to the shift value.

3.3.2.3 Subprogram COMBINE

The function of Subprogram COMBINE is to use the results from Subprograms FOUND and SAP to determine the response of the soil/structure system. Several different techniques for carrying out this function have been considered in the course of this program (see Werner, 1976b). However, the technique described in this section has been selected and incorporated into Subprogram COMBINE, since it offers the following significant advantages:

- It provides a combined superstructure/foundation/soil system impedance matrix that is of the lowest possible order (equal to the number of foundation degrees of freedom). This simplifies its inversion when determining the system response.

- It represents the superstructure by using a normal mode technique that features efficient convergence properties.

The basic technique is an extension of an approach described by Clough and Penzien (1975) for analyzing structures subjected to multiple-support motions. The various steps in the technique are outlined as follows:

- Partition the equations of motion of the superstructure/foundation system according to degrees of freedom of the superstructure and of the foundation elements, i.e.,

$$\begin{bmatrix} M_1 & 0 \\ 0 & M_2 \end{bmatrix} \begin{Bmatrix} \ddot{y}_1 \\ \ddot{y}_2 \end{Bmatrix} + \begin{bmatrix} C_{11} & C_{12} \\ C_{21} & C_{22} \end{bmatrix} \begin{Bmatrix} \dot{y}_1 \\ \dot{y}_2 \end{Bmatrix} + \begin{bmatrix} K_{11} & K_{12} \\ K_{21} & K_{22} \end{bmatrix} \begin{Bmatrix} y_1 \\ y_2 \end{Bmatrix} = \begin{Bmatrix} 0 \\ P \end{Bmatrix} \qquad (3\text{-}1)$$

where

$\{y_1\}$ = Degrees of freedom of superstructure $= \{Y_1\}e^{i\omega t}$

$\{y_2\}$ = Degrees of freedom of foundation $= \{Y_2\}e^{i\omega t}$

$[M],[C],[K]$ = Mass, damping, and stiffness matrices, respectively

$\{P\}$ = Vector of forces applied at foundation/soil interfaces $= \{P_o\}e^{i\omega t}$

and the damping matrix $[C]$ is expressed as

$$[C] = \left[\begin{array}{c|c} C_{11} & C_{12} \\ \hline C_{21} & C_{22} \end{array}\right] = \alpha[M] + \beta[K] \qquad (3\text{-}2)$$

in which α and β are selected to provide representative damping ratios for the superstructure (as defined by $[M_1]$ and $[K_{11}]$).

- Express the superstructure response, $\{y_1\}$, as the superposition of a pseudostatic component, $\{y_1^s\}$, and a dynamic component, $\{y_1^d\}$:

$$\{y_1\} = \{y_1^s\} + \{y_1^d\} \qquad (3\text{-}3)$$

- Express the pseudostatic displacement component, $\{y_1^s\}$, in terms of the foundation degree-of-freedom vector, $\{y_2\}$ using the relationship

$$\{y_1^s\} = [R^s]\{y_2\} = [R^s]\{Y_2\}e^{i\omega t} \qquad (3\text{-}4)$$

where

$$[R^s] = -[K_{11}]^{-1}[K_{12}]$$

This accounts for the superstructure response and internal stresses induced by relative static displacements of its foundations.

- Compute the dynamic response component, $\{y_1^d\} = \{Y_1^d\}e^{i\omega t}$, from a normal mode expansion of the upper set of equations in Equation 3-1, which corresponds to the superstructure system defined by $[M_1]$, $[K_{11}]$, and $[C_{11}]$ and to a

fixed base configuration for the superstructure. This results in

$$\{Y_1^d\} = [R^d]\{Y_2\} = [R^d]\{Y_2\}e^{i\omega t} \qquad (3\text{-}5)$$

where

$$[R^d] = -[\phi][S]_D^{-1}[\phi]^T\left[-\omega^2[M_1][R^s] + i\omega\left[[C_{11}][R^s] + [C_{12}]\right]\right]$$

in which $[\ ]_D$ refers to a diagonal matrix, and

$[\phi]$ = Modal matrix for fixed-base superstructure configuration

$[S]_D = -\omega^2[I]_D + i\omega\left[\alpha[I]_D + \beta[\omega_n^2]_D\right] + [\omega_n^2]_D$

$[I]_D$ = Unit diagonal matrix

$[\omega_n^2]_D$ = Diagonal matrix in which the nth diagonal element contains the square of the eigenvalue for the nth mode

- Incorporate $\{Y_1^s\}$ (from Eq. 3-4) and $\{Y_1^d\}$ (from Eq. 3-5) into the second set of partitioned equation of motions in Equation 3-1. This set of equations takes the form

$$[K_a]\{Y_2\} = \{P_o\} \qquad (3\text{-}6)$$

where

$[K_a]$ = Superstructure/foundation dynamic impedance matrix

$$= -\omega^2[M_2] + [K_{21}]\left[[R^s]+[R^d]\right] + [K_{22}] + i\omega\left[[C_{22}] + [C_{21}]\left[[R^s]+[R^d]\right]\right]$$

and

$$\{Y_2\} = \{Y_2\}e^{i\omega t}$$

$$\{P\} = \{P_o\}e^{i\omega t}$$

$[C_{21}]$, $[C_{22}]$ = Damping matrices defined in Equation 3-2.

- Express $\{P_o\}$ as the superposition of the foundation/soil driving forces and resisting forces, i.e.,

$$\{P_o\}e^{i\omega t} = \{F^D\}e^{i\omega t} + \{F^R\}e^{i\omega t} \qquad (3\text{-}7)$$

where

$\{F^D\}$ = Vector of driving force amplitudes* (Fig. 3-3a)

$\{F^R\}$ = Vector of resisting force amplitudes
$= -[K_b]\{Y_2\}$

$[K_b]$ = Soil/foundation impedance matrix* (Fig. 3-3b)

- Substitute Equation 3-7 into 3-6, thereby coupling the superstructure/foundation system with the massless-foundation/soil/incident-wave system as represented by the above driving and resisting forces.† Obtain the resulting foundation response as:

$$\{Y_2\} = [K_a + K_b]^{-1}\{F^D\} \qquad (3\text{-}8)$$

- Compute the corresponding superstructure displacements by using Equation 3-3 after substituting the above computed values of $\{Y_2\}$ into Equations 3-4 and 3-5.

---

*Computed in Subprogram FOUND.

†This step assures that the forces applied to the foundations by these systems are in a state of dynamic equilibrium and that the two systems are bonded together at the foundation locations.

3.3.3 OUTPUT PHASE

The purpose of the output phase of CAST1 is to provide the output required for evaluation of the system response characteristics. This output is presented in printed and plotted form as described below.

3.3.3.1 Printed Output

Before describing the printed output of the system response results, it is appropriate to note that, although not specifically indicated in Figure 3-2, each subprogram in CAST1 provides an echo-print of the input to that subprogram as well as the results of its computations. For example, Subprogram GREEN prints out the array of frequency-dependent Green's functions, whereas, for each given set of soil properties and incident wave characteristics, Subprogram FOUND prints out the complex foundation/soil compliance matrix, the impedance matrix, and the driving force vector for each excitation frequency.* Subprogram SAP prints out the superstructure stiffness and mass matrices (see Eq. 3-1) as well as the fixed-base mode shapes and frequencies. It also prints out the foundation mass matrix.

The printout of the system-response results are provided by Subprogram COMBINE for each combination of parameters that define the superstructure, foundation, soil, and incident wave. The results are printed as the real and imaginary parts of the complex, steady-state displacement of each degree of freedom at all foundation and superstructure node points. This printout is preceded by an echo-print of all data input into COMBINE by the other subprograms, and by a printout of the superstructure/foundation/soil impedance matrix, which is formed in COMBINE prior to the computation of the system displacement results.

---

*The excitation frequencies are expressed in dimensionless form, as discussed in Section 4.2.

3.3.3.2 Plotted Output--Subprogram PLOT

In addition to the printout described above, Subprogram COMBINE provides a data tape that contains the records of the computed displacement response and, for each record, the corresponding dimensionless frequency, angles of incidence, and shear wave velocity. This tape is used as input to Subprogram PLOT, whose function is to provide two main graphic forms of the system response, as described below.

a. Frequency-Dependent Response Plots

The first graphic form produced by Subprogram PLOT corresponds to plots of the frequency-dependent response amplitude and phase angle at any specified degree of freedom. Examples of these plots are shown in Figures 3-4a and 3-4b.* These figures show that the amplitudes and phase angles are plotted in terms of a dimensionless frequency parameter, R_L, which is defined in Section 4.2. Other parameters denoted in the plots are (1) N/C--the node point (N) and component number (C) of the degree-of-freedom response being plotted†; (2) TH and TV--the angles of incidence θ_H and θ_V defined in Figure 3-1; and (3) WS--the shear wave velocity of the elastic half-space.

It is noted that Subprogram PLOT provides the following useful options that can be employed when obtaining frequency-dependent response plots: (1) the scales along the ordinate and abscissa can either be defined by the program or selected by the user; (2) either a single curve or several overlaid curves can be provided on a single frame; and (3) the phase angles can be plotted directly from the information on the data tape, (which may produce discontinuities in the resulting curve), or, alternatively, they can be automatically modified by factors of $\pm 2n\pi$ ($n = 1, 2, \ldots$) to generate smooth and continuous phase angle vs. frequency curves.

*These plots show results from the single-span bridge analysis described in Chapter 4 and depicted in Figure 4-1.

†The components are numbered as 1 to 6. Components 1, 2, and 3 represent translational displacements along the x, y, and z axes, respectively, whereas Components 4, 5, and 6 represent rotations about these axes.

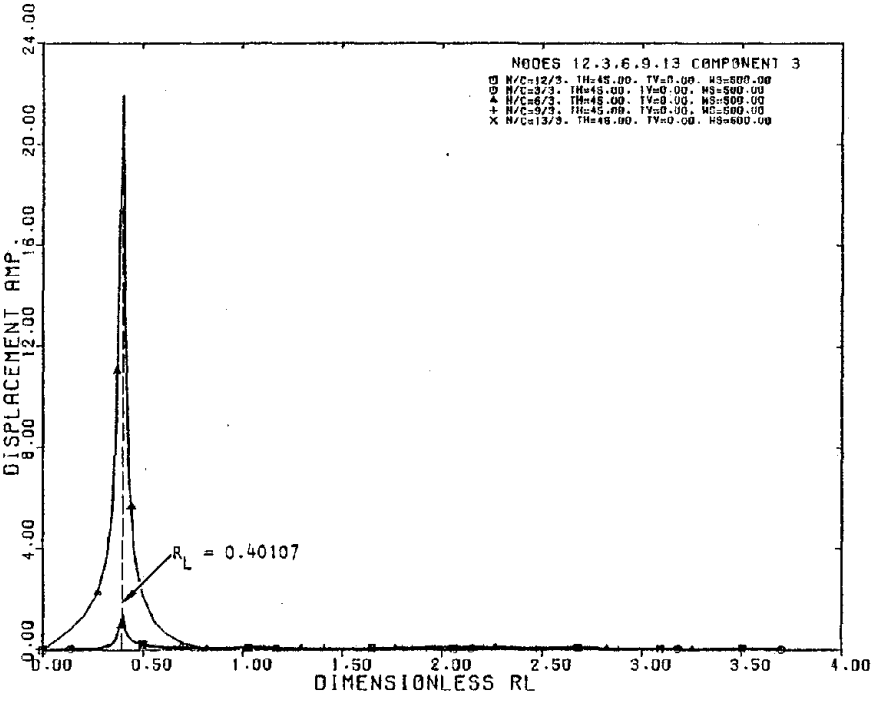

(a) Amplitude

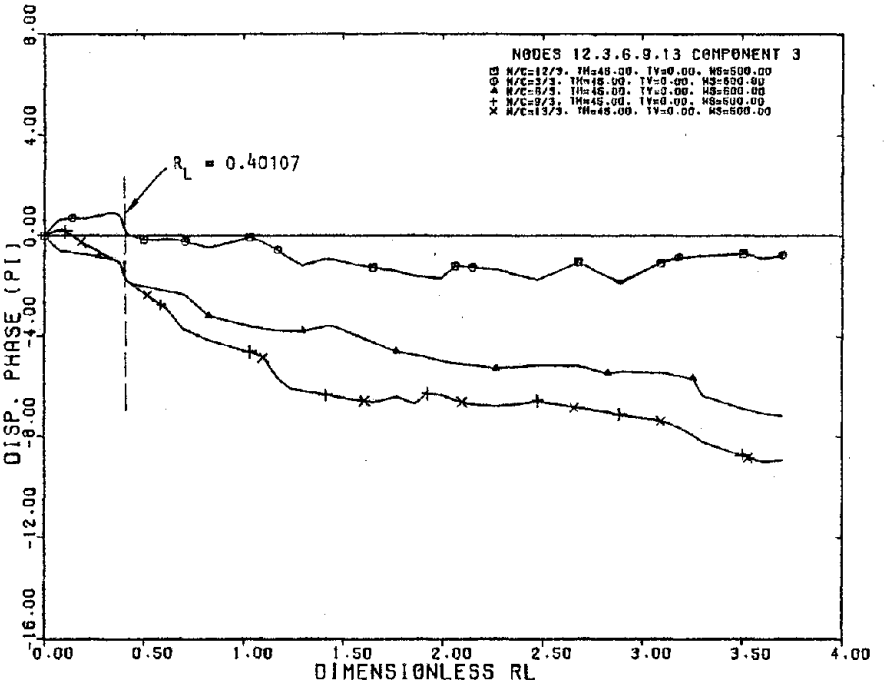

(b) Phase angle

FIGURE 3-4. FREQUENCY-DEPENDENT AMPLITUDE AND PHASE ANGLE PLOTS

b. Deformed Shape Plots

The second graphic form of the response results is the three-dimensional plot of the deformed shape of the structure at different times during its steady-state response to a given incident wave with a particular excitation frequency. Such plots are developed as follows:

1. Select an excitation frequency at which the deformed shape plots are to be obtained. This frequency should correspond to the occurrence of significant response of the soil/structure system, and should be identified from examination of the frequency-dependent response amplitude and phase angle plots.

2. Identify particular times during the structure response at this excitation frequency for which deformed shape plots will be obtained. This is carried out by constructing time histories of steady-state displacement response for selected degrees of freedom along the structure, using the simple expression

$$u_i(t) = A_i \sin(\omega t - \alpha_i) \qquad (3\text{-}9)$$

where, for the ith degree of freedom

$u_i(t)$ = Steady-state displacement at time t

A_i, α_i = Amplitude and phase angle respectively, as computed from the system response analysis

ω = Excitation frequency (rad/sec) identified in Step 1

Overlaid time-history plots for the various degrees of freedom, as obtained using Equation 3-9, can be used to identify particular times at which significant structure responses are taking place.

3. Using the information determined from Steps 1 and 2, together with the structure geometry and complex displacements at each degree of freedom, apply Subprogram PLOT to obtain the deformed-shape plots at each discrete time.

An example development of deformed shape plots is provided by applying this procedure to results from the single-span bridge analysis described in Chapter 4. The configuration and node-point numbers of this bridge model are shown in Figure 4-1. By applying the above three steps, deformed shape plots for the bridge response to incident SH-waves with θ_H = 45 deg, θ_V = 0 deg, are developed as follows:

1. From examination of the frequency-dependent response plots shown in Figure 3-4, a significant peak in the vertical displacement (Component 3) is seen to occur at the midspan of the bridge (Node 6) when the dimensionless excitation frequency is such that R_L = 0.40107.* Therefore deformed shape plots will be obtained for this frequency.

2. Time-history plots of the vertical displacements induced at various structure node points for this excitation are shown in Figure 3-5. The figure indicates that the response characteristics at this frequency can be well represented by providing deformed shape plots at times given by ωt = 0.4, 0.9, 1.4, and 1.9.

3. The resulting deformed shape plots at these discrete times are shown in Figure 3-6.

The above example features only one response component--the vertical response--that was of importance. However, it is conceivable that, at a given

*This response is shown in Figures 3-4a and 3-4b by the curves denoted by N/C = 6/3 and by the triangular symbols.

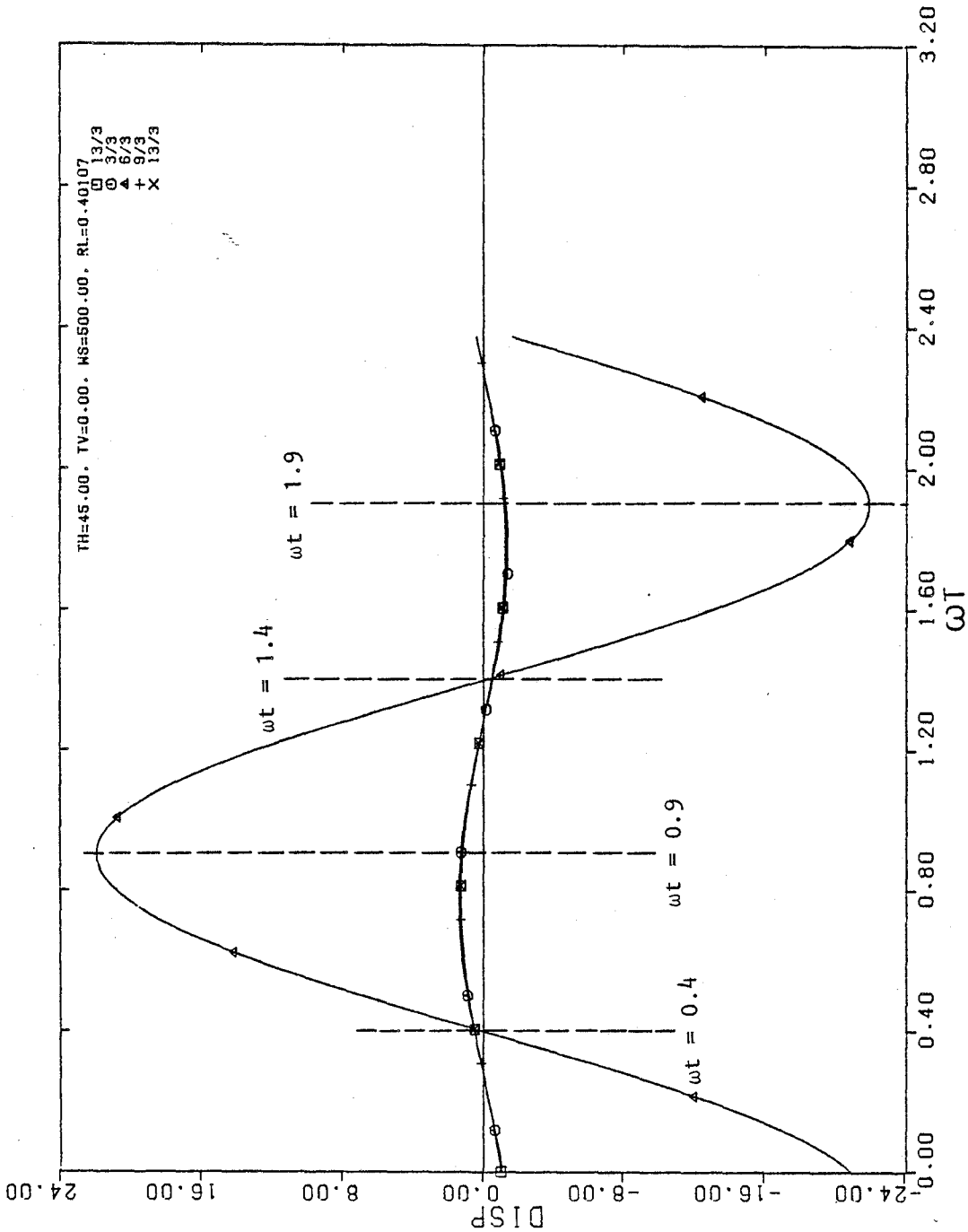

FIGURE 3-5. DISPLACEMENT TIME-HISTORIES USED TO CONSTRUCT DEFORMED-SHAPE PLOT

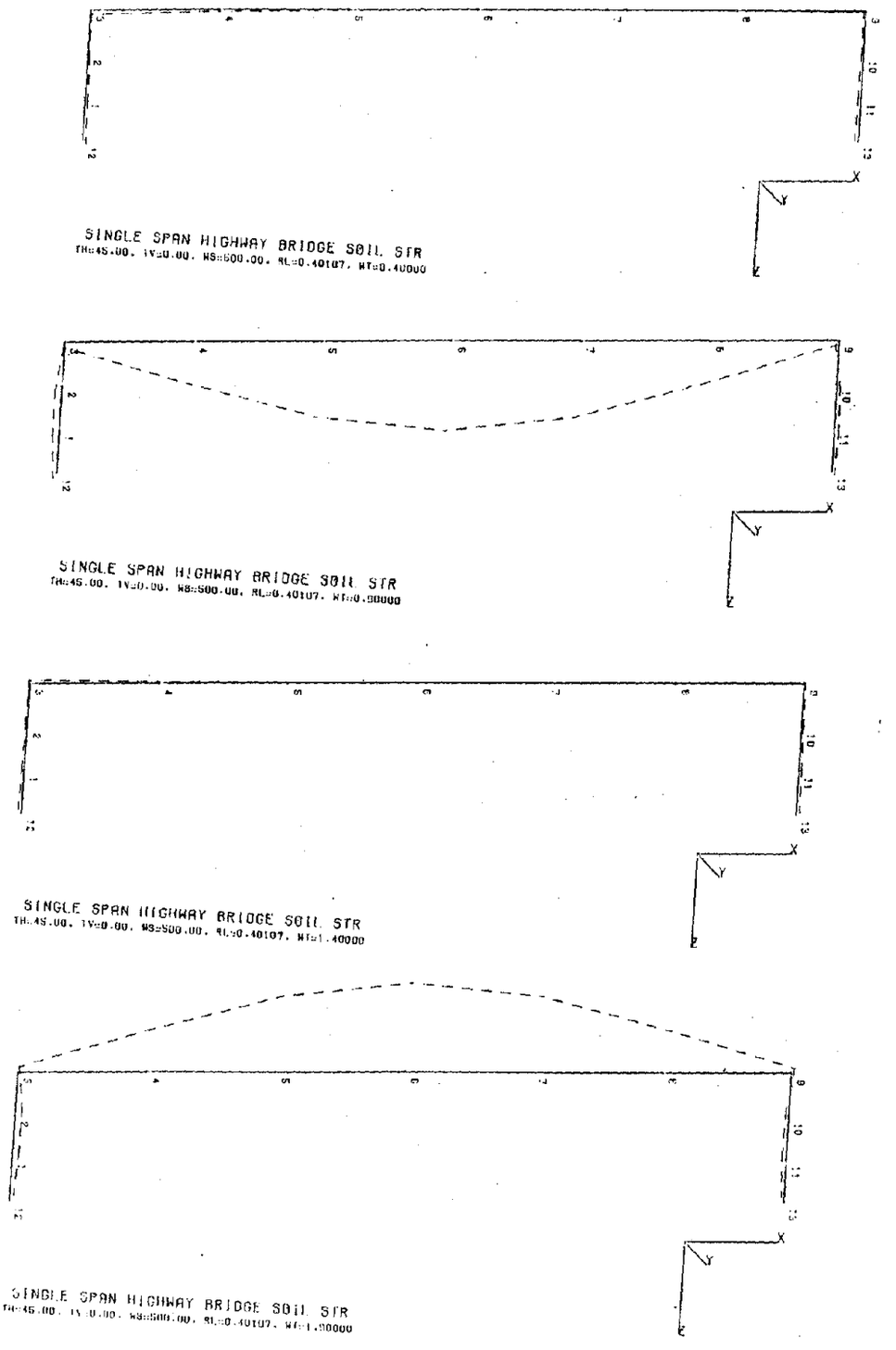

FIGURE 3-6. DEFORMED-SHAPE PLOTS

frequency, more than one response component may be of interest. For this case, it will be necessary to develop and examine time-history plots for each of the significant response components to define the discrete times at which the deformed shapes should be plotted.

3.4 POSSIBLE EXTENSIONS OF CAST1 METHODOLOGY

Although CAST1 in its present form already represents a valuable analytical tool, there are several areas that can be further developed to increase its technical capabilities and ease of implementation. Plans along these lines are discussed in the following paragraphs.

3.4.1 EXTENSION TO INCLUDE ARBITRARY TRANSIENT EXCITATIONS

The methodology in its present form considers only harmonic incident waves. As noted in Section 3.2.3, this is no technical limitation since any transient excitation can be expressed using Fourier Transform techniques as the superposition of a series of harmonic excitations that cover a broad frequency band. Therefore, to provide a means for considering arbitrary transient input motions, an existing Fast-Fourier-Transform program will soon be incorporated into CAST1. This planned extension requires only a minimum programming effort, and it will greatly expand the usefulness of CAST1 to earthquake-related problems.

3.4.2 COMPUTATION OF MOMENTS AND STRESSES

The structure response now computed by CAST1 takes the form of steady-state displacements at each degree-of-freedom along the structure. This capability, although useful for gaining insight into some fundamental aspects of traveling wave effects on structure response, does not yet provide complete information for design applications; such applications require knowledge of moments and stresses within the structure as well as displacements and deformed shapes. Therefore, CAST1 will be extended to compute moments and stresses for any of the element types used to model the structure (see

Table 3-1). This will involve the use of element stiffness matrices generated by Subprogram SAP together with the complex displacements determined in Subprogram COMBINE. No difficulty is involved with incorporating computations of this type into CAST1, although some programming effort will be required to format and organize the results so that they may be presented in the most useful form possible.

3.4.3 FOUNDATION AND SOIL REPRESENTATION

At present, the CAST1 methodology is based on rigid foundations of arbitrary shape that rest on the surface of an elastic half-space. To make this representation more general, it is planned to: (1) modify the soil model to correspond to a viscoelastic, horizontally-layered medium, and (2) incorporate foundation-embedment effects. This modified representation of the soil medium, by itself, will involve the implementation of Green's functions developed for point loads on the surface of a viscoelastic, layered medium; i.e., a revised Subprogram GREEN will be required. Computerized techniques for developing such Green's functions are available and can be easily incorporated into the methodology. The additional inclusion of foundation embedment effects will involve the use of Green's functions recently developed by Luco (1977) to represent a point source within a viscoelastic, layered medium. A sizeable programming effort is anticipated for incorporating these Green's functions into this methodology.

3.4.4 SUBPROGRAM INTERFACING

Another extension being considered would modify the existing interfaces between the subprograms so that CAST1 can be more easily applied. One possible modification would incorporate several of the subprograms as subroutines under a single mainline program, thereby eliminating much of the data-handling and subprogram interfacing that is now required. However, the modification also has certain disadvantages; for example, the single combined program could require extensive in-core storage that, in turn, could influence computer run times, particularly for large problems. These various considerations will be weighed when deciding whether to carry out this modification.

CHAPTER 4

AN EXAMPLE ANALYSIS OF A SINGLE-SPAN BRIDGE ON A SOFT SOIL MEDIUM SUBJECTED TO INCIDENT SH-WAVES

This chapter presents results obtained by applying CAST1 to the analysis of a simple, single-span bridge structure that rests on the surface of a soft soil medium and is subjected to traveling SH-waves. The purpose of these calculations is to demonstrate (1) some basic phenomena and the potential importance of traveling-wave effects and (2) the usefulness of CAST1 as a technique for studying these effects.

4.1 SYSTEM DESCRIPTION

4.1.1 STRUCTURE

The single-span bridge considered in the following calculations consists of a road deck supported at either end by identical end walls and spread-footing foundations. The road deck has a uniform box-girder cross section and is 120-ft long by 60-ft wide. The end walls are 20-ft high, and the spread footings have a plan dimension of 70 ft by 10 ft and rest on the surface of the soil medium (Fig. 4-1a).

The bridge is modeled by a series of beam elements, whose lengths are shown in Figure 4-1b and whose section properties and material properties are listed in Table 4-1. This use of beam elements provides a satisfactory representation of the structure response for the purposes of this example. The foundations are rigid in this model and the structure is undamped.

The fixed-base mode shapes and frequencies of the superstructure, as computed by Subprogram SAP, are shown in Figure 4-2. The out-of-plane modes are seen to have significantly higher frequencies than do the corresponding in-plane modes, a direct result of the greater stiffness of the structure in the y-direction. A total of 29 modes was used to characterize

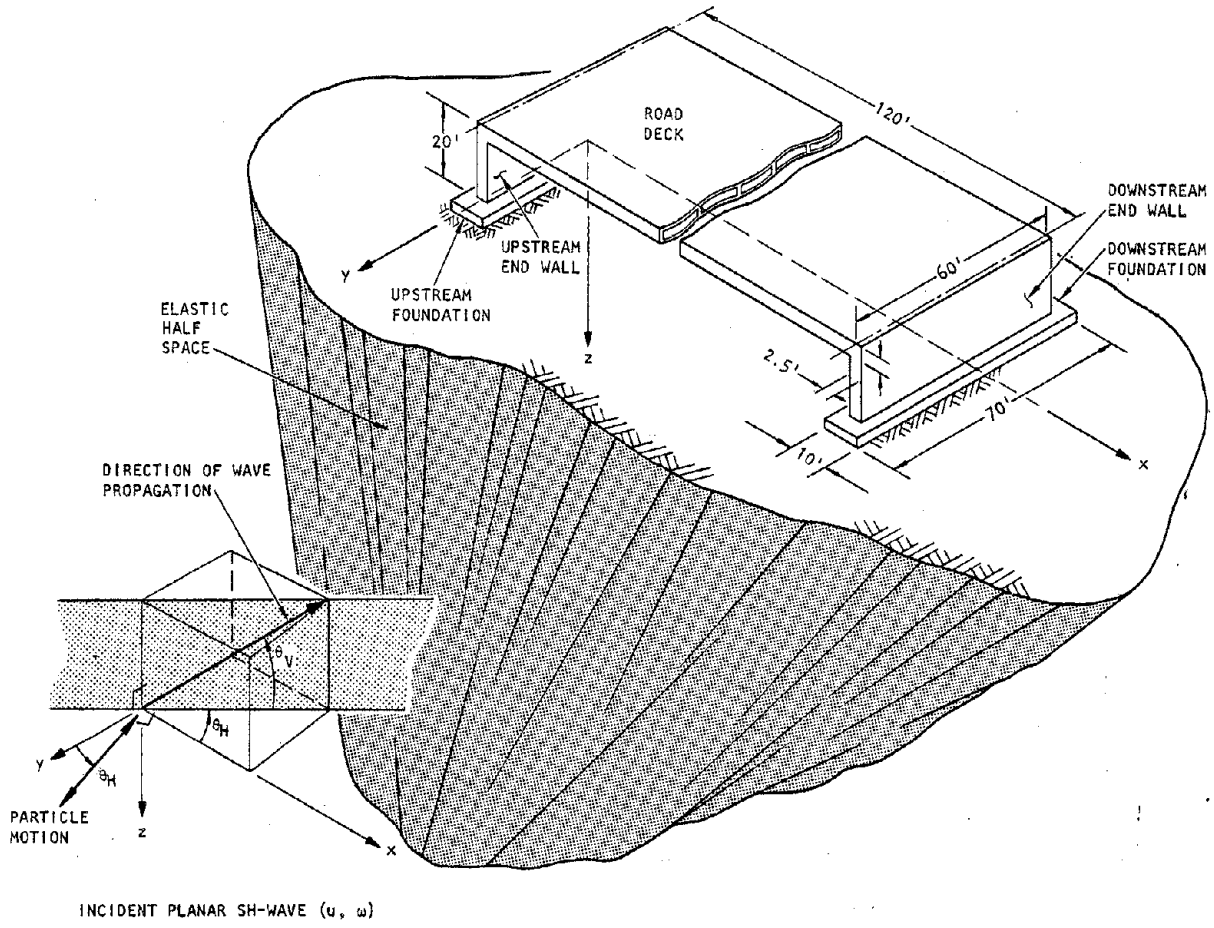

(a) System configuration

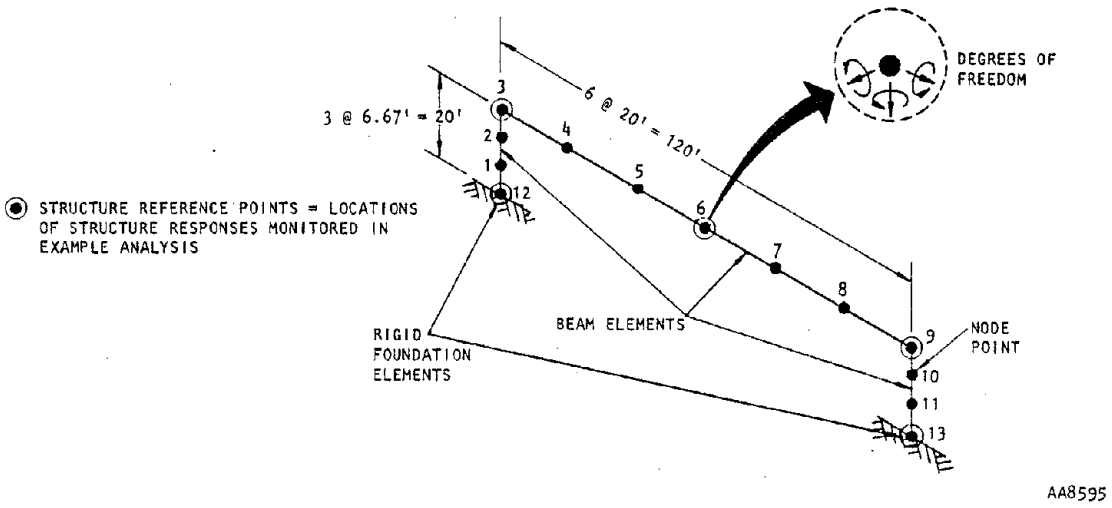

(b) Structure model

FIGURE 4-1. SOIL/STRUCTURE SYSTEM CONFIGURATION AND MODEL CONSIDERED IN EXAMPLE ANALYSIS

TABLE 4-1. SECTION PROPERTIES AND MATERIAL PROPERTIES CONSIDERED IN EXAMPLE ANALYSIS

Element	Cross Sectional Area, ft^2	Moment of Inertia, ft^4		
		About Strong Axis	About Weak Axis	Torsion
Road Deck	9.82 x 10	3.56×10^4	3.29×10^2	1.01×10^3
End Walls	1.48×10^2	4.28×10^4	7.69 x 10	3.08×10^2

(a) Superstructure section properties

Element	Shear Wave Velocity, fps	Unit Weight, pcf	Poisson's Ratio
Elastic Half Space	500	110	0.33
Superstructure	6900	150	0.15

(b) Material properties

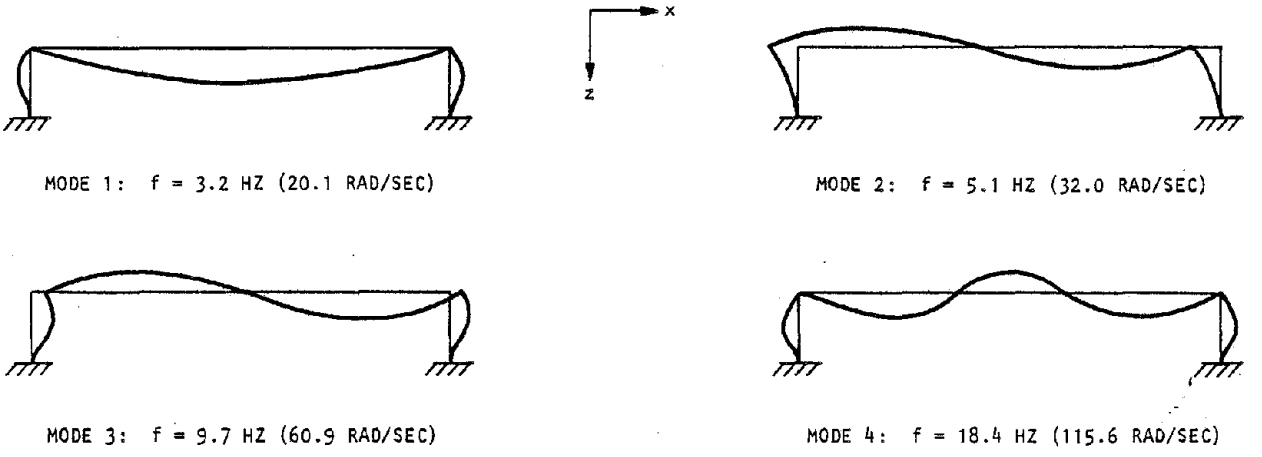

(a) In-plane modes (significant response in x-z plane)

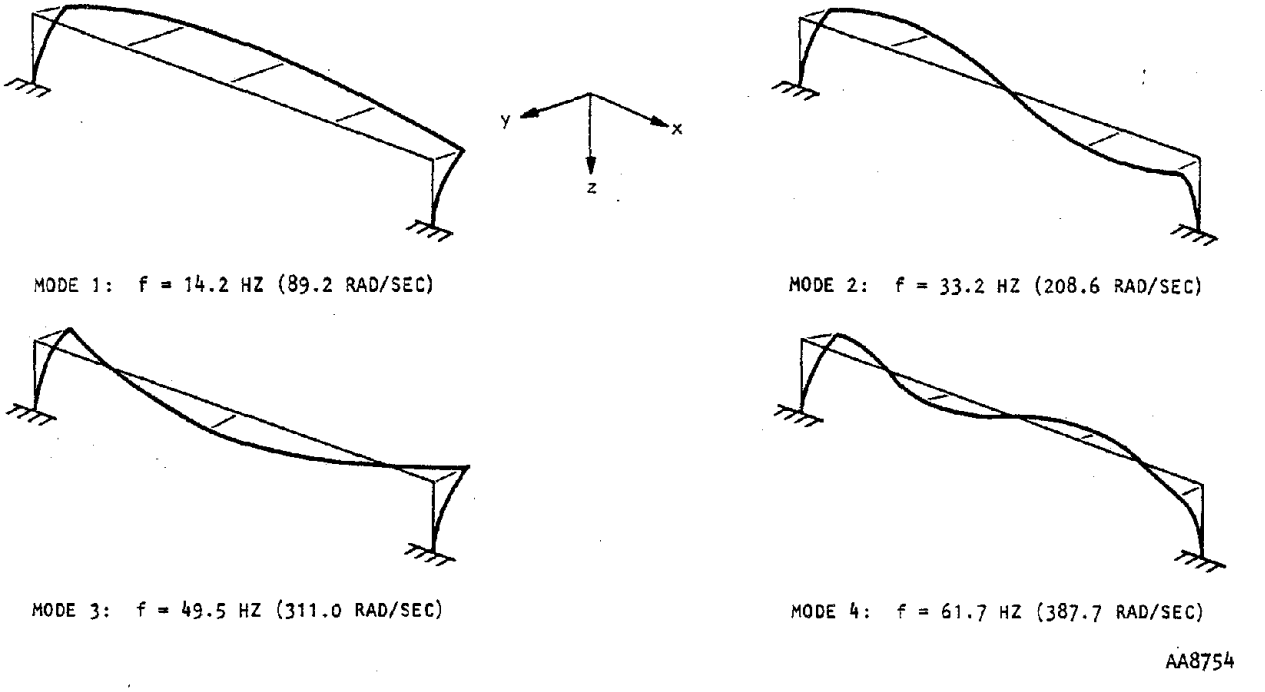

(b) Out-of-plane modes (significant response in y-direction)

FIGURE 4-2. FIXED-BASE MODE SHAPES AND FREQUENCIES OF SUPERSTRUCTURE

the superstructure, in order to provide adequate convergence of the response computations within the range of excitation frequencies considered in this analysis (up to 25 Hz).

4.1.2 SOIL MEDIUM

The soil medium is represented as an elastic half-space with material properties shown in Table 4-1b. Its low shear wave velocity (500 fps chosen for this example) is representative of a soft soil material for which traveling wave effects at a given excitation frequency will be more pronounced than for stiffer media with a higher shear wave velocity.

4.1.3 INPUT MOTIONS

The input motions for analysis of this soil/structure system consist of plane harmonic SH-waves. For such waves, the particle motion is always directed parallel to the ground surface and is normal to the direction of the wave propagation (Fig. 4-1a). In this analysis, the particle motion is assigned an amplitude of 1.0 (surface amplitude 2.0) and a zero phase angle at the upstream foundation, which is the origin of the coordinate system for these analyses. The orientation of the particle motions and the direction of wave propagation is defined by the two angles of incidence, θ_H and θ_V, that are defined in Figure 4-1a. Nine combinations of these angles, which comprise three values each of θ_H and θ_V, have been considered. The three values of θ_H are:

- θ_H = 0 deg. The incident SH-waves propagate in a vertical plane parallel to the x-z plane. The corresponding particle motions are directed parallel to the y-axis, or normal to the span of the bridge.

- θ_H = 90 deg. The incident SH-waves propagate in a vertical plane normal to the x-z plane. The corresponding particle motions are directed normal to the y-axis, or parallel to the span of the bridge.

- θ_H = 45 deg. The incident SH-waves propagate in a vertical plane oriented at an angle of 45 deg with the x-z plane. The corresponding particle motions are directed at an angle of 45 deg from the positive y-axis.

For each of the above θ_H angles, three different values of θ_V are considered. These θ_V values each specify a direction of propagation of the wave within the plane defined by θ_H, and are as follows:

- θ_V = 90 deg. The incident waves are propagating along a path normal to the ground surface; i.e., they are vertically incident waves. For such waves, the particle motions applied at each point along the structure foundation are identical in amplitude and phase--i.e., there is no traveling-wave effect. This corresponds to the case most commonly considered in current engineering practice.

- θ_V = 0 deg. The incident waves are propagating along a path parallel to the ground surface; i.e., they are horizontally incident waves.

- θ_V = 45 deg. The incident waves are propagating along a path that makes an angle of 45 deg with the ground surface.

4.2 FORM OF RESULTS

The results of the calculations are presented in three different forms. The first two forms are displacement amplitude plots and tabulations of displacement amplitudes and phase angles. They are provided at five different locations along the structure, termed "structure reference points." These locations correspond to the upstream and downstream foundations, the tops of the upstream and downstream end walls, and the midspan of the road deck (Fig. 4-1b).

The third form of the results consists of deformed-shape plots of the structure response. These plots are provided for particular excitation frequencies and angles of incidence at which significant structure responses are indicated by the frequency-dependent displacement amplitudes and phase angles. As noted in Chapter 3, the deformed-shape plots are obtained directly from the computed displacement amplitudes and phase angles for each degree of freedom. They define the three-dimensional response at discrete times during the application of the incident waves.

For each form of the results, the excitation frequencies are represented in terms of a dimensionless frequency parameter, R_L, defined as

$$R_L = \frac{\ell}{\lambda} = \frac{\ell\omega}{2\pi V_s} \qquad (4\text{-}1)$$

where

ℓ = Structure dimension

λ = Actual wavelength of the incident wave

V_s = Shear wave velocity of elastic half-space

ω = Excitation frequency, rad/sec

The parameter ℓ in the above expression is a characteristic structure dimension that is selected according to the orientation of the propagation path of the incident wave, as defined by θ_H. Its selection for the three values of θ_H considered in these calculations is shown in Table 4-2. Also, with regard to Equation 4-1, it is recognized that the system response is more directly related to the apparent wavelength, as projected onto the ground surface, than to the actual wavelength. However, since the apparent wavelength, λ_a, computed as

$$\lambda_a = \frac{\lambda}{\cos \theta_V} \qquad (4\text{-}2)$$

TABLE 4-2. DEPENDENCE OF DIMENSIONLESS FREQUENCY ON θ_H

Angle of Incidence, θ_H, deg	Orientation of Incident Wave Propagation Path	Definition of ℓ (Eq. 4-1)		Dimensionless Frequency, R_L (Eq. 4-1)
		Description	Numerical Value (Fig. 4-1)	
0	Within vertical plane parallel to x-z plane of bridge	Distance between the two bridge foundations	120 ft	$R_{L_x} = \frac{120 \text{ ft} \times \omega}{2\pi V_s}$
90	With vertical plane normal to x-z plane of bridge (or parallel to y-z plane)	Length of foundations along y-axis	70 ft	$R_{L_y} = \frac{70 \text{ ft} \times \omega}{2\pi V_s}$
45	Within vertical plane oriented at 45 deg to x-z plane	Same as for θ_H = 0 deg and 90 deg		R_{L_x} and R_{L_y}

approaches infinity as θ_V approaches 90 deg, it is not possible to represent the frequency dependence of the response for this condition. For this reason, the actual wavelength is represented in Equation 4-1, although the frequency shift between certain results for θ_V = 0 deg and 45 deg that is caused by the apparent wavelength effect, will be discussed in the sections that follow.

4.3 RESULTS FOR INCIDENT SH-WAVES WITH θ_H = 0 DEG

The first set of results corresponds to incident SH-waves that propagate in a vertical plane parallel to the x-z plane of the bridge and apply particle motions directed along the y-axis (θ_H = 0 deg, as shown in Fig. 4-1a). For this case, the frequency-dependent response is expressed in terms of the dimensionless frequency parameter R_{L_x}, defined in Table 4-2. Also, as can be seen in Figure 4-1a, the x-dimension of each foundation (10 ft) is small when compared to the overall bridge span (120 ft). Therefore, the particle motions from incident waves with θ_H = 0 deg result in almost concentrated point loads that are applied at either end of the bridge.

4.3.1 RESPONSE TO INCIDENT WAVES WITH θ_V = 90 DEG

The response of the bridge to vertically incident SH-waves oriented at θ_H = 0 deg is described in terms of displacements along the y-axis and rotations about the z-axis. These results are provided in the frequency-dependent response plots of Figure 4-3, the tabulations of amplitudes and displacements in Table 4-3, and the deformed-shape plots of Figure 4-4. They indicate the following trends:

- The largest displacement amplitudes occur when R_{L_x} = 1.03, which corresponds to the wavelength of the incident wave being about equal to the span length (Fig. 4-3a).

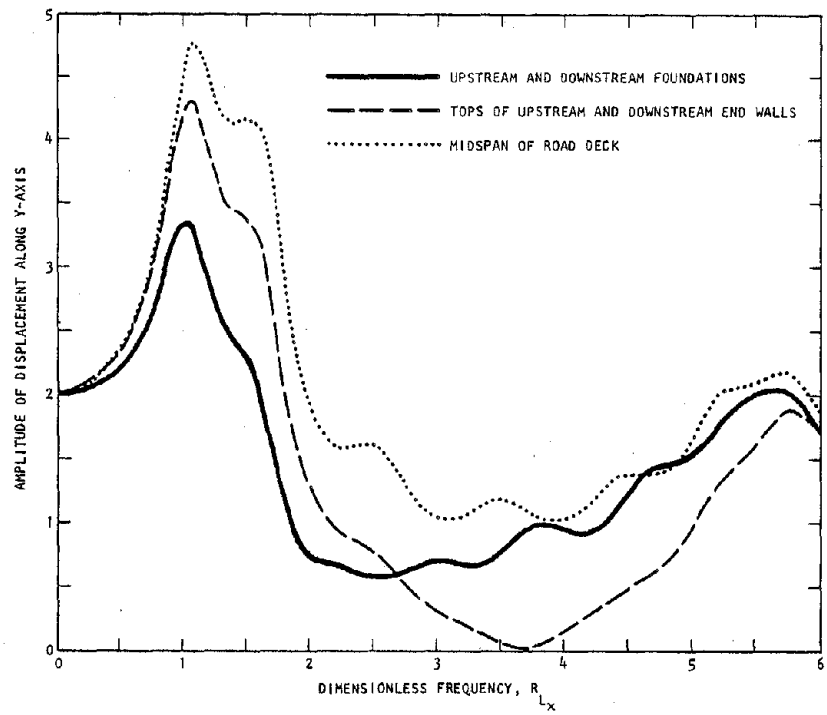

(a) Displacement along y-axis

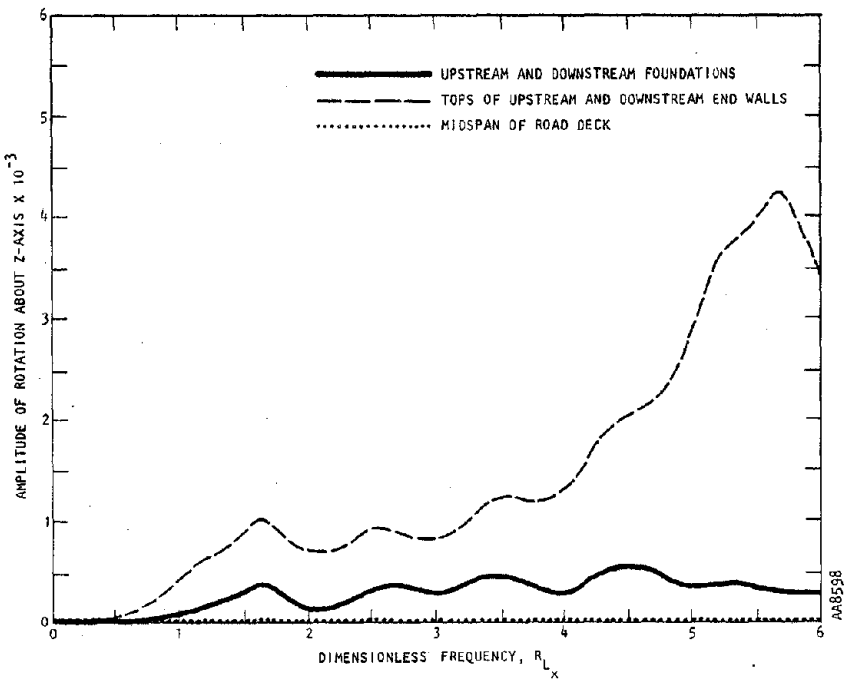

(b) Rotations about z-axis

FIGURE 4-3. FREQUENCY-DEPENDENT RESPONSE AMPLITUDES OF BRIDGE SUBJECTED TO INCIDENT SH-WAVES WITH θ_H = 0 DEG, θ_V = 90 DEG

TABLE 4-3. AMPLITUDES AND PHASE ANGLES OF BRIDGE RESPONSE TO INCIDENT SH-WAVES WITH θ_H = 0 DEG

Angle of Incidence, θ_V, deg	Description of Response	Component of Response	Dimensionless Frequency, R_{L_x}	Upstream Foundation		Downstream Foundation		Top of Upstream End Wall		Top of Downstream End Wall		Midspan of Road Deck	
				Amplitude	Phase Angle, rad	Amplitude	Phase Angle, rad	Amplitude	Phase Angle, rad	Amplitude	Phase Angle, rad	Amplitude	Phase Angle, rad
90	Symmetric Response	Displacement along y-axis	1.03	3.363	-0.174π	3.363	-0.174π	4.311	-0.206π	4.311	-0.206π	4.762	-0.206π
			2.00	0.687	-0.376π	0.687	-0.376π	1.221	-0.709π	1.221	-0.709π	1.853	-0.709π
			5.73	2.063	-0.265π	2.063	-0.265π	1.889	-0.237π	1.889	-0.237π	2.221	0.763π
		Rotation about z-axis	1.0	0.078×10^{-3}	0.807π	0.078×10^{-3}	-0.193π	0.463×10^{-3}	-0.177π	0.463×10^{-3}	0.823π	~ 0	--
			2.0	0.152×10^{-3}	0.554π	0.152×10^{-3}	-0.446π	0.698×10^{-3}	-0.709π	0.698×10^{-3}	0.29π	~ 0	--
			5.73	0.260×10^{-3}	0.462π	0.260×10^{-3}	-0.538π	4.251×10^{-3}	0.763π	4.251×10^{-3}	-0.237π	~ 0	--
0	Antisymmetric Response	Displacement along y-axis	0.5	2.100	-0.004π	2.100	0.996π	2.137	-0.005π	2.137	0.995π	~ 0	--
			1.5	3.056	-0.165π	3.057	0.835π	3.662	-0.198π	3.664	0.802π	~ 0	--
			4.5	0.601	-0.292π	0.601	0.706π	0.563	-0.676π	0.568	0.324π	0.003	-0.806π
		Rotation about z-axis	0.5	0.223×10^{-3}	-0.864π	0.233×10^{-3}	0.819π	2.943×10^{-3}	0.995π	2.943×10^{-3}	0.995π	2.964×10^{-3}	0.995π
			1.5	0.415×10^{-3}	0.990π	0.643×10^{-3}	0.613π	4.998×10^{-3}	0.802π	5.000×10^{-3}	0.802π	5.124×10^{-3}	0.802π
			4.5	0.487×10^{-3}	-0.410π	0.859×10^{-3}	0.252π	0.680×10^{-3}	0.323π	0.700×10^{-3}	0.323π	0.871×10^{-3}	0.324π
	Symmetric Response	Displacement along y-axis	1.0	3.338	-0.150π	3.337	-0.150π	4.218	-0.177π	4.217	-0.178π	4.630	-0.177π
			2.0	0.666	-0.375π	0.660	-0.377π	1.178	-0.707π	1.182	-0.710π	1.790	-0.709π
			5.73	1.080	-0.075π	0.985	0.091π	0.654	-0.003π	1.181	-0.051π	1.074	-0.968π
		Rotation about z-axis	1.0	0.205×10^{-3}	-0.666π	0.267×10^{-3}	-0.470π	0.459×10^{-3}	-0.182π	0.459×10^{-3}	0.828π	0.006×10^{-3}	-0.703π
			2.0	0.249×10^{-3}	-0.715π	0.495×10^{-3}	-0.569π	0.679×10^{-3}	-0.713π	0.669×10^{-3}	0.294π	0.009×10^{-3}	0.920π
			5.73	0.827×10^{-3}	-0.696π	0.713×10^{-3}	-0.208π	1.784×10^{-3}	-0.981π	2.339×10^{-3}	0.041π	0.464×10^{-3}	0.114π
	Whipping Response	Displacement along y-axis	0.75	2.489	0.017π	2.402	0.447π	2.744	0.007π	2.623	0.428π	2.230	0.212π
			1.25	1.580	-0.143π	3.429	-0.693π	1.619	-0.262π	4.453	-0.722π	2.865	-0.616π
			1.75	2.536	-0.411π	1.293	0.375π	3.776	-0.490π	0.879	0.266π	2.179	-0.429π
45	Antisymmetric Response	Displacement along y-axis	$0.5\sqrt{2}$	2.212	-0.016π	2.212	0.984π	2.305	-0.019π	2.305	0.981π	~ 0	--
		Rotation about z-axis	$0.5\sqrt{2}$	0.230×10^{-3}	-0.905π	0.254×10^{-3}	0.791π	3.170×10^{-3}	0.981π	3.170×10^{-3}	0.980π	3.201×10^{-3}	0.981π
	Symmetric Response	Displacement along y-axis	$\sqrt{2}$	2.331	-0.335π	2.329	-0.335π	3.373	-0.425π	3.374	-0.426π	4.094	-0.426π
	Whipping Response	Displacement along y-axis	$0.75\sqrt{2}$	3.522	-0.089π	2.136	0.305π	4.374	-0.101π	2.548	0.231π	3.373	0.017π

AA8771

Note: Incident wave motions defined to have a surface amplitude of 2.0 and a zero phase angle at the upstream foundation, which is the origin of the coordinate system for this analysis.

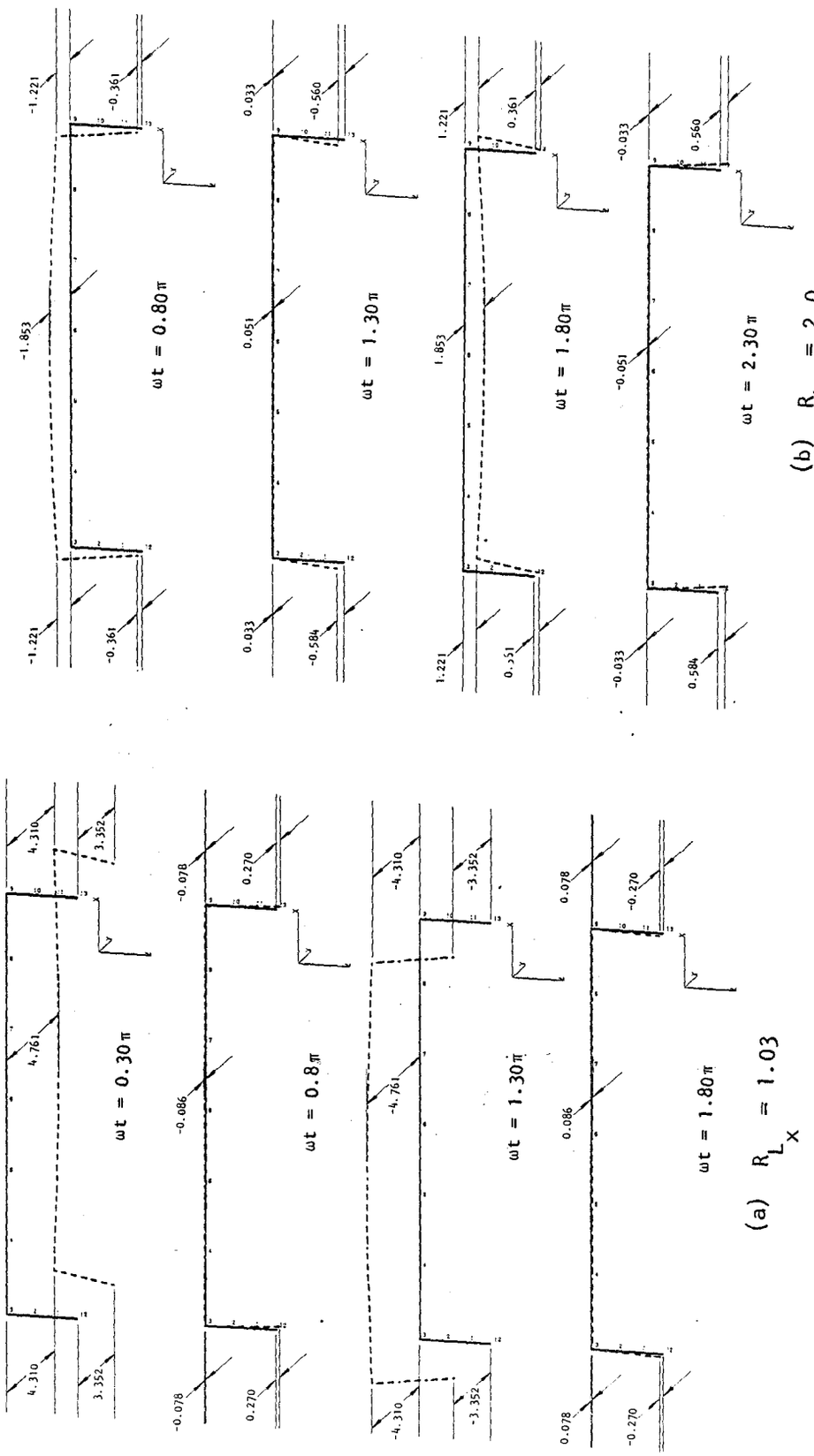

FIGURE 4-4. DEFORMED SHAPES OF BRIDGE SUBJECTED TO INCIDENT SH-WAVES WITH θ_H = 0 DEG, θ_V = 90 DEG

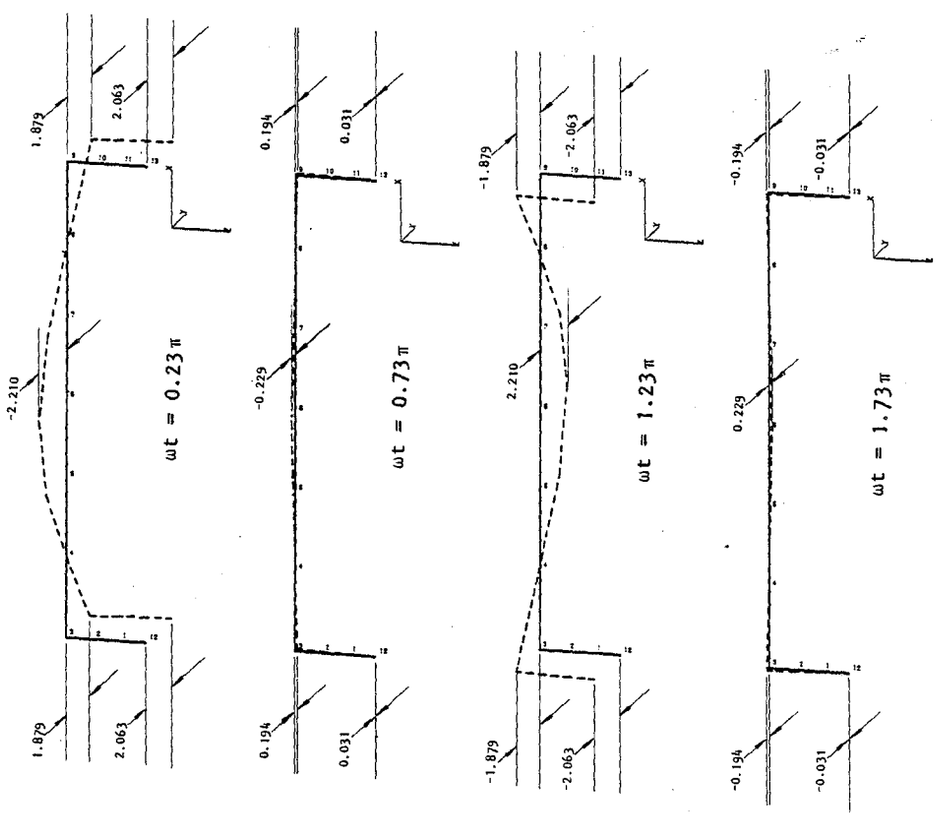

(c) $R_{L_x} = 5.73$

FIGURE 4-4. (CONCLUDED)

- Bridge response amplitudes are symmetric about the midspan of the bridge, for all excitation frequencies (Table 4-3, Fig. 4-4). This follows from the symmetry of the structure and the fact that free-field motions of identical amplitude and phase are applied to each foundation when $\theta_V = 90$ deg.

- At low excitation frequencies, rigid body translations of the foundations and the entire bridge are predominant (Fig. 4-4a). However, as the frequency increases, the bending deformations of the road deck (in the x-y plane) become increasingly more significant (Figs. 4-4b, 4-4c).

- At higher frequencies (as represented by $R_{L_X} = 5.73$), the tops of the end walls undergo relatively large rotations about the z-axis, which follow from the significant bending that is taking place in the road deck (Fig. 4-4c). Large differences in the amplitudes of these rotations at the tops of the end walls relative to those at the foundations indicate that the end walls are being subjected to large torsional deformations at these frequencies (Table 4-3).

- The peak displacements induced by the vertically-incident waves occur at a much lower frequency (4.29 Hz, which corresponds to $R_{L_X} = 1.03$) than that of the fundamental out-of-plane, fixed-base mode (14.2 Hz) which is shown in Figure 4-2b. The displacement patterns are also very different for the two cases. The structure response to the vertically-incident waves with $R_{L_X} = 1.03$ corresponds essentially to vibration of a nearly rigid bridge on a soft soil medium. In contrast, the soil is assumed rigid for the fixed-base mode, and the mode shape is dominated by bending deformations of the end walls and the road deck.

4.3.2 RESPONSE TO INCIDENT WAVES WITH θ_V = 0 DEG

As the angle of incidence, θ_V, decreases from 90 deg, the phase difference between the particle motions applied to each foundation becomes more significant. This phase difference is maximized when θ_V = 0 deg; that is, when the waves are horizontally incident.

Frequency-dependent amplitudes of displacement along the y-axis and rotation about the z-axis, as induced by the SH-waves with $\theta_H = \theta_V$ = 0 deg, are plotted in Figures 4-5a and 4-5b respectively. These figures and the tabulated amplitudes and phase angles (Table 4-3) show three distinct patterns of response that occur at particular sets of excitation frequencies. These correspond to antisymmetric response of the structure, symmetric response, and whipping response.

4.3.2.1 Antisymmetric Response when $\theta_H = \theta_V$ = 0 Deg

When odd multiples of the half-wavelength of the incident wave are approximately equal to the bridge span, (i.e., when R_{L_X} = 0.5, 1.5, etc.), the free-field displacements applied to each foundation are of equal amplitude and opposite phase (Fig. 4-6a). The bridge response characteristics at these frequencies are indicated by Figure 4-5, Table 4-3, and the deformed shape plots in Figure 4-7. Analysis results are summarized as follows:

- The structure displacements are essentially antisymmetric about the midspan of the road deck (Table 4-3, Fig. 4-7).
- At lower frequencies (R_{L_X} = 0.5, 1.5) the road deck is undergoing large rigid body rotations about the z-axis that are much greater than the corresponding rotations of the foundation elements (Fig. 4-5b, Table 4-3). Therefore, the end walls are being subjected to significant torsional deformations.

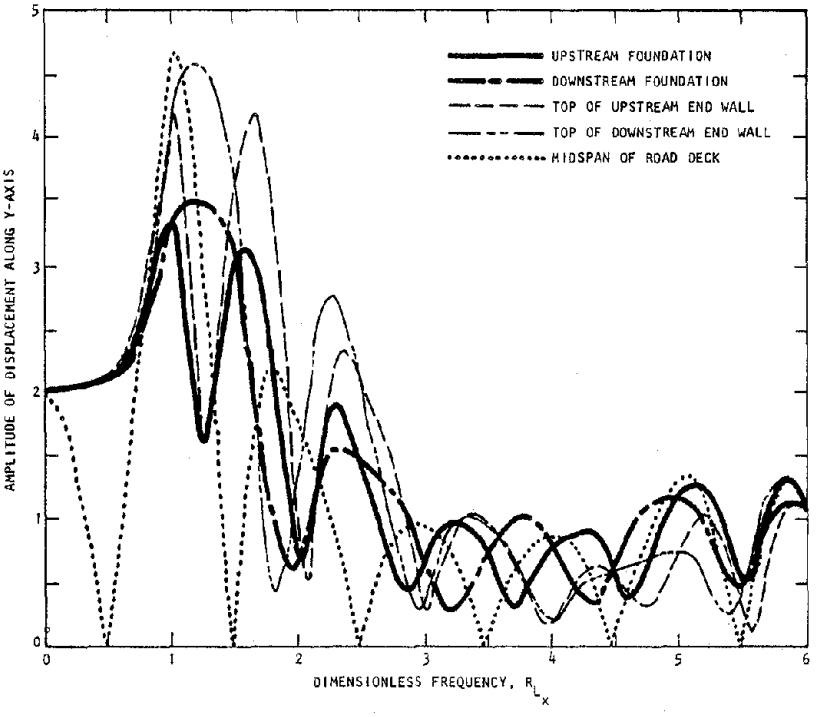

(a) Displacements along y-axis

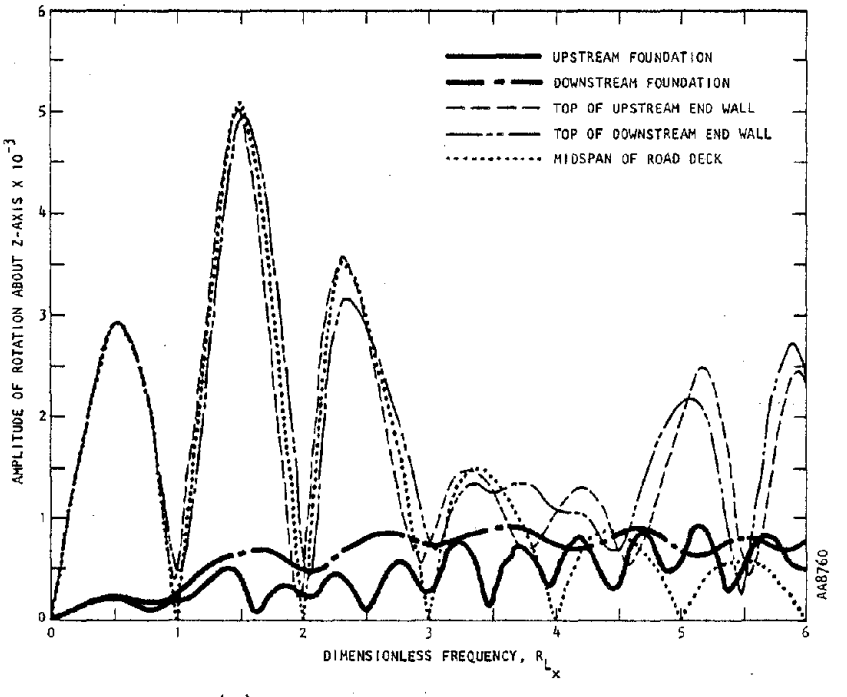

(b) Rotations about z-axis

FIGURE 4-5. FREQUENCY-DEPENDENT RESPONSE AMPLITUDES OF BRIDGE SUBJECTED TO INCIDENT SH-WAVES WITH θ_H = 0 DEG, θ_V = 0 DEG

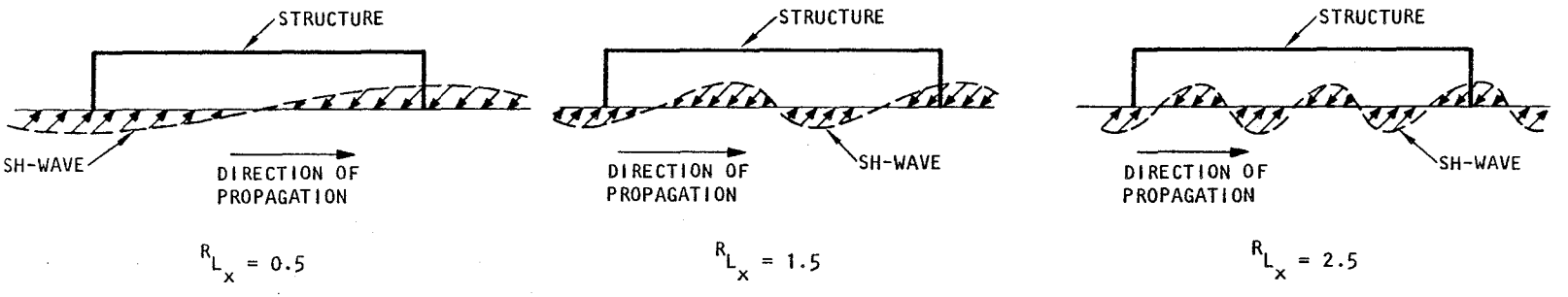

(a) Incident waves causing antisymmetric response of structure

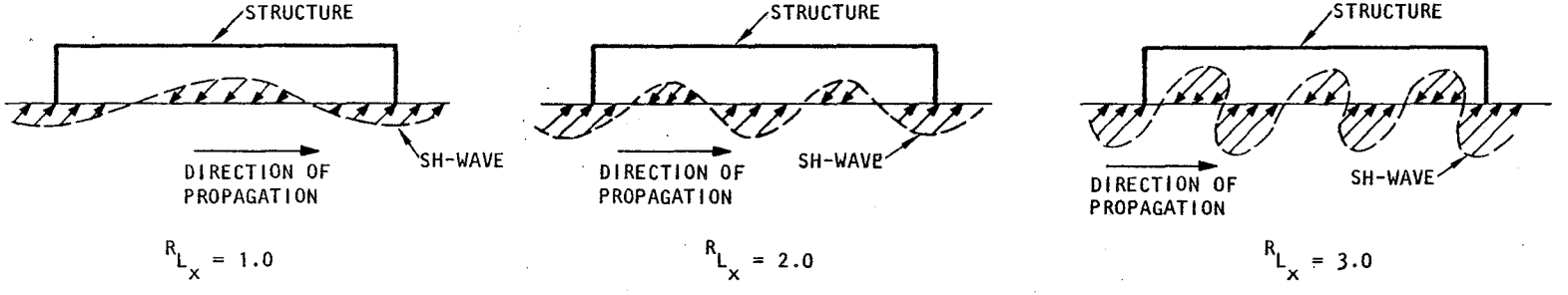

(b) Incident waves causing symmetric response of structure

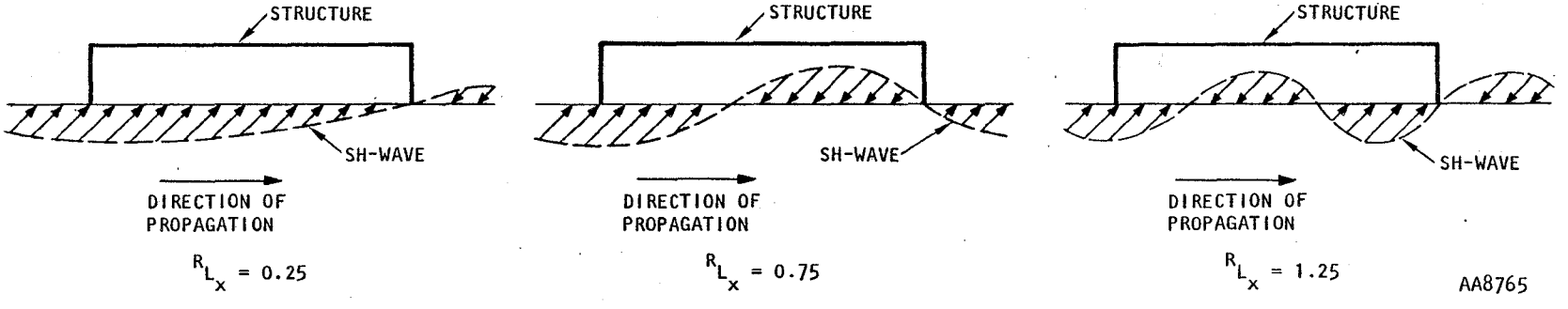

(c) Incident waves causing whipping response of structure

FIGURE 4-6. INFLUENCE OF WAVELENGTH OF INCIDENT WAVES ON STRUCTURE RESPONSE CHARACTERISTICS -- θ_H = 0 DEG, θ_V = 0 DEG

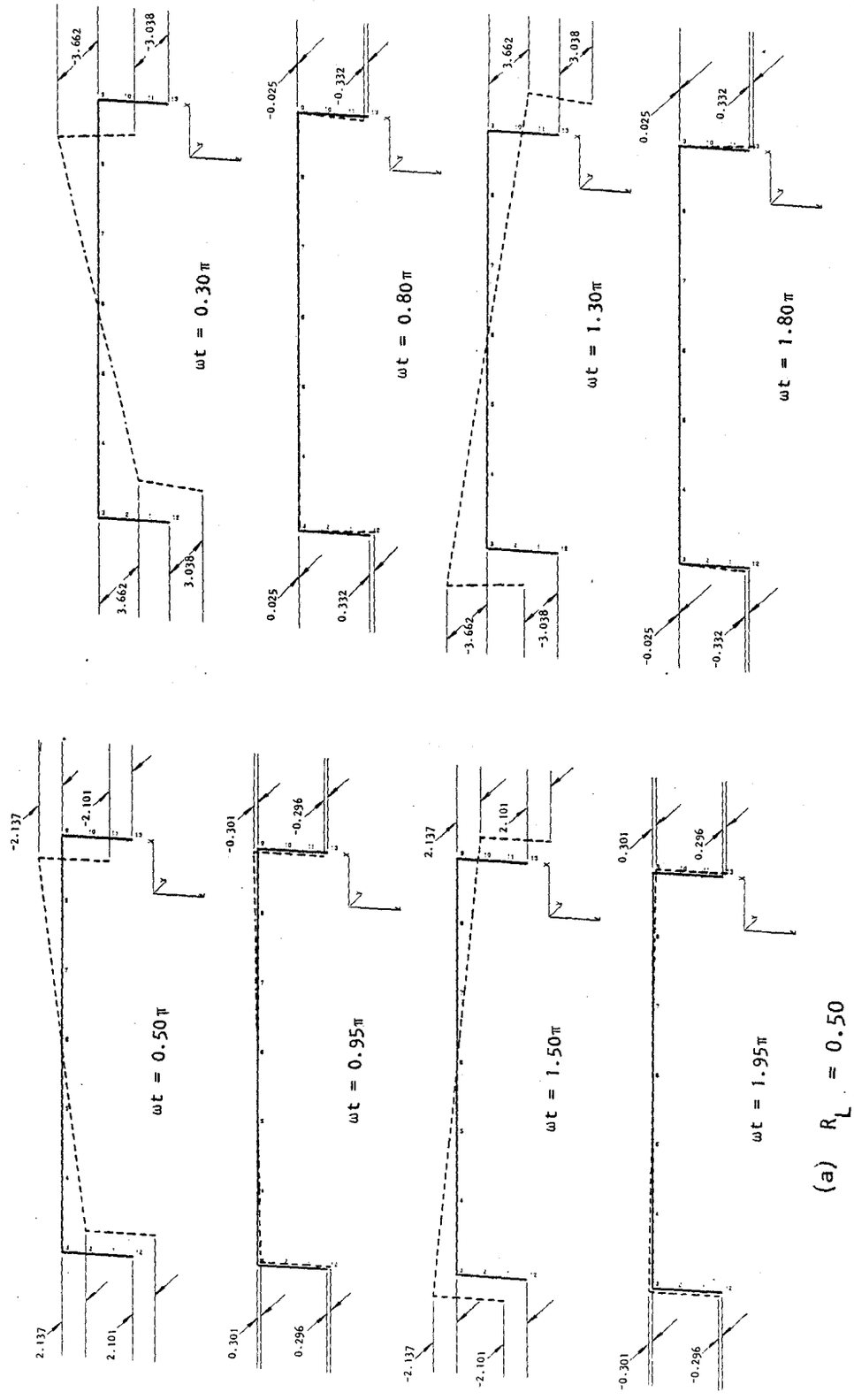

(a) $R_{L_x} = 0.50$ (b) $R_{L_x} = 1.5$

FIGURE 4-7. DEFORMED SHAPES OF BRIDGE SUBJECTED TO INCIDENT SH-WAVES WITH $\theta_H = 0$ DEG, $\theta_V = 0$ DEG (ANTISYMMETRIC RESPONSE)

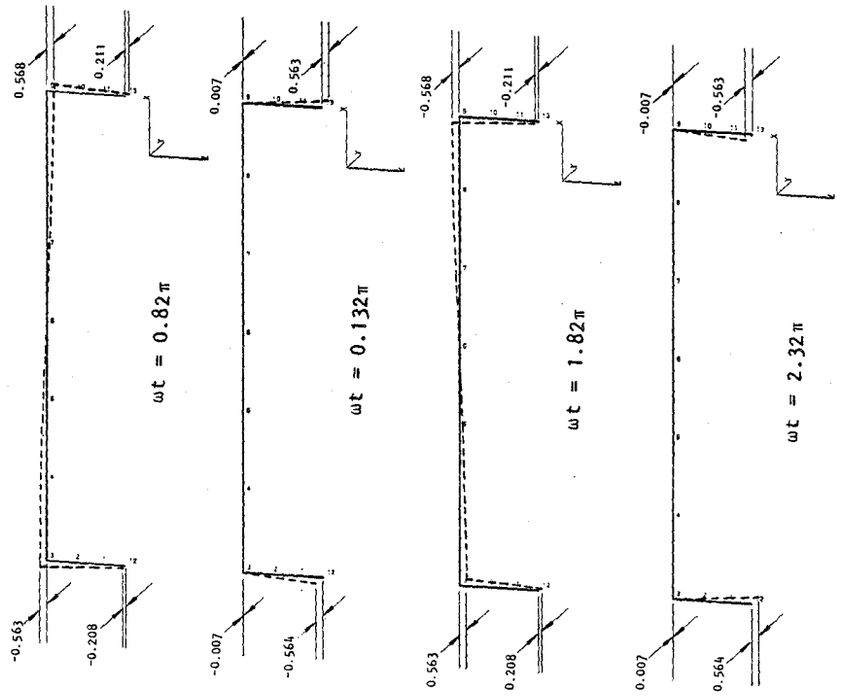

(c) $R_{L_x} = 4.50$

FIGURE 4-7. (CONCLUDED)

- At higher frequencies (e.g., $R_{L_x} = 4.5$) the road deck rotations about the z-axis are smaller and comparable in magnitude to the foundation rotation. Rotation amplitudes and phase angles vary along the length of the road deck, suggesting bending in the x-y plane (Table 4-3).

- In general, the largest response amplitudes occur when R_{L_x} is less than about 3 and greater than about 0.25 (Fig. 4-5).

4.3.2.2 Symmetric Response when $\theta_H = \theta_V = 0$ Deg

A second important response pattern occurs when integer multiples of the wavelength are equal to the structure span length (i.e., when $R_{L_x} = 1.0, 2.0$, etc.). For these conditions, the free-field y-displacements applied at each foundation have equal amplitude and phase (Fig. 4-6b). The corresponding bridge response characteristics are shown in Figure 4-5, Table 4-3, and Figure 4-8. These results are summarized as follows:

- The structure response is essentially symmetric about the midspan of the road deck (Table 4-3, Fig. 4-8).

- At the tops of the end walls, the rotations about the z-axis are quite small and are about equal to the corresponding rotations of the foundation elements. This indicates that the torsional deformations of the end walls are small by comparison to those induced during the antisymmetric response described previously. These rotations essentially vanish at the midspan of the road deck, which is consistent with the observed symmetry of the structure response (Fig. 4-5b, Table 4-3).

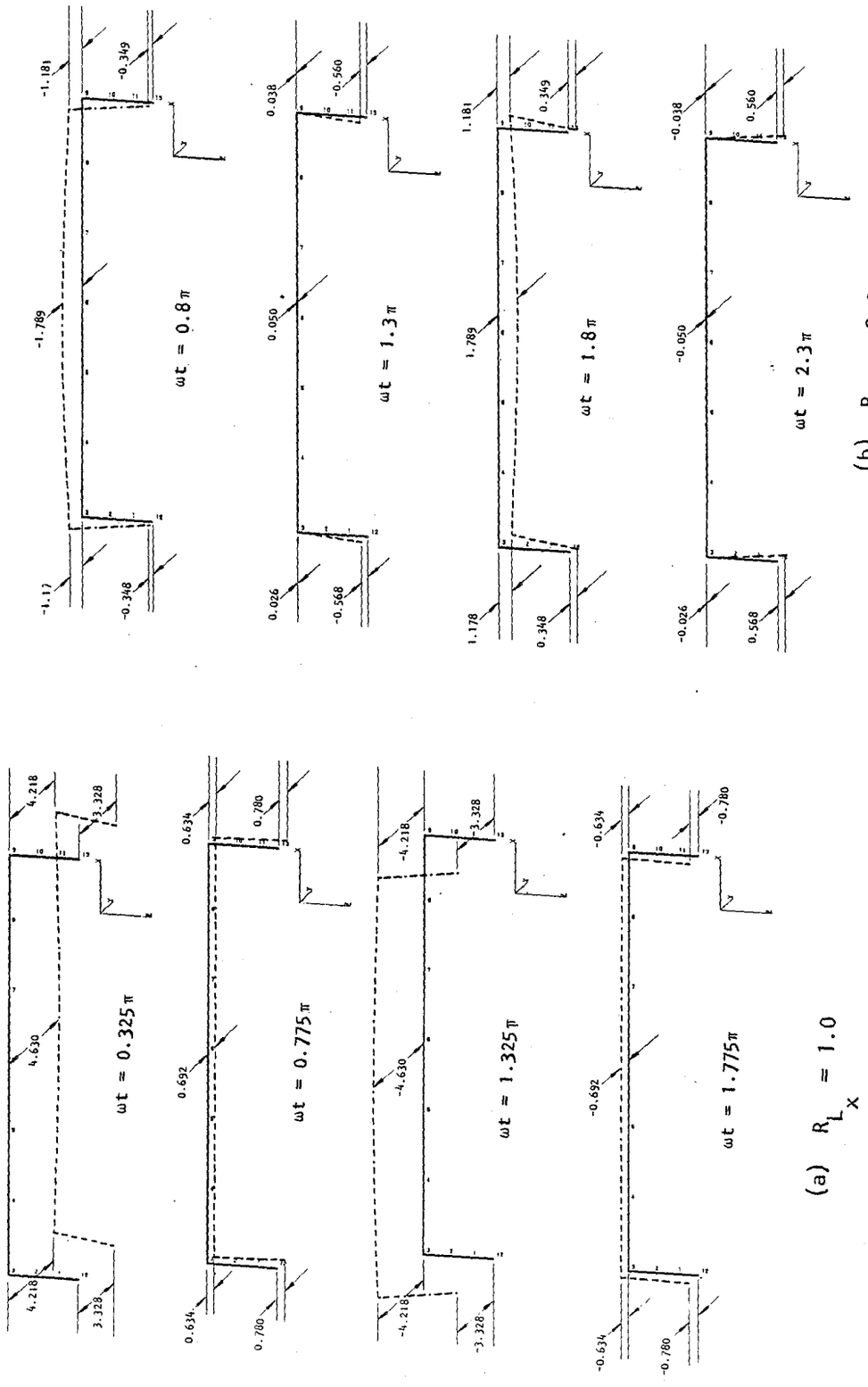

(a) $R_{L_x} = 1.0$ (b) $R_{L_x} = 2.0$

FIGURE 4-8. DEFORMED SHAPES OF BRIDGE SUBJECTED TO INCIDENT SH-WAVES WITH $\theta_H = 0$ DEG, $\theta_V = 0$ DEG (SYMMETRIC RESPONSE)

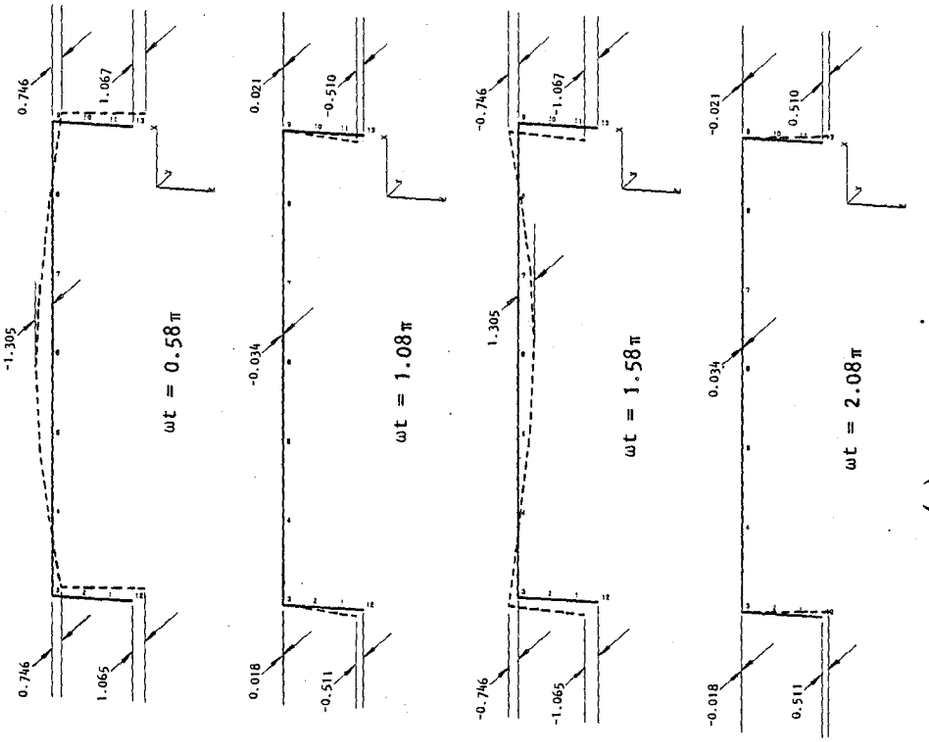

(c) $R_{L_x} = 5.0$

FIGURE 4-8. (CONCLUDED)

- At lower excitation frequencies (R_{L_X} = 1.0), the symmetric response is dominated by rigid body translations along the y-axis and rocking rotations of the end walls and foundations about the x-axis. The amplitudes and phase angles of these response quantities are similar to those induced by the vertically incident waves (Table 4-3, Figs. 4-4a and 4-8a).

- At higher excitation frequencies (R_{L_X} = 5.0), the bending deformations of the road deck (in the x-y plane) become more predominant. This is also true when vertically incident waves are applied, although the displacement amplitudes are much larger for that case--probably because of its different wave-scattering characteristics, which are more important at higher frequencies (Figs. 4-4c, 4-8c, Table 4-3).

4.3.2.3 Whipping Response when $\theta_H = \theta_V$ = 0 Deg

Examination of the frequency-dependent displacement amplitudes (Fig. 4-5a) indicates the presence of prominent amplitude peaks that do not correspond to either antisymmetric or symmetric response. For example, at R_{L_X} = 1.25, the displacement amplitudes along the downstream end wall are seen to be significant, whereas at R_{L_X} = 1.75 significant displacement peaks occur along the upstream end wall. Although not obvious from Figure 4-5a, this behavior corresponds to a general pattern of structure response that occurs when excitation frequencies are such that $R_{L_X} \approx$ 0.25, 0.75, 1.25, 1.75, etc.; for such cases, the incident free-field motions reach their maximum value at one foundation while, at the same time, they nearly vanish at the other foundation (Fig. 4-6c). The resulting structure response is depicted in the deformed-shape plots provided in Figure 4-9 and is summarized as follows:

- The structure response consists primarily of rigid body rotations of the bridge, about a center of rotation whose position along the span of the bridge is changing with time.

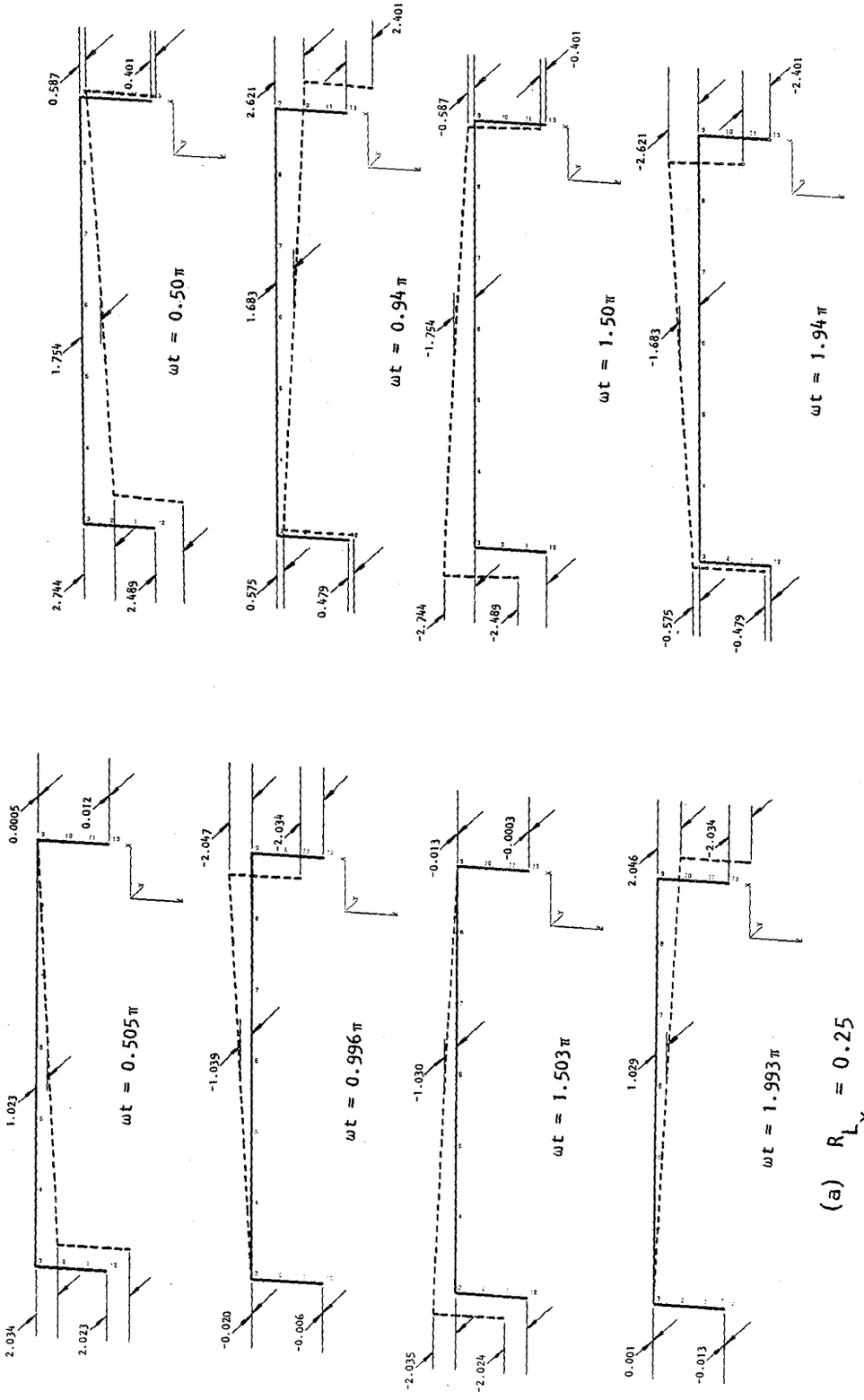

(a) $R_{L_x} = 0.25$

(b) $R_{L_x} = 0.75$

FIGURE 4-9. DEFORMED SHAPES OF BRIDGE SUBJECTED TO INCIDENT SH-WAVES WITH $\theta_H = 0$ DEG, $\theta_V = 0$ DEG (WHIPPING RESPONSE)

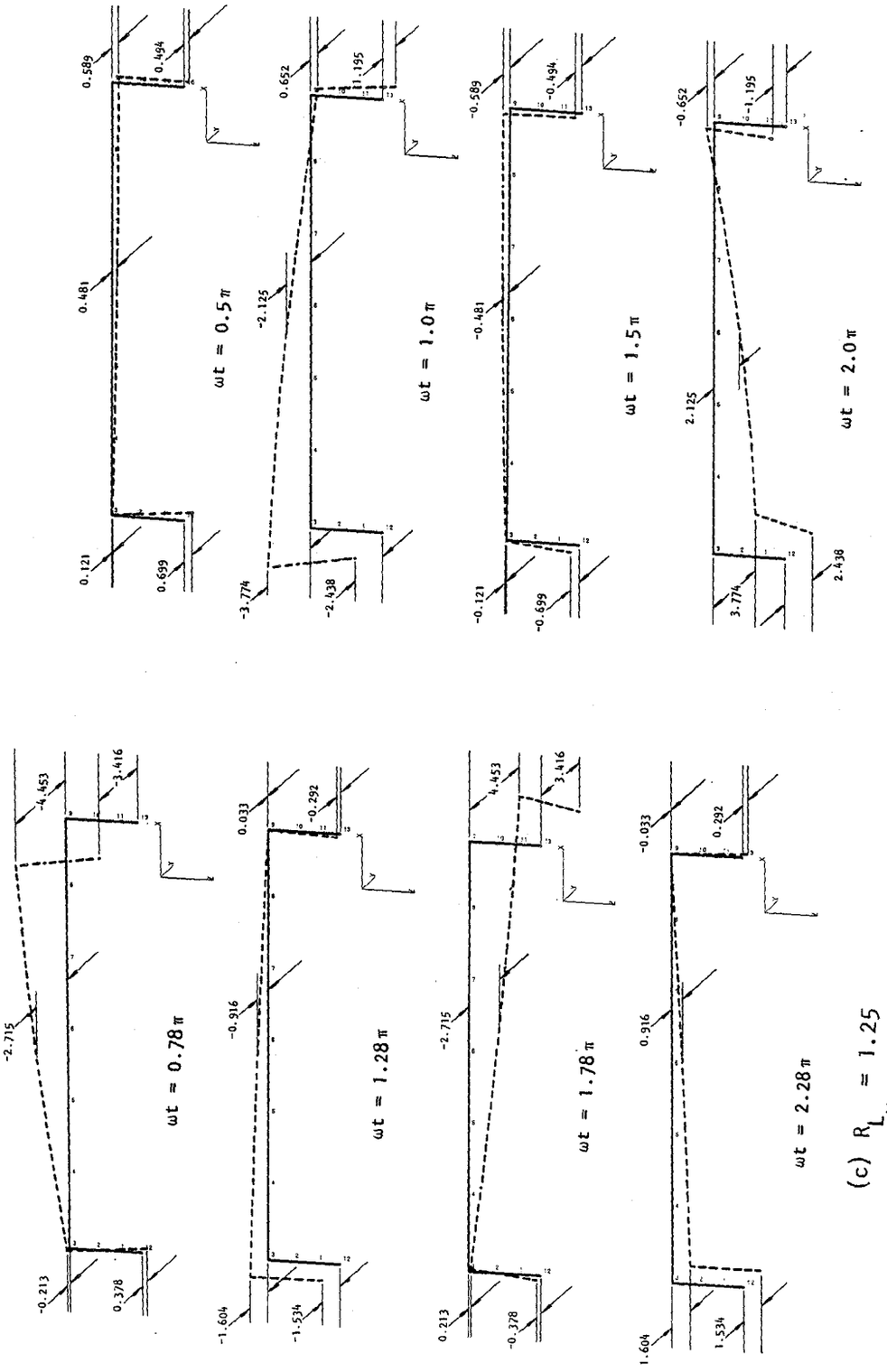

FIGURE 4-9. (CONCLUDED)

- At certain times during the steady-state response, this center of rotation is located at or near the upstream end wall; at such times, the displacement of the upstream end wall is quite small, while the displacement of the downstream wall attains its maximum value. At subsequent times, the center of rotation shifts toward the downstream end wall, resulting in successively increasing displacements of the upstream wall and successively decreasing displacements of the downstream wall. When the center of rotation reaches the downstream wall, its displacements are minimized and those of the upstream wall are maximized. The steady-state response cycle is completed as the center of rotation shifts back toward the upstream end wall.

- Such behavior, in which one end wall reaches its maximum displacement while the other end wall reaches its minimum displacement, is called a "whipping response."

- At low excitation frequencies (for example, $R_{L_X} = 0.25$), the whipping response is characterized almost entirely by rigid-body rotations of the road deck about the z-axis and essentially pure translations of each end wall in the y-direction. Also, the peak displacement amplitudes of each end wall are nearly equal to each other and to those of the incident wave; the phase angles, however, are different (Table 4-3).

- At higher excitation frequencies ($R_{L_X} = 1.25, 1.75$), certain aspects of these response characteristics are modified. First, bending deformations in the plane of the road deck are more significant. Also, the end walls exhibit prominent rocking motions (i.e., rotations about the x-axis) as well as translational motions, and the peak foundation displacements are noticeably larger than are the free-field particle displacements. Finally, the tops of the two end walls have markedly different peak displacements that attain larger values than at the lower frequencies.

4.3.3 RESPONSE TO INCIDENT WAVES WITH θ_V = 45 DEG

When the bridge is subjected to incident SH-waves with θ_H = 0 deg and θ_V = 45 deg, displacements along the y-axis and rotations about the z-axis occur as shown in Figures 4-10a and 4-10b. Amplitudes and phase angles of these response components are tabulated in Table 4-3 and deformed-shape plots are provided in Figure 4-11. These results indicate the following trends:

- The structure response characteristics are generally quite similar to those previously discussed for the case of incident SH-waves with θ_V = 0 deg (Sec. 4.3.2). Antisymmetric, symmetric, and whipping responses of the structure can be observed at discrete excitation frequencies.

- The primary difference between these results and those for θ_V = 0 deg is the particular values of the excitation frequencies at which the above-indicated responses occur. When θ_V = 45 deg, the antisymmetric, symmetric, and whipping modes of response occur at frequencies that are increased by a factor of about $\sqrt{2}$ over the corresponding frequencies at which these responses occur when θ_V = 0 deg (Table 4-3, Fig. 4-10).

- The above frequency shift can be attributed to the change in the apparent wavelength, as discussed in Section 4.2. To illustrate, it was shown in Section 4.3.2.1 that, when θ_V = 0 deg, antisymmetric response first occurs when

$$R_{L_x} = \frac{\ell}{\lambda} = 0.5 \qquad (4\text{-}3a)$$

or when

$$\ell = 0.5\lambda \qquad (4\text{-}3b)$$

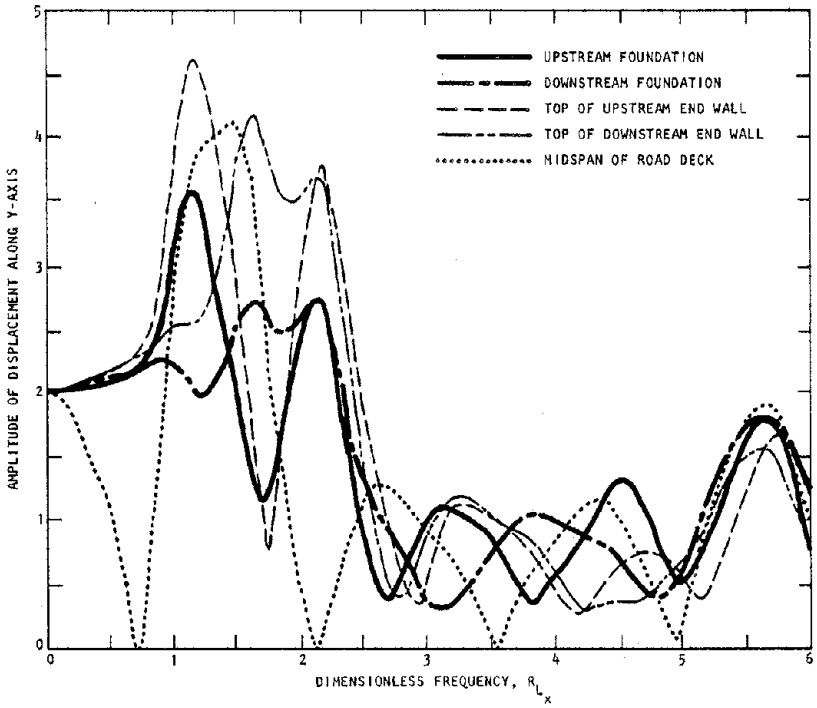

(a) Displacement along y-axis

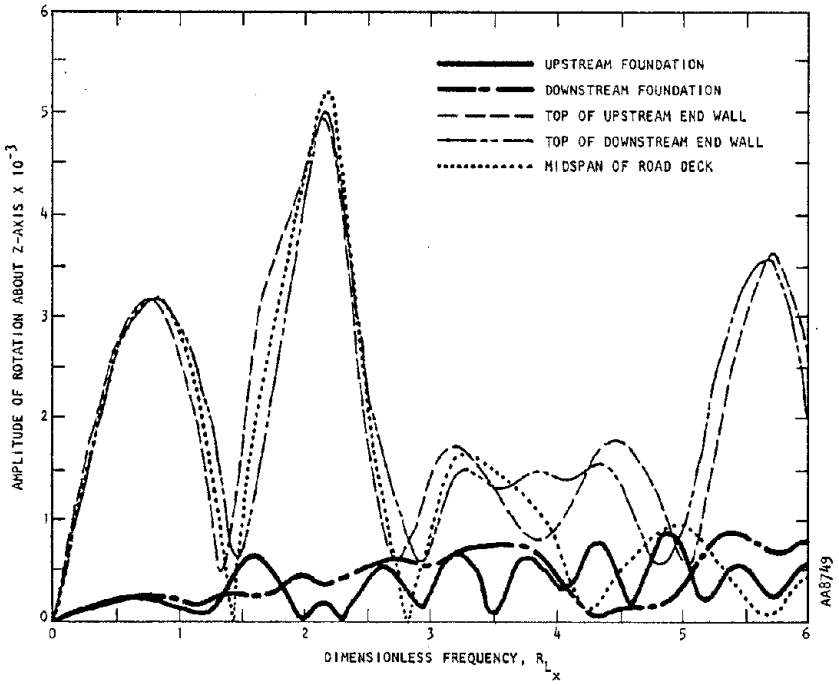

(b) Rotation about z-axis

FIGURE 4-10. FREQUENCY-DEPENDENT RESPONSE AMPLITUDES OF BRIDGE SUBJECTED TO INCIDENT SH-WAVES WITH θ_H = 0 DEG, θ_V = 45 DEG

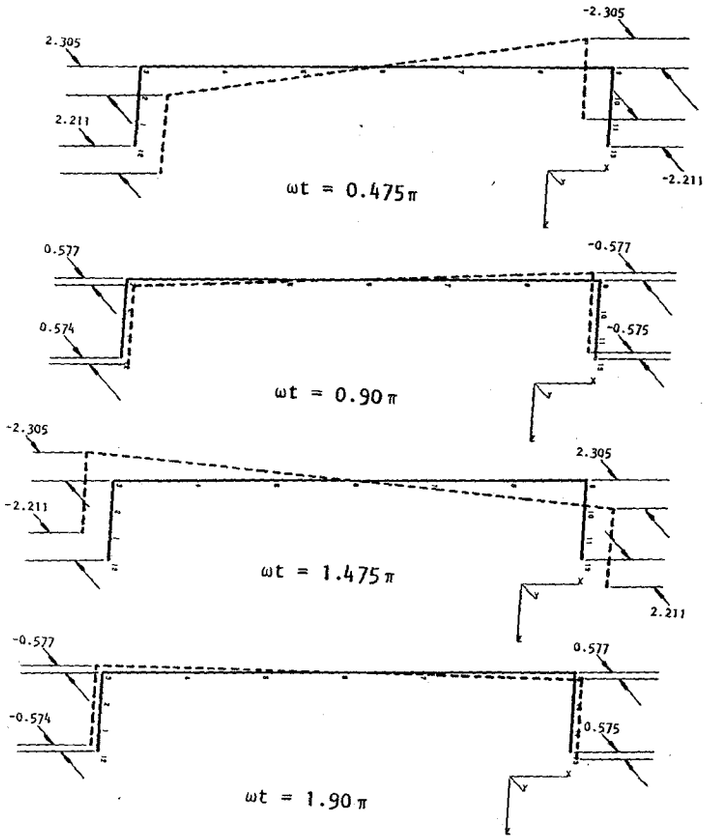

(a) Antisymmetric response at $R_{L_x} = 0.707\ (0.5\sqrt{2})$

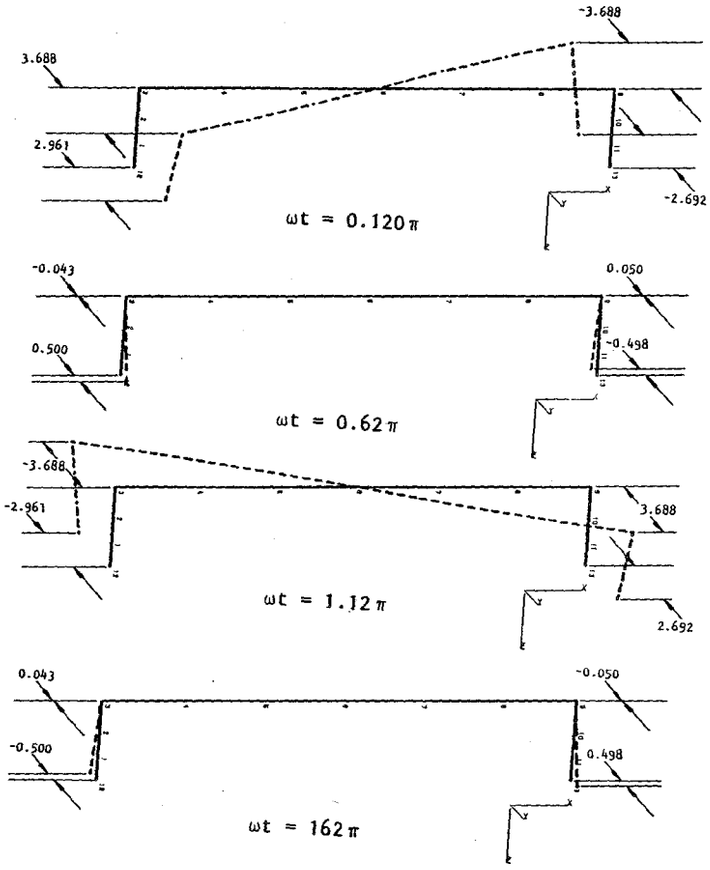

(b) Antisymmetric response at $R_{L_x} = 2.124\ (1.50\sqrt{2})$

FIGURE 4-11. DEFORMED SHAPES OF BRIDGE SUBJECTED TO INCIDENT SH-WAVES WITH $\theta_H = 0$ DEG, $\theta_V = 45$ DEG

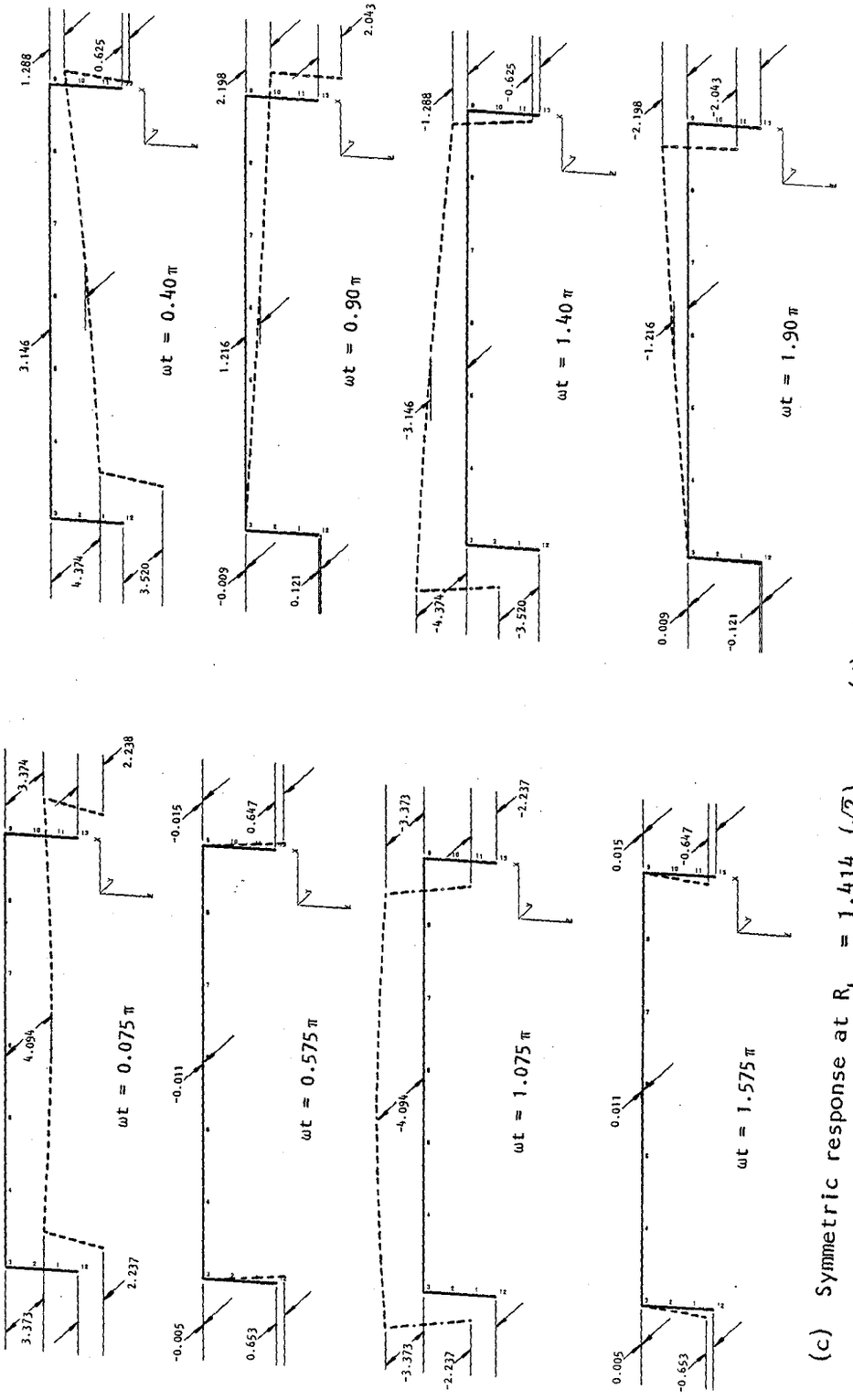

(d) Whipping response at $R_{L_x} = 1.061\ (0.75\sqrt{2})$

(c) Symmetric response at $R_{L_x} = 1.414\ (\sqrt{2})$

FIGURE 4-11. (CONCLUDED)

where ℓ is the span length, and λ is the wavelength of the incident wave. Now, when $\theta_V = 0$ deg, the wavelength along the ray path, λ, is identical to the apparent surface wavelength, λ_a (see Eq. 4-2). For other values of θ_V, Equations 4-3a and 4-3b can be generalized by replacing λ with λ_a, i.e.,

$$\ell = 0.5\lambda_a \tag{4-3c}$$

Substituting Equation 4-2 into Equation 4-3c yields

$$\ell = 0.5\frac{\lambda}{\cos \theta_V} \tag{4-3d}$$

Next it may be recalled that R_{L_x} is defined in terms of the actual wavelength, λ, rather than the apparent wavelength, λ_a. Therefore, Equation 4-3d indicates that for $\theta_V = 0$ deg, ($\cos \theta_V = 1.0$), antisymmetric response occurs when

$$R_{L_x} = \frac{\ell}{\lambda} = 0.5 \tag{4-3e}$$

whereas, when $\theta_V = 45$ deg ($\cos \theta_V = \frac{1}{\sqrt{2}}$), this response occurs when

$$R_{L_x} = 0.5\sqrt{2} \tag{4-3f}$$

- These results show that for $\theta_V = 45$ deg, the excitation frequency at which antisymmetric response first occurs is increased by a factor of $\sqrt{2}$. The same factor can be applied to the other frequencies at which antisymmetric, symmetric, and whipping response occurred when $\theta_V = 0$ deg, to determine the corresponding frequencies for $\theta_V = 45$ deg.

4.4 RESULTS FOR INCIDENT SH-WAVES WITH θ_H = 90 DEG

The second set of results corresponds to incident SH-waves that propagate in a plane parallel to the y-z plane of the bridge and apply particle motions directed along the x-axis (i.e., θ_H = 90 deg, as shown in Fig. 4-1a). Since these motions are applied to the foundation/soil system along the 70-ft length of each foundation, this length defines the dimensionless frequency parameter, R_{L_y}, used in presenting the frequency-dependent response results for this case (see Table 4-2).

There are two ways in which this case differs from the θ_H = 0 deg condition previously described in Section 4.3. First, the dynamic loads may no longer be thought of as discrete point loads applied at the ends of the bridge span; instead they correspond to loads that are continuously distributed along a large foundation dimension (Sec. 4.4.1). Second, the bridge will be more flexible when subjected to inertial loads oriented along the x-axis--the direction of the particle motions applied by the incident waves for this case.

4.4.1 DYNAMIC LOADS

Prior to assessing the response of the bridge to incident SH-waves with θ_H = 90 deg, it is instructive to first consider the nature of the dynamic loads applied by such waves. These loads, depicted in Figure 4-12, are applied along the length of the foundation with a nonuniform load distribution that is changing with time as the wave propagates.

The nonuniform loads can be considered to be comprised of various combinations of symmetric components (with respect to the x-axis) and antisymmetric components, as shown in Figure 4-12.* The nature of these load components is as follows:

- The symmetric load components with half-wavelengths comparable to or longer than the foundation length will result in significant

*This can be visualized as a Fourier series decomposition of the nonuniform load distribution into even (symmetric) components and odd (antisymmetric) components.

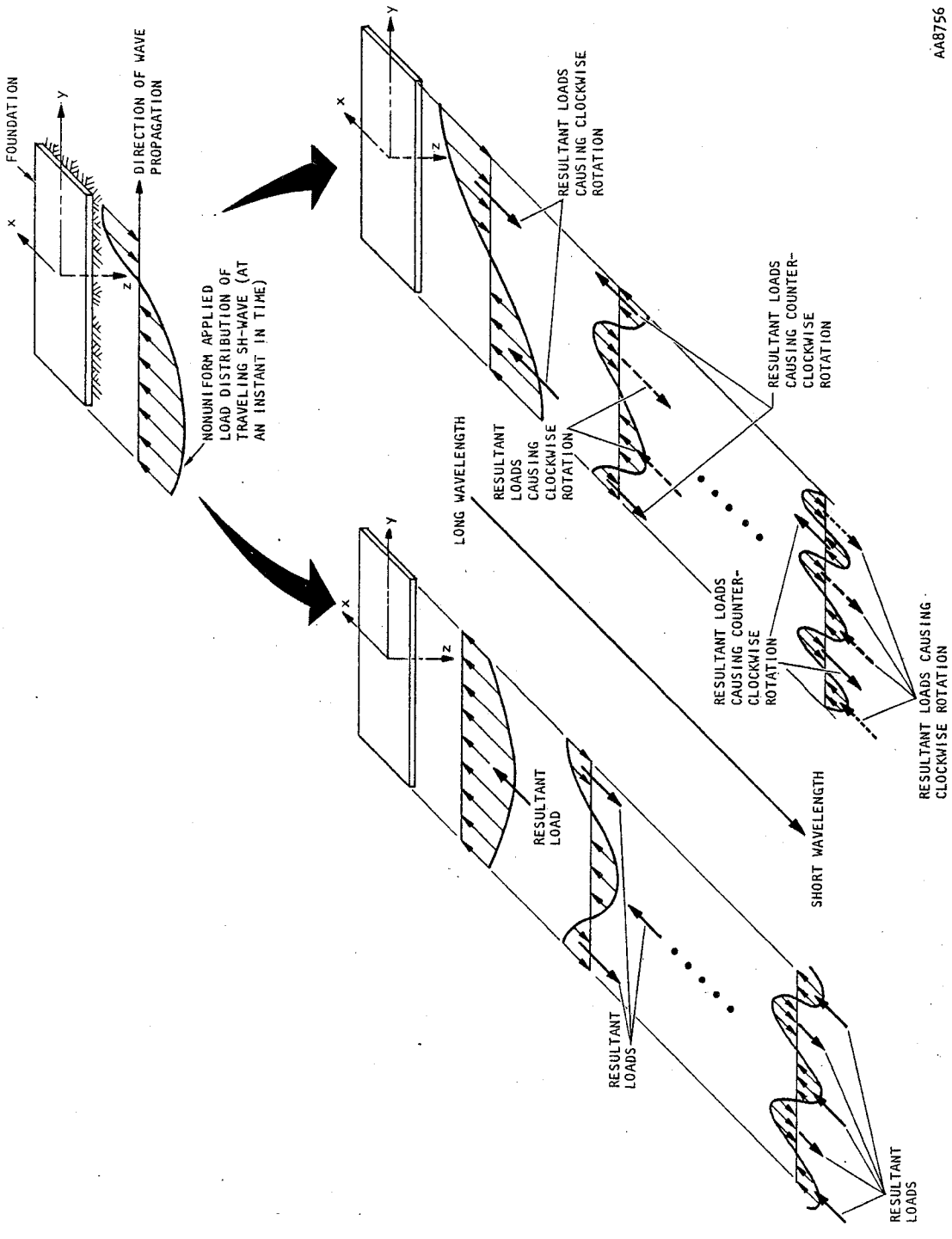

(a) Symmetric load components (b) Antisymmetric load components

FIGURE 4-12. DECOMPOSITION OF NONUNIFORM LOAD DISTRIBUTION INTO SYMMETRIC AND ANTISYMMETRIC COMPONENTS

net loads that will tend to drive the foundation horizontally in the x-direction (Fig. 4-12a).

- The symmetric load components whose wavelengths are short compared to the foundation length will not be as effective in driving the structure horizontally. This is because such loadings are self-equilibrating; i.e., they include both positive and negative load components that tend to cancel one another and reduce the net load applied to the foundation (Fig. 4-12a).

- The antisymmetric load components with wavelengths roughly comparable to the foundation length will tend to rotate the foundation about its z-axis (Fig. 4-12b).

- The antisymmetric load components with wavelengths that are short compared to the foundation length will have a reduced ability to rotate the foundation. This is because such loadings induce several sets of resultant forces whose moments tends to cancel one another (Fig. 4-12b).

The above discussion pertains to nonvertically incident SH-waves for which traveling wave effects are present. Loads applied to the foundation by vertically incident waves are considerably simpler, because such waves have infinite apparent wavelengths; therefore motions applied at all points along the foundations are identical in amplitude and phase. Since the resulting loads are uniform and for $\theta_H = 90$ deg are symmetric about the x-axis, they do not induce any antisymmetric load components for symmetric foundations. Therefore, vertically incident SH-waves with $\theta_H = 90$ deg will excite the foundation horizontally but will not induce any rotations about the z-axis.

4.4.2 STRUCTURE RESPONSE CHARACTERISTICS

The components of the structure response discussed below for this case are the displacements along the x-axis and the rotations about the z-axis. These results are presented for θ_V = 0 deg, 45 deg, and 90 deg in tabulated form (Table 4-4) and in the form of frequency-dependent amplitude curves (Figs. 4-13, 4-14, and 4-15, respectively). Deformed-shape plots for θ_V = 0 deg and 90 deg are also presented (Fig. 4-16).

4.4.2.1 Rotations about the z-Axis when θ_H = 90 Deg and θ_V = 0, 45, and 90 Deg

- When θ_V = 0 deg and 45 deg, the foundations exhibit rotations about the z-axis that are much greater than those of the road deck (Figs. 4-13b, 4-14b; Table 4-4). This indicates that the traveling SH-waves are causing large torsional deformations in the end walls.

- The amplitudes of the foundation rotations are greatest at lower frequencies (Figs. 4-13b, 4-14b; Table 4-4). These low-frequency amplitudes are induced by antisymmetric components of the nonuniformly distributed foundation loading. At higher frequencies (i.e., shorter wavelengths), the rotation amplitudes are limited by the self-equilibrating characteristics of the foundation loading (Sec. 4.4.1).

- The peak amplitudes of these rotations are about the same for θ_V = 0 deg and θ_V = 45 deg, although the peaks extend over a frequency range that is about 40% wider when θ_V = 45 deg (Figs. 4-13b, 4-14b; Table 4-4). This wider frequency range is attributable to apparent wavelength effects discussed earlier (Sec. 4.3.3).

TABLE 4-4. AMPLITUDES AND PHASE ANGLES OF BRIDGE RESPONSE TO INCIDENT SH-WAVES WITH θ_H = 90 DEG

Description of Predominant Response	Dimensionless Frequency, R_{L_y}	Angle of Incidence, θ_V, deg	Component of Response	Foundations		Tops of End Walls		Midspan of Road Deck	
				Amplitude	Phase Angle, rad	Amplitude	Phase Angle, rad	Amplitude	Phase Angle, rad
Sidesway of bridge	0.412	0	Displacement along x-axis	3.788	0.762π	18.667	0.758π	18.773	0.758π
			Rotation about z-axis	4.640×10^{-3}	-0.497π	0.149×10^{-3}	-0.589π	0.125×10^{-3}	-0.608π
		45	Displacement along x-axis	4.568	0.758π	22.541	0.755π	22.670	0.755π
			Rotation about z-axis	3.608×10^{-3}	-0.497π	0.116×10^{-3}	-0.589π	0.010×10^{-3}	-0.608π
		90	Displacement along x-axis	5.425	0.756π	26.797	0.753π	26.950	0.753π
			Rotation about z-axis	0.0	--	0.0	--	0.0	--
Peak rotation of foundations about z-axis	0.613	0	Rotation about z-axis	5.368×10^{-3}	-0.491π	0.169×10^{-3}	-0.618π	0.143×10^{-3}	-0.644π
	0.947	45	Rotation about z-axis	5.414×10^{-3}	-0.478π	0.172×10^{-3}	-0.841π	0.166×10^{-3}	-0.896π
	--	90	Rotation about z-axis	0.0	--	0.0	--	0.0	--

Note: Incident wave motions defined to have a surface amplitude of 2.0 and a zero phase angle at the upstream foundation, which is the origin of the coordinate system for this analysis.

AA8770
R-7720-4514

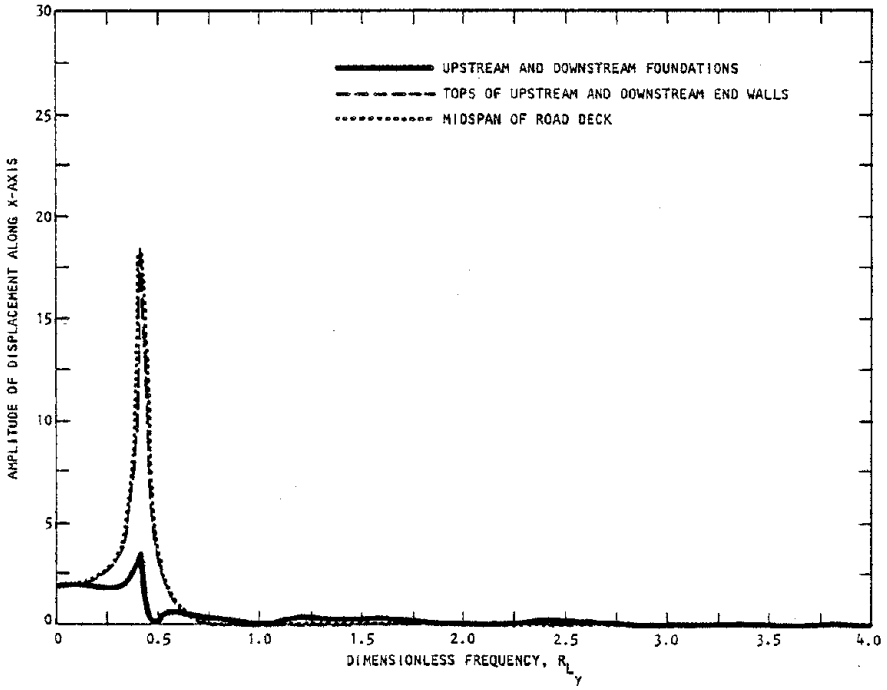

(a) Displacement along x-axis

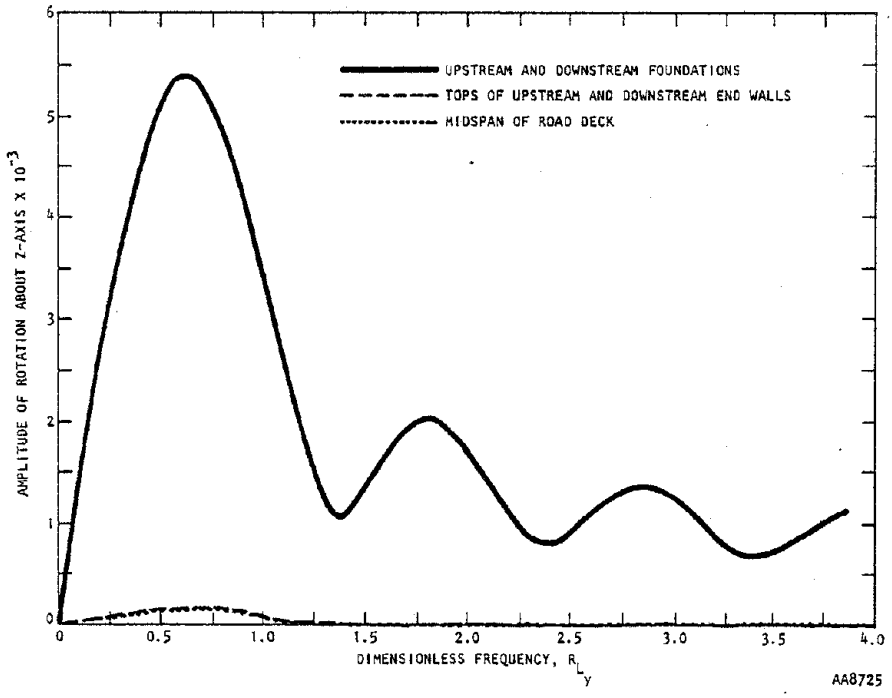

(b) Rotation about z-axis

FIGURE 4-13. FREQUENCY-DEPENDENT RESPONSE AMPLITUDES OF BRIDGE SUBJECTED TO INCIDENT SH-WAVES WITH θ_H = 90 DEG, θ_V = 0 DEG

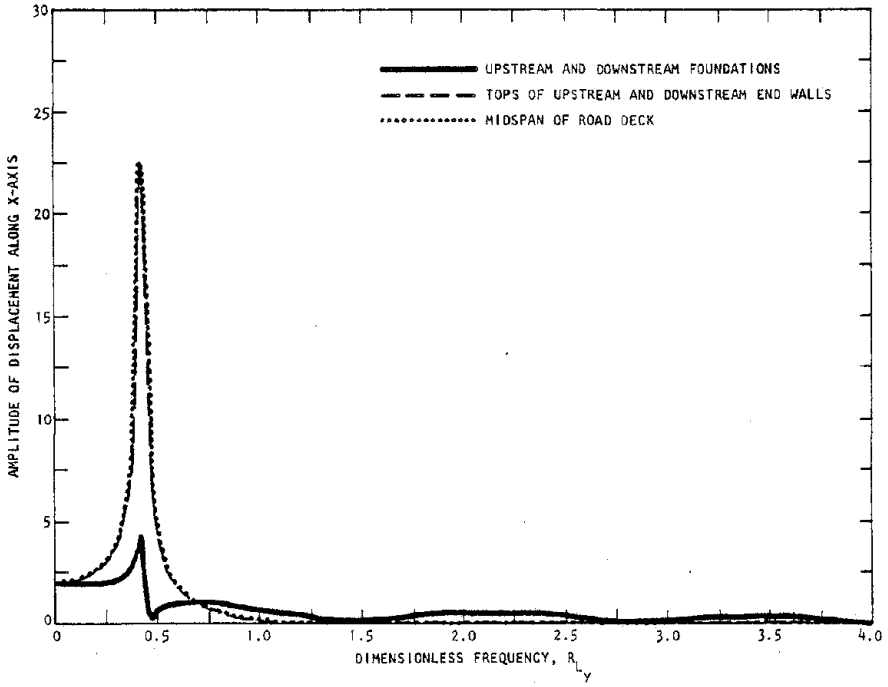

(a) Displacement along x-axis

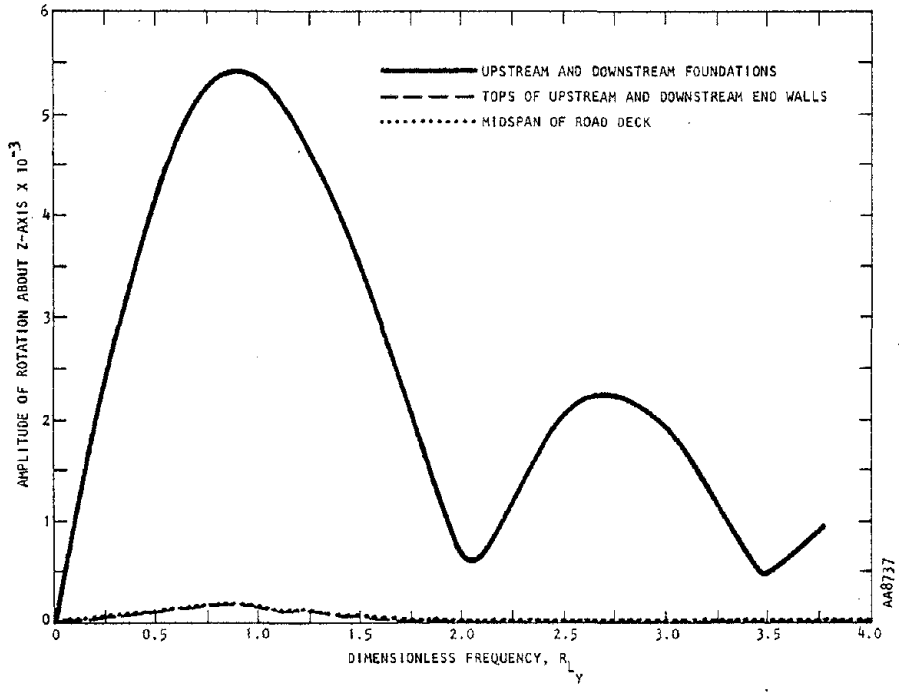

(b) Rotation about z-axis

FIGURE 4-14. FREQUENCY-DEPENDENT RESPONSE AMPLITUDES OF BRIDGE SUBJECTED TO INCIDENT SH-WAVES WITH θ_H = 90 DEG, θ_V = 45 DEG

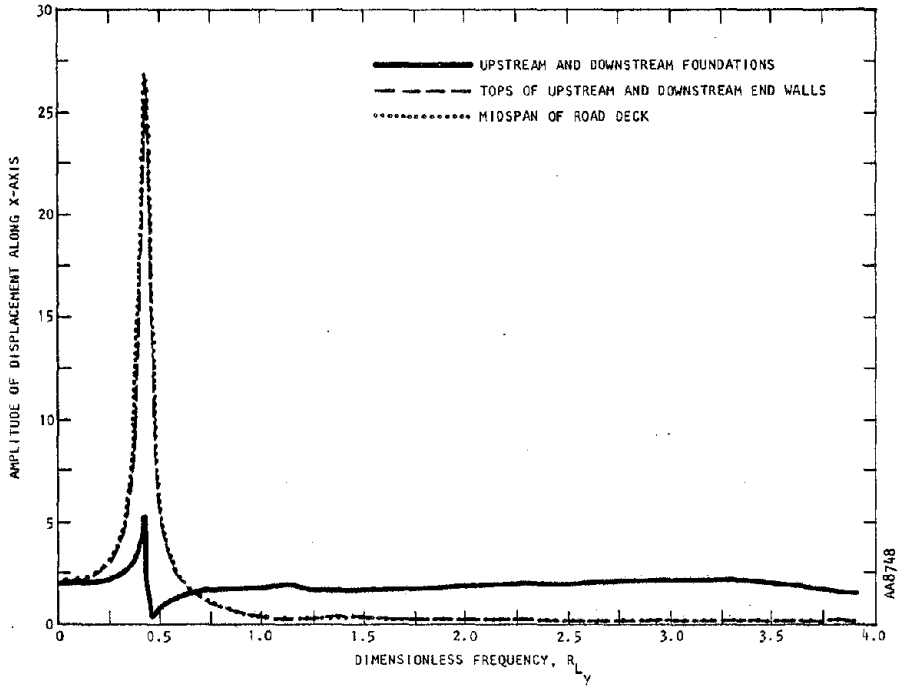

(a) Displacement along x-axis

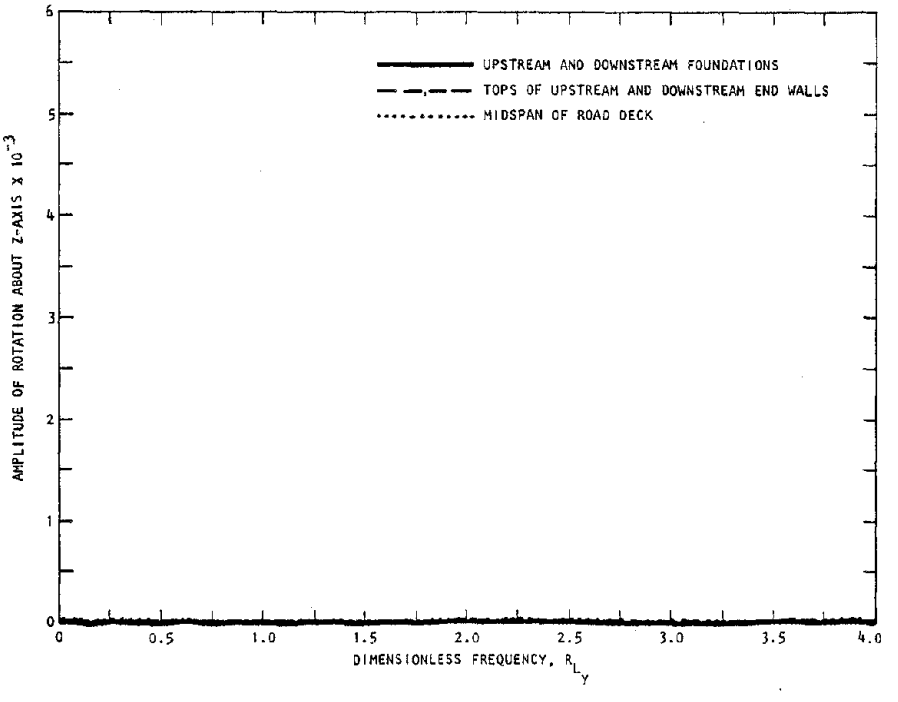

(b) Rotation about z-axis

FIGURE 4-15. FREQUENCY-DEPENDENT RESPONSE AMPLITUDES OF BRIDGE SUBJECTED TO INCIDENT SH-WAVES WITH θ_H = 90 DEG, θ_V = 90 DEG

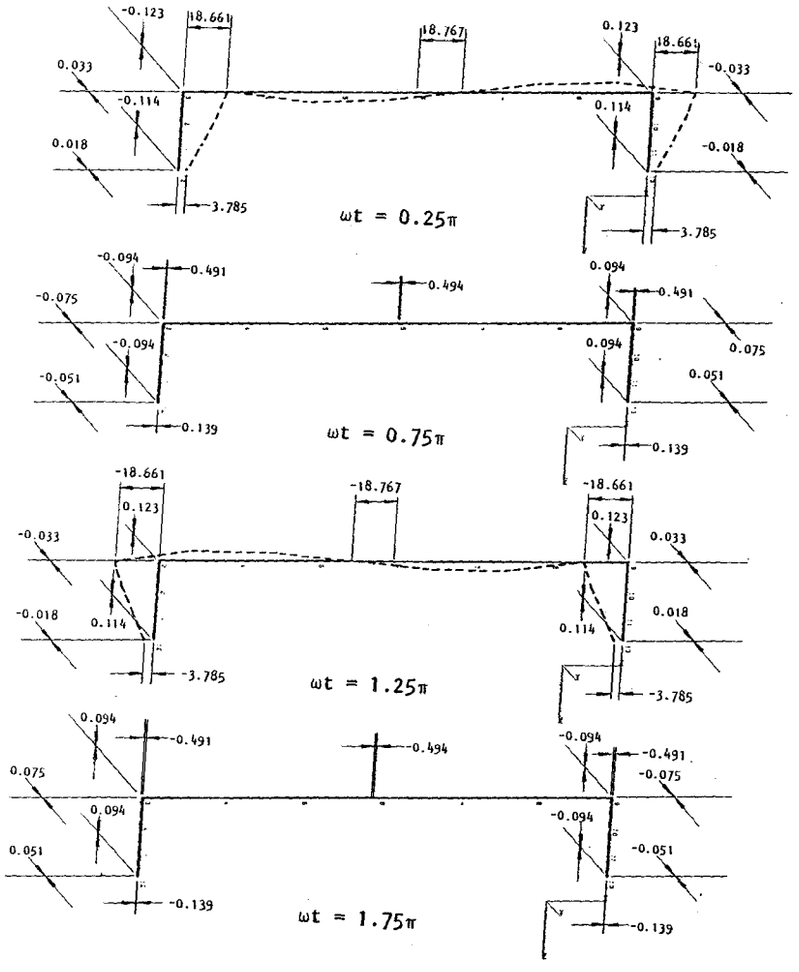

(a) θ_V = 0 DEG

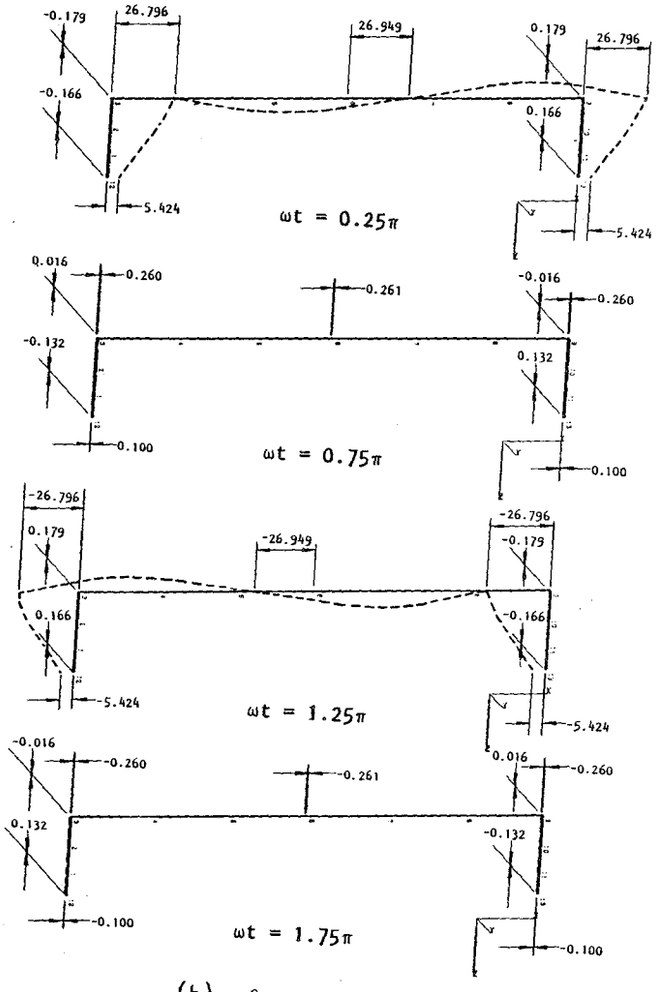

(b) θ_V = 90 DEG

FIGURE 4-16. DEFORMED SHAPES OF BRIDGE SUBJECTED TO INCIDENT SH-WAVES WITH θ_H = 90 DEG, θ_V = 0 DEG AND 90 DEG (R_{L_y} = 0.412)

- No rotations about the z-axis are induced when vertically incident SH-waves (θ_V = 90 deg) are applied (Fig. 4-15b). This is because such waves produce only uniformly distributed foundation loads that cannot rotate the foundation (Sec. 4.4.1).

4.4.2.2 Displacements along the x-Axis when θ_H = 90 Deg and θ_V = 0, 45, and 90 Deg

- Displacement curves for all three θ_V values exhibit significant amplification of the road-deck displacement relative to that of the foundations. This amplification occurs only within a single narrow-banded frequency range. It is quite large, ranging from about 18.7 (for θ_V = 0 deg) to nearly 27.0 (when θ_V = 90 deg) (Table 4-4).

- These amplifications and the deformed shape plots of the structure indicate sidesway bending deformations in the end wall, together with rigid body rotations of the foundations and end walls that will be important because of the underlying soft soil medium (Fig. 4-16).

- The frequency at which these large displacement amplifications occur is independent of θ_V; i.e., for all three θ_V angles considered, the peak is centered about a dimensionless frequency defined by R_{L_y} = 0.412, which corresponds to an excitation frequency of 2.94 Hz. Furthermore, the deformed shape of the structure response is also essentially independent of θ_V.

- The above result indicates that the structure response at R_{L_y} = 0.412 is not influenced much by traveling wave effects. Rather, it is dominated by a resonance condition caused by application of symmetric load components (Fig. 4-12) with excitation frequencies identical to the natural frequency of the first sidesway mode of the soil/structure system.

- The sidesway motions exhibited by the deformed shapes shown in Figure 4-16 are similar to those of Mode 2 of the in-plane fixed-base structure modes shown in Figure 4-2a. However, the frequency of Mode 2 (5.1 Hz) is much higher than the resonant frequency for the present case (2.94 Hz, which corresponds to $R_{L_y} = 0.412$). This indicates that the soft soil medium, which is incorporated in the present case, has a significant effect in reducing the frequency of this sidesway mode of vibration.

- The resonant frequency displacement amplitudes at $R_{L_y} = 0.412$ are seen to increase as θ_V varies from 0 deg to 45 deg to 90 deg (Table 4-4). This can be attributed to the increase in apparent wavelength of the incident waves that results when θ_V is increased. The longer apparent wavelengths result in foundation loadings that are more nearly uniformly distributed across the length of the foundation. Such loadings will have the greatest tendency to drive the structure horizontally (causing the largest displacements in the x-direction) and the least tendency to rotate the foundation about its z-axis. This trend is clearly evident in Table 4-4.

4.5 RESULTS FOR INCIDENT SH-WAVES WITH $\theta_H = 45$ DEG

The final set of results corresponds to incident SH-waves that (1) propagate in a vertical plane oriented at 45 deg from the x-z plane; and (2) apply particle motions directed at 45 deg from the positive y-axis ($\theta_H = 45$ deg, as shown in Fig. 4-1a). This case is significant because, unlike the results already presented for $\theta_H = 0$ deg and 90 deg, the resultant particle motions are not directed along either of the principal axes of the structure. Therefore, the results for $\theta_H = 45$ deg can be used to evaluate the extent to which three-dimensional coupling effects influence the bridge response characteristics. These results are expressed in terms of both dimensionless frequency parameters, R_{L_x} and R_{L_y}, which are defined in Table 4-2.

4.5.1 RESPONSE TO INCIDENT WAVES WITH θ_V = 90 DEG

The response of the bridge to SH-waves with θ_H = 45 deg and θ_V = 90 deg is presented in terms of displacements along the x-, y-, and z-axes and rotations about the z-axis only. Amplitudes and phase angles of these response components are tabulated in Table 4-5, and the amplitudes are plotted vs. R_{L_X} and R_{L_Y} in Figure 4-17. Deformed shape plots of the structure response are provided in Figure 4-18. These results are summarized below for the various response components.

4.5.1.1 Displacements along the x-Axis when θ_H = 45 Deg and θ_V = 90 Deg

- The bridge response to vertically incident waves is dominated by displacements of the road deck along the x-axis that are very large in comparison to the corresponding foundation displacements. These amplified sidesway motions occur over a very narrow frequency range centered about R_{L_Y} = 0.423. The peak amplitudes of these displacements reach values that exceed 25.0 at the various structure reference points along the road deck (Fig. 4-17a, Table 4-5).

- The above behavior is very similar to that induced by vertically incident waves with θ_H = 90 deg. In fact, the peak amplitudes of the displacements and the frequency at which they occur are nearly identical for these two cases (Fig. 4-15a, Table 4-4).

4.5.1.2 Displacements along the z-Axis when θ_H = 45 Deg and θ_V = 90 Deg

- The displacements along the z-axis are small compared to the x- and y-displacements and are not significant for this case (Fig. 4-17b, Table 4-5).

TABLE 4-5. AMPLITUDES AND PHASE ANGLES OF BRIDGE RESPONSE TO INCIDENT SH-WAVES WITH θ_H = 45 DEG

Angle of Incidence, θ_V, deg	Description of Predominant Response	Dimensionless Frequency		Component of Response	Upstream Foundation		Downstream Foundation		Top of Upstream End Wall		Top of Downstream End Wall		Midspan of Road Deck	
		R_{L_x}	R_{L_y}		Amplitude	Phase Angle Rad	Amplitude	Phase Angle Rad	Amplitude	Phase Angle Rad	Amplitude	Phase Angle Rad	Amplitude	Phase Angle Rad
90	Sidesway of bridge	0.726	0.423	Displacement along x-axis	4.011	-0.480π	4.011	-0.480π	25.268	-0.485π	25.268	-0.485π	25.421	-0.485π
	Peak displacement of bridge along y-axis	1.061	0.619	Displacement along y-axis	2.349	-0.197π	2.349	-0.197π	3.050	-0.233π	3.050	-0.233π	3.390	-0.223π
	Bending of road deck in x-y plane and maximum torsion of end walls	5.657	3.300	Displacement along y-axis	1.467	-0.230π	1.467	-0.230π	1.287	-0.192π	1.287	-0.192π	1.561	0.808π
				Rotation about z-axis	0.196×10^{-3}	0.511π	0.196×10^{-3}	0.511π	2.952×10^{-3}	0.808π	2.952×10^{-3}	0.808π	~0	--
0	Vertical displacement of road deck	0.687	0.401	Displacement along z-axis	1.356	0.274π	1.271	0.278π	1.387	0.277π	1.302	0.281π	21.950	0.400π
				Displacement along x-axis	1.112	-0.448π	0.934	0.597π	0.368	-0.667π	0.613	0.646π	0.493	-0.654π
				Rotation about y-axis	9.468×10^{-3}	0.319π	6.374×10^{-3}	-0.693π	30.573×10^{-3}	-0.582π	32.114×10^{-3}	0.414π	0.319×10^{-3}	-0.623π
	Peak rotation of road deck about z-axis	0.657	0.383	Displacement along y-axis	1.328	-0.016π	1.331	-0.937π	1.368	-0.020π	1.374	-0.937π	0.198	-0.483π
				Rotation about z-axis	2.452×10^{-3}	-0.515π	2.495×10^{-3}	0.588π	1.871×10^{-3}	-0.972π	1.873×10^{-3}	-0.984π	1.887×10^{-3}	-0.978π
	Peak rotation of foundations about z-axis	1.414	0.825	Rotation about z-axis	3.853×10^{-3}	-0.481π	3.792×10^{-3}	-0.492π	0.336×10^{-3}	-0.501π	0.227×10^{-3}	0.832π	0.137×10^{-3}	-0.768π
45	Sidesway of bridge	0.726	0.423	Displacement along z-axis	0.683	0.190π	0.482	0.102π	0.701	0.191π	0.489	0.107π	8.399	0.303π
				Displacement along x-axis	1.045	-0.823π	2.022	-0.855π	9.620	-0.849π	9.733	-0.847π	9.735	-0.848π
				Rotation about y-axis	39.700×10^{-3}	0.164π	28.100×10^{-3}	0.130π	9.801×10^{-3}	-0.049π	26.660×10^{-3}	0.217π	8.497×10^{-3}	-0.855π
	Vertical displacement of road deck	0.687	0.401	Displacement along z-axis	1.298	0.422π	1.201	0.413π	1.330	0.425π	1.228	0.416π	20.931	0.456π
				Displacement along x-axis	2.198	-0.398π	0.793	-0.749π	5.306	-0.487π	5.541	-0.486π	5.453	-0.486π
				Rotation about y-axis	24.500×10^{-3}	0.496π	9.720×10^{-3}	0.555π	21.610×10^{-3}	-0.421π	38.272×10^{-3}	0.551π	4.209×10^{-3}	-0.487π
	Peak rotation of road deck about z-axis	0.974	0.568	Displacement along y-axis	1.387	-0.034π	1.444	-0.998π	1.477	-0.045π	1.557	-0.997π	0.128	-0.630π
				Rotation about z-axis	2.514×10^{-3}	-0.511π	2.593×10^{-3}	0.546π	2.079×10^{-3}	0.983π	2.078×10^{-3}	0.970π	2.106×10^{-3}	0.976π
	Peak rotation of foundation about z-axis	2.223	1.297	Rotation about z-axis	3.988×10^{-3}	-0.472π	3.982×10^{-3}	-0.700π	0.649×10^{-3}	-0.941π	0.477×10^{-3}	0.877π	0.564×10^{-3}	0.970π

Note: Incident wave motions defined to have a surface amplitude of 2.0 and a zero phase angle at the upstream foundation, which is the origin of the coordinate system for this analysis.

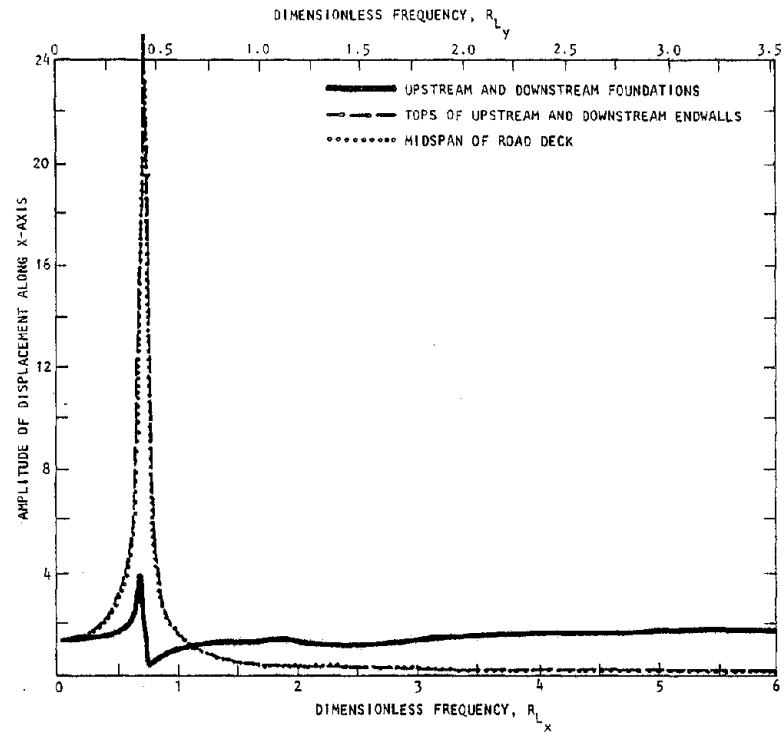

(a) Displacement along x-axis

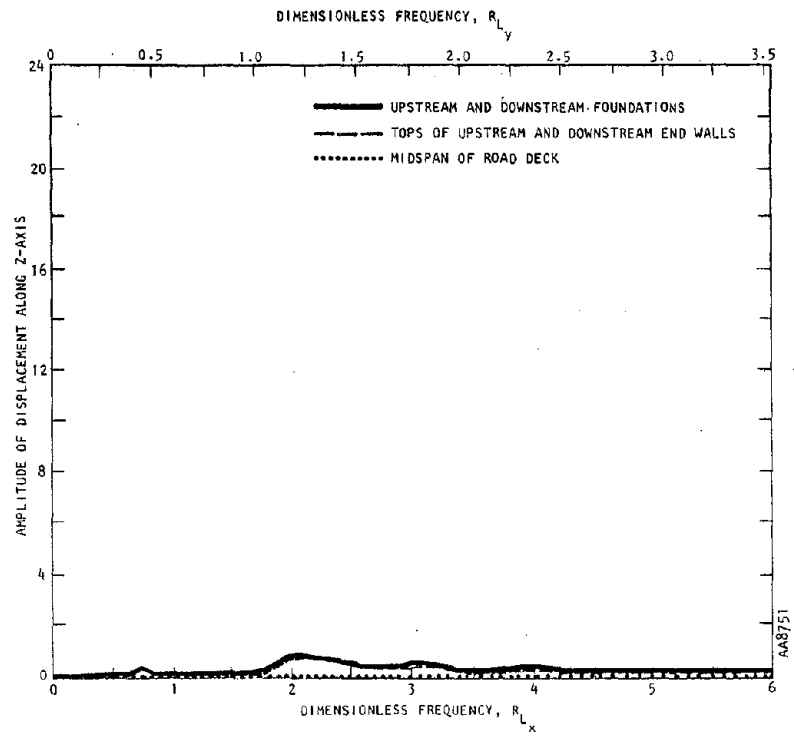

(b) Displacement along z-axis

FIGURE 4-17. FREQUENCY-DEPENDENT RESPONSE AMPLITUDES OF BRIDGE SUBJECTED TO INCIDENT SH-WAVES WITH θ_H = 45 DEG, θ_V = 90 DEG

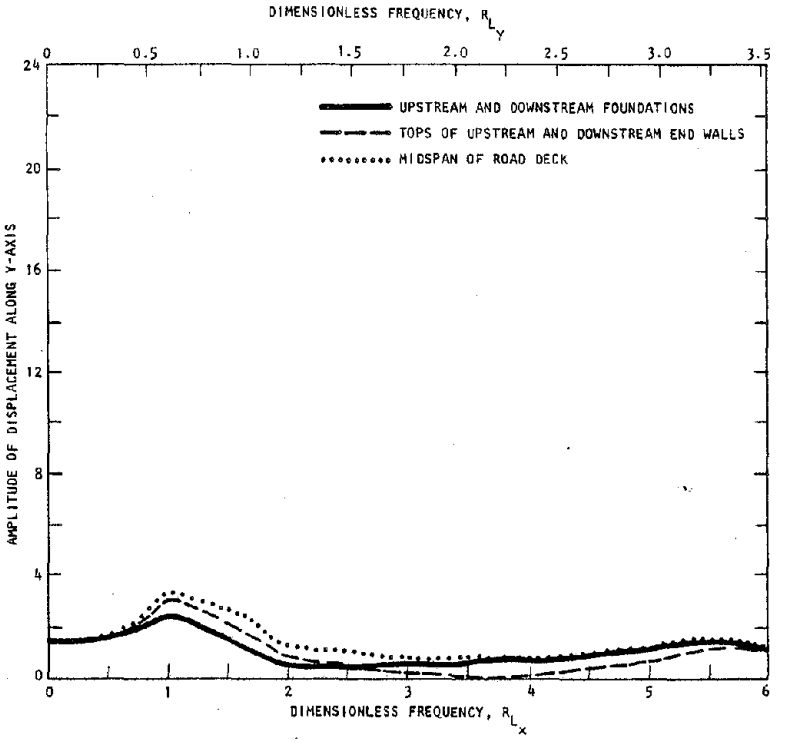

(c) Displacement along y-axis

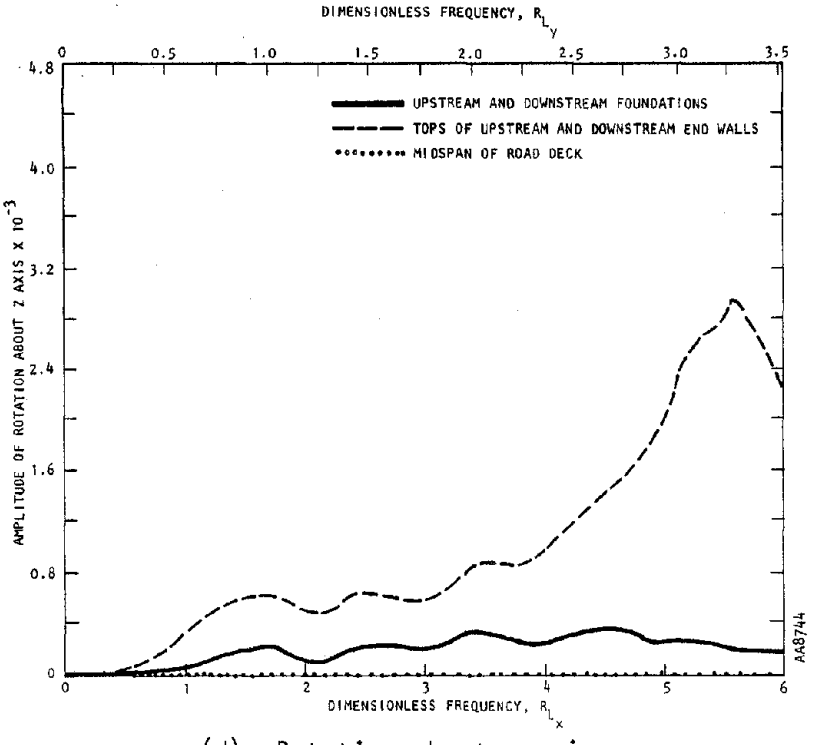

(d) Rotation about z-axis

FIGURE 4-17. (CONTINUED)

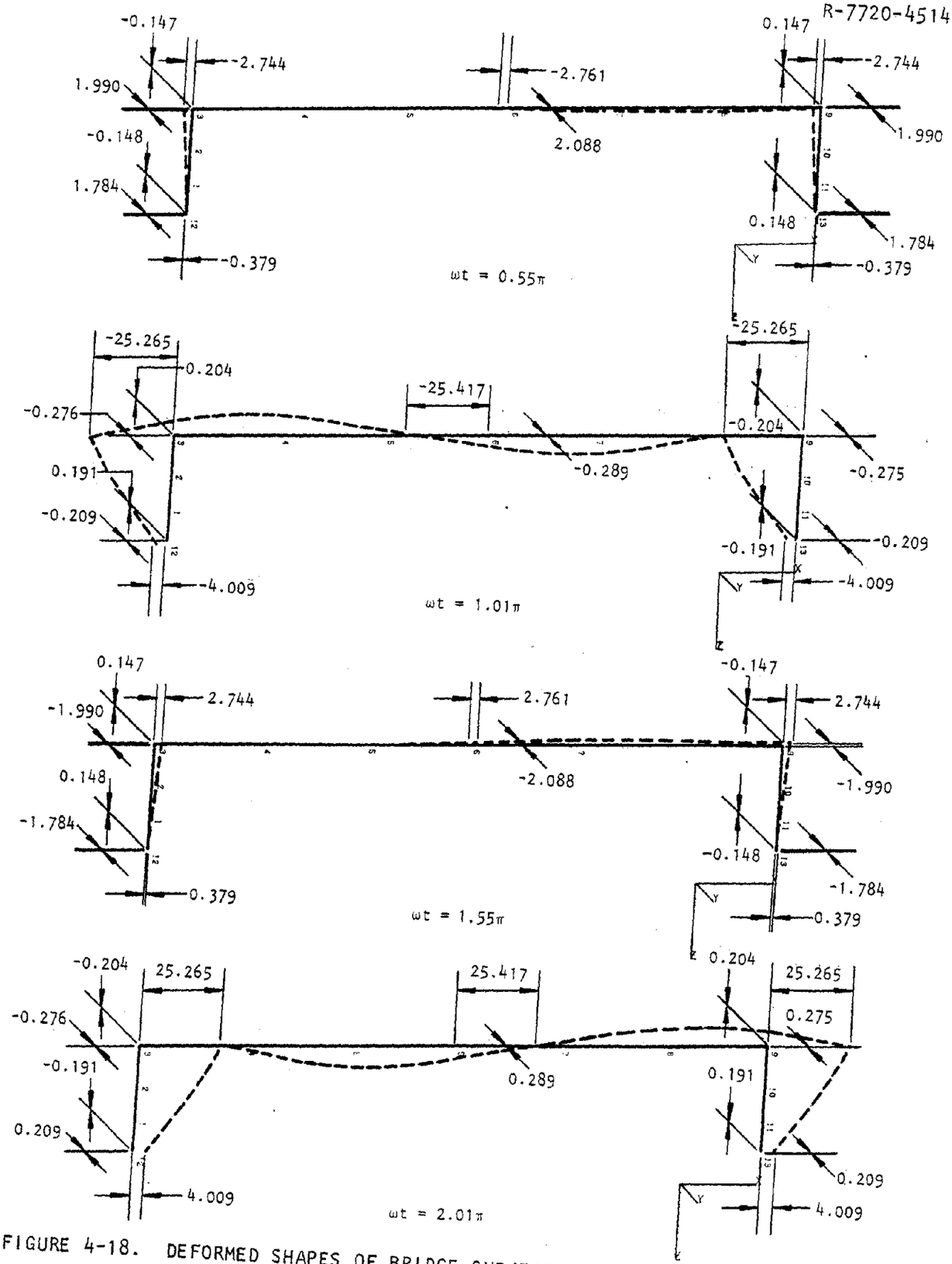

FIGURE 4-18. DEFORMED SHAPES OF BRIDGE SUBJECTED TO INCIDENT SH-WAVES WITH θ_H = 45 DEG, θ_V = 90 DEG (R_{L_x} = 0.423)

4.5.1.3 Displacements along the y-Axis when θ_H = 45 Deg and θ_V = 90 Deg

- The peak displacements along the y-axis are small in comparison to the peak displacements along the x-axis. They are, however, noticeably larger than the y-component of the peak free-field displacement (Fig. 4-17c, Table 4-5).

- The displacement vs. frequency curves exhibit peak amplitudes at R_{L_x} = 1.06 and 5.66 (Fig. 4-17c, Table 4-5). These are quite similar to the frequencies at which displacement peaks are induced by the vertically incident waves with θ_H = 0 deg (Fig. 4-3a, Table 4-3).

- The amplitudes of the peak displacements are about 70% of those resulting from the vertically incident waves with θ_H = 0 deg. This ratio corresponds closely to the ratio between the free-field y-displacement components for θ_H = 45 deg and 0 deg, which is 0.707 (Tables 4-3, 4-5).

4.5.1.4 Rotations about the z-Axis when θ_H = 45 Deg and θ_V = 90 Deg

- Significant rotations of the road deck about the z-axis occur only at higher frequencies (R_{L_x} = 5.66). The corresponding rotations of the foundation are small at all frequencies (Fig. 4-17d). This behavior is similar to that induced by vertically incident waves with θ_H = 0 deg (Fig. 4-3b).

- The amplitudes of the peak rotations are about 70% of those caused by the vertically incident waves with θ_H = 0 deg. Again, this ratio is very similar to the ratio between the free-field y-displacement components for θ_H = 45 deg and 0 deg (Tables 4-3, 4-5).

4.5.2 RESPONSE TO INCIDENT WAVES WITH θ_V = 0 DEG

The general features of the structure response to incident SH-waves with θ_H = 45 deg and θ_V = 0 deg are depicted by plots of frequency-dependent displacements along the x-, y-, and z-axes and rotations about the z-axis (Figs. 4-19a through 4-19d). These figures indicate that significant response components are the vertical displacements along the road deck and the rotations of the road deck and foundations about the z-axis. Amplitudes and phase angles of these response components are shown in Table 4-5. Deformed shape plots of the structure response to these incident waves are presented in Figure 4-20.

4.5.2.1 Vertical Displacements of Road Deck when θ_H = 45 Deg and θ_V = 0 Deg

The most prominent feature of the bridge response for this case is the large vertical displacements of the road deck and its accompanying bending deformations in the x-z plane. The main characteristics of this response are the following:

- The significant amplification of the midspan vertical displacement occurs over a very narrow frequency range centered about R_{L_x} = 0.688. This corresponds to an excitation frequency of 2.86 Hz.

- The amplitudes and phase angles of the vertical displacement at the two ends of the road deck (i.e., at the tops of the two end walls) are nearly identical to one another (Table 4-5). This indicates that the vertical displacements are essentially symmetric about the midspan of the bridge. The symmetry of these displacements is also clearly shown by the deformed-shape plots of the response at this excitation frequency (Fig. 4-20).

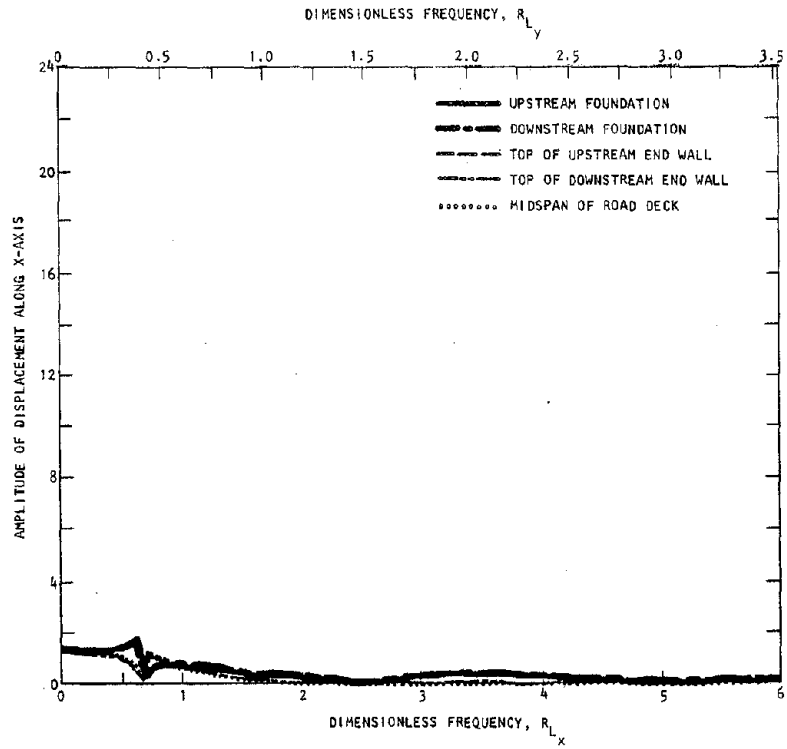

(a) Displacement along x-axis

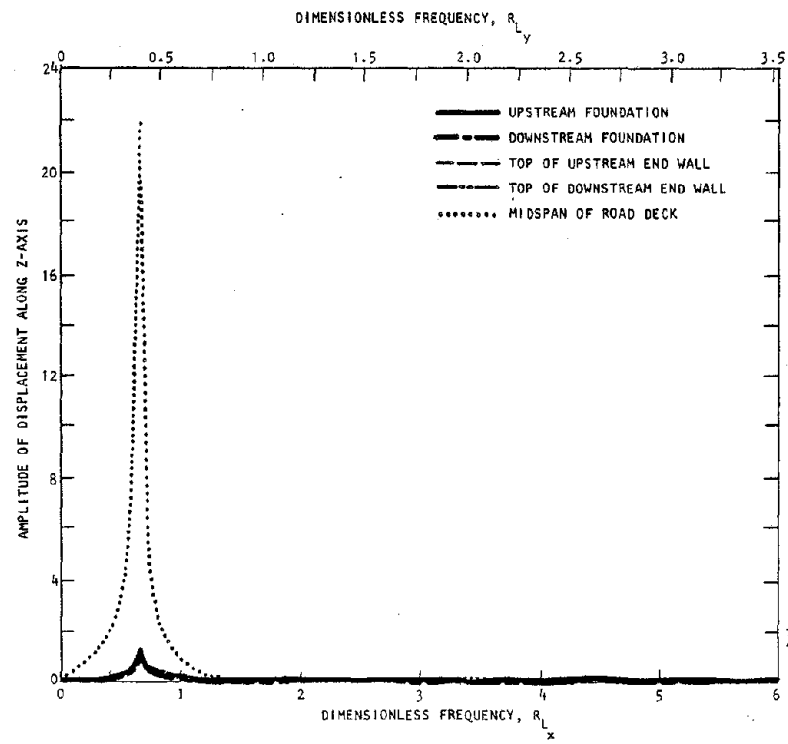

(b) Displacement along z-axis

FIGURE 4-19. FREQUENCY-DEPENDENT RESPONSE AMPLITUDES OF BRIDGE SUBJECTED TO INCIDENT SH-WAVES WITH θ_H = 45 DEG, θ_V = 0 DEG

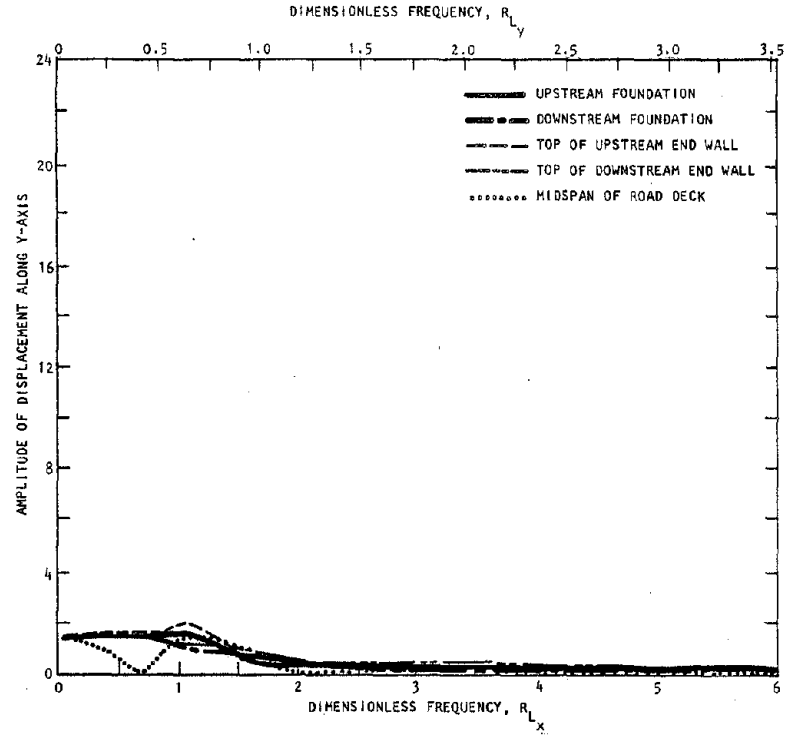

(c) Displacement along y-axis

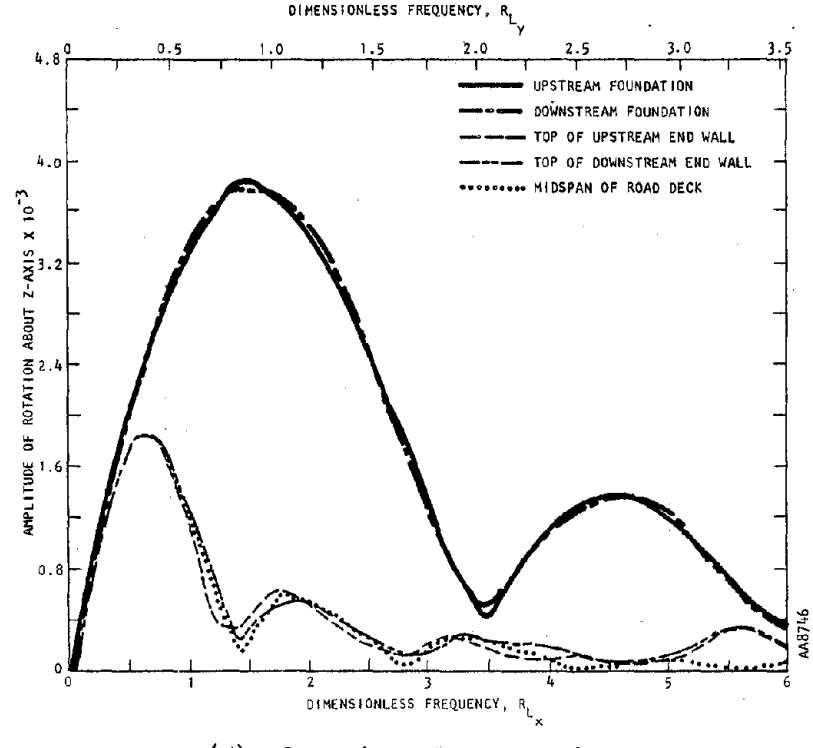

(d) Rotation about z-axis

FIGURE 4-19. (CONTINUED)

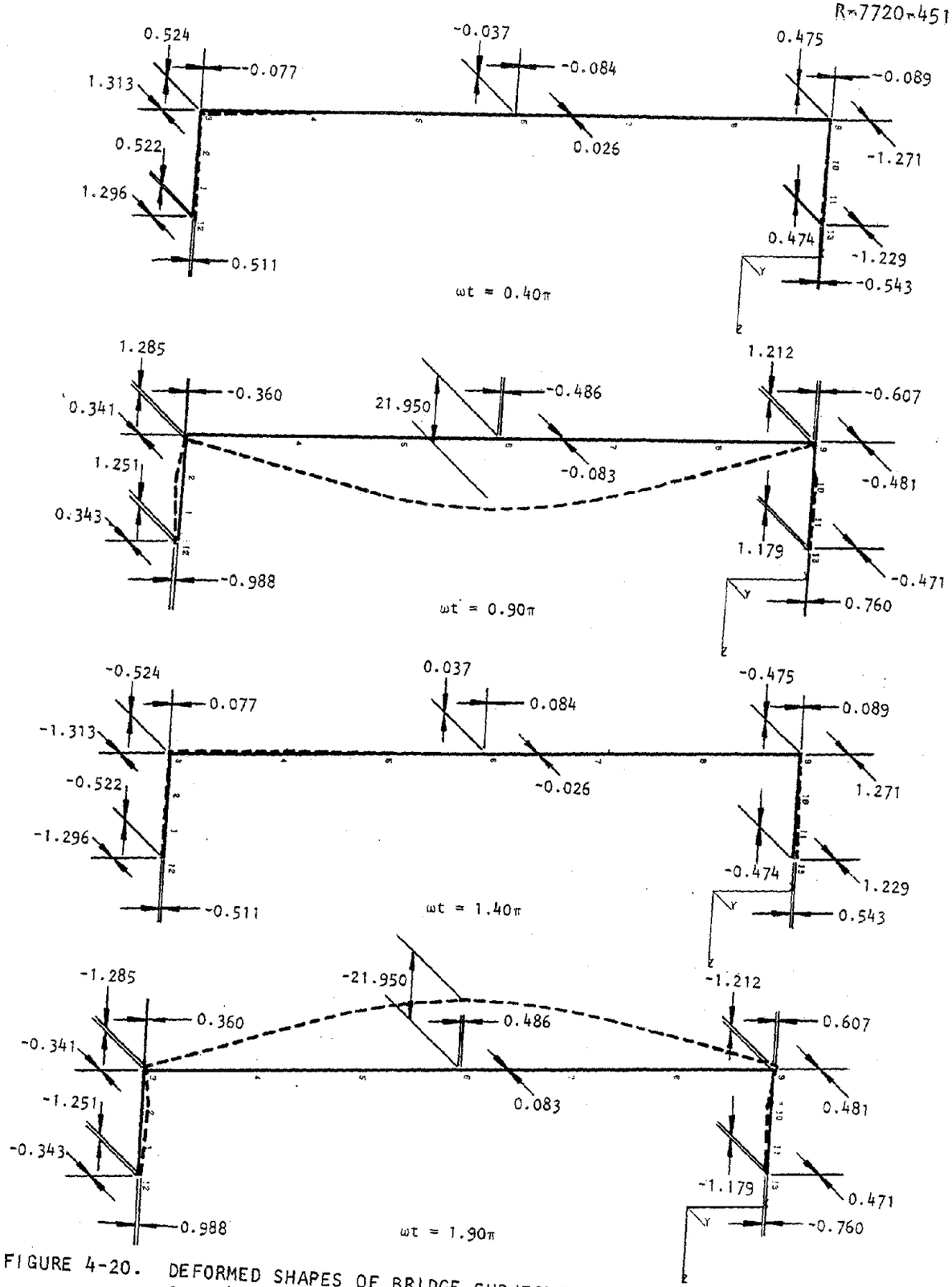

FIGURE 4-20. DEFORMED SHAPES OF BRIDGE SUBJECTED TO INCIDENT SH-WAVES WITH θ_H = 45 DEG, θ_V = 0 DEG (R_{L_x} = 0.401)

- The deformed shape of the bridge for this case (Fig. 4-20) closely resembles the mode shape of the first in-plane fixed-base mode indicated in Figure 4-2a. The natural frequency of this fixed-base mode (3.16 Hz) is only slightly higher than the resonant frequency for the present case (2.86 Hz), which includes the soft soil medium. This relatively slight difference in frequency is due to the fact that the effects of the soil deformation are not as significant for the present case as, say, for the sidesway response induced by the incident waves with θ_H = 90 deg. For this latter case, the presence of the soft soil medium was shown to reduce the frequency by about 40% below that of the corresponding fixed-base mode (Sec. 4.4.2.2).

It is of interest to explore the mechanism by which *vertical* motions are induced in the road deck by these incident waves of propagating *horizontal* motion. From an examination of the amplitudes and phase angles of the bridge response (Table 4-5), the following mechanism becomes apparent:

- The wavelength of the incident SH-waves for this case, as projected along the x-z plane of the structure, is such that each foundation experiences displacements along the x-axis and rotations about the y-axis that are of opposite phase.

- These foundation displacements and rotations induce bending of the end walls in the x-z plane. This bending causes significant in-plane rotations (about the y-axis) at the top of each end wall which are of essentially equal amplitude and opposite phase.

- In addition to its bending deformations, the end walls also transmit in-phase vertical motions that are developed at the foundation through the coupling terms in the foundation/soil impedance matrix. The resulting vertical motions at the top of each end wall are of nearly equal amplitude and phase.

- The road deck can now be visualized as an elastically supported beam whose supports are subjected to equal vertical (transverse) displacements and equal-and-opposite end rotations. These support motions will induce vertical displacements that are symmetric relative to the midspan of the beam. When their frequency reaches the natural frequency of the beam, a resonance condition occurs; this, in turn, results in the significant vertical displacements at the midspan of the road deck that are indicated in Figures 4-19b and 4-20.

4.5.2.2 Rotations of Foundations about z-Axis when θ_H = 45 Deg and θ_V = 0 Deg

Another important feature of the bridge response for this case is that of significant torsional deformations of the end walls associated with large rotations of the foundations about the z-axis. These rotations have the following characteristics:

- Large foundation rotations of this type were previously noted for the case of nonvertically incident SH-waves with θ_H = 90 deg; such rotations were attributed to antisymmetric components of the nonuniformly distributed loads oriented along the x-axis and applied by the waves as they propagate along the y-dimension of the foundation (Sec. 4.4.1). The foundation rotations induced by the waves with θ_H = 45 deg can be explained by the same mechanism.

- The peaks and valleys of the frequency-dependent rotation curve for θ_H = 45 deg and θ_V = 0 deg occur at dimensionless frequencies that are greater, by a factor of approximately $\sqrt{2}$, than the frequencies at the peaks and valleys of the corresponding curve for θ_H = 90 deg and θ_V = 0 deg (see Figs. 4-13b, 4-19d, and Tables 4-4, 4-5). This is due to an apparent wavelength effect that corresponds to the increase in the wavelength

as it is projected from the true direction of propagation of the incident wave along the ground surface (at θ_H = 45 deg) to the y-axis of the structure.

- The peak amplitudes of the foundation rotations for the θ_H = 45 deg case are about 70% of those for the θ_H = 90 deg case. This ratio corresponds closely to the ratio between the free-field x-displacement components for θ_H = 45 deg and θ_H = 90 deg, which is 0.707 (Tables 4-4, 4-5).

4.5.2.3 Rotations of the Road Deck about the z-Axis when θ_H = 45 Deg and θ_V = 0 Deg

A third aspect of the bridge response, that is of interest for comparison with the θ_H = 0 deg results, is the rotations of the road deck about the z-axis. These rotations have the following characteristics:

- For horizontally incident waves with θ_H = 0 deg, it is recalled that peak values of the rotations of the road deck about the z-axis were observed when R_{L_X} = 0.5, 1.5, etc. These rotations were accompanied by peak displacements along the y-axis that were antisymmetric about the midspan of the bridge (Sec. 4.3.2.1).

- Table 4-5 and Figure 4-19d indicate that horizontally incident waves with θ_H = 45 deg exhibit a similar response pattern when R_{L_X} = 0.657. This pattern is not predominant at higher frequencies, however, as it is for the θ_H = 0 deg results (see Fig. 4-5b). The dimensionless frequency at which this behavior first occurs for the θ_H = 45 deg case (R_{L_X} = 0.657) is increased relative to the corresponding frequency for θ_H = 0 deg (R_{L_X} = 0.5) by a factor of 1.31, which is close to the $\sqrt{2}$ factor that arises from apparent wavelength effects.

4.5.3 RESPONSE TO INCIDENT WAVES WITH θ_V = 45 DEG

The response of the bridge to incident SH-waves with $\theta_H = \theta_V = 45$ deg is presented in Figure 4-21 as plots of frequency-dependent displacements along the x-, y-, and z-axes and rotations about the z-axis. In addition, amplitudes and phase angles of these response components are tabulated in Table 4-5, and deformed-shape plots are shown in Figure 4-22.

4.5.3.1 Displacements along x- and z-Axes when $\theta_H = \theta_V = 45$ Deg

The x- and z-displacements caused by incident SH-waves with $\theta_H = \theta_V = 45$ deg are compared below to the corresponding displacements induced by incident waves with $\theta_H = 45$ deg and $\theta_V = 0$ deg and 90 deg (Secs. 4.5.1, 4.5.2).

- For the case involving SH-waves with $\theta_H = 45$ deg and $\theta_V = 90$ deg, the in-phase free-field x-displacements caused large horizontal sidesway motions (within a narrow frequency band) and relatively small vertical motions of the bridge. In contrast, for the $\theta_H = 45$ deg and $\theta_V = 0$ deg case, the out-of-phase x-displacements and y-rotations of the free-field motions at the two foundations were seen to cause significant vertical displacements in the road deck (also within a narrow frequency band) and only small x-displacements. The center frequencies of the narrow frequency bands for the two cases are quite similar. For the $\theta_V = 90$ deg case, $R_{L_y} = 0.423$ (i.e., $R_{L_x} = 0.726$) whereas for the $\theta_V = 0$-deg results, the center frequency corresponds to $R_{L_y} = 0.401$ (i.e., $R_{L_x} = 0.688$).

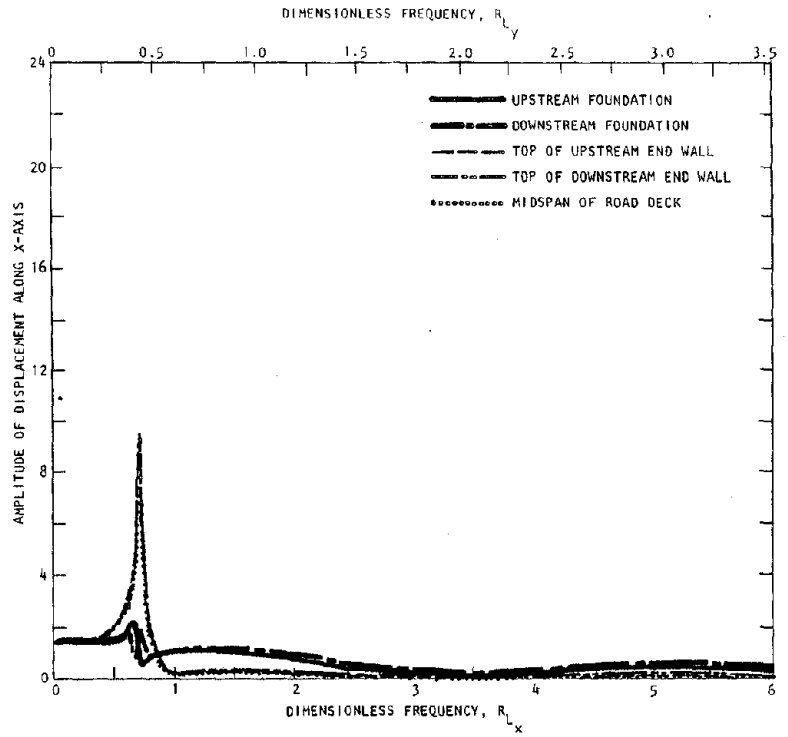

(a) Displacement along x-axis

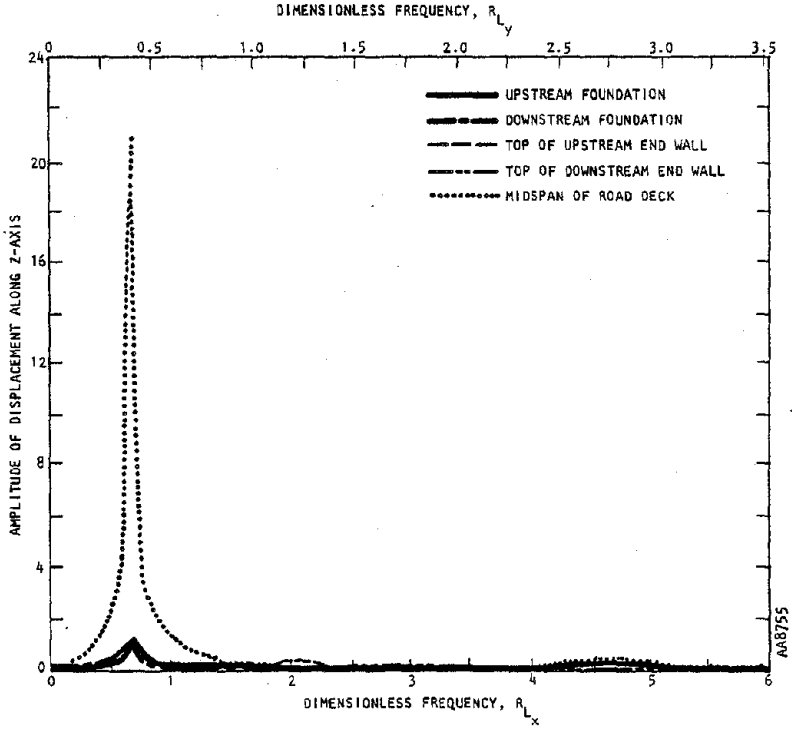

(b) Displacement along z-axis

FIGURE 4-21. FREQUENCY-DEPENDENT RESPONSE AMPLITUDES OF BRIDGE SUBJECTED TO INCIDENT SH-WAVES WITH θ_H = 45 DEG, θ_V = 45 DEG

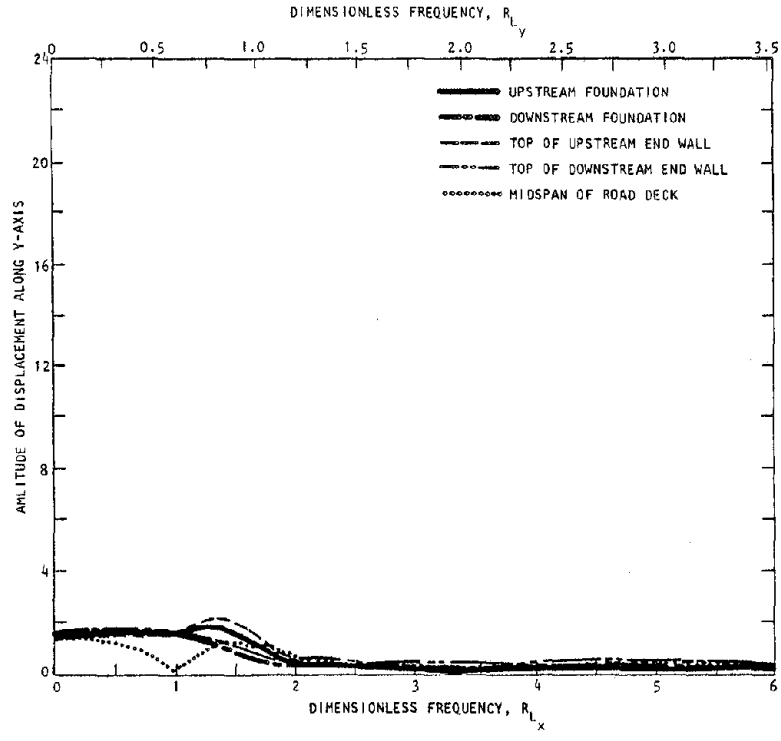

(c) Displacement along y-axis

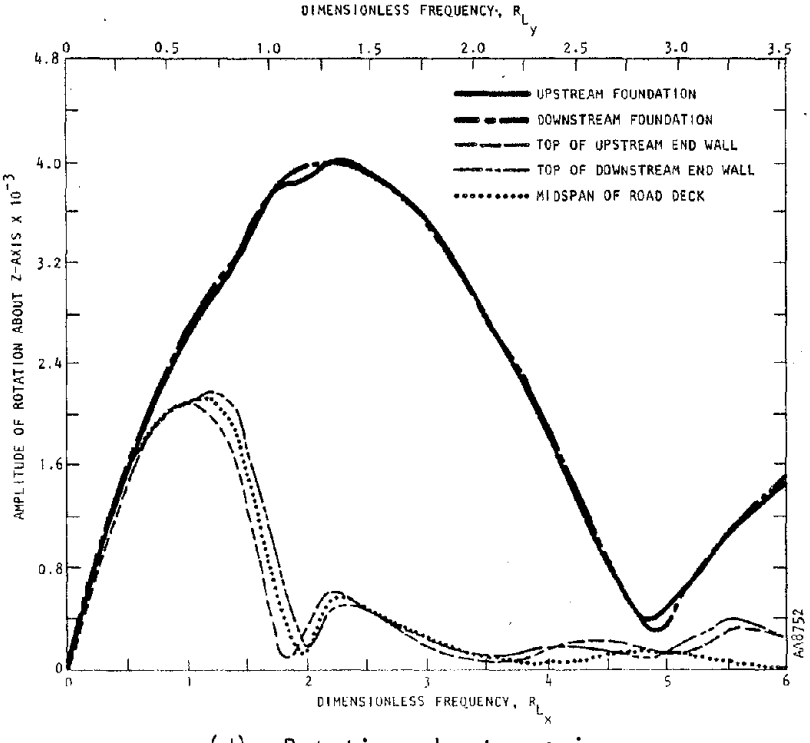

(d) Rotation about z-axis

FIGURE 4-21. (CONTINUED)

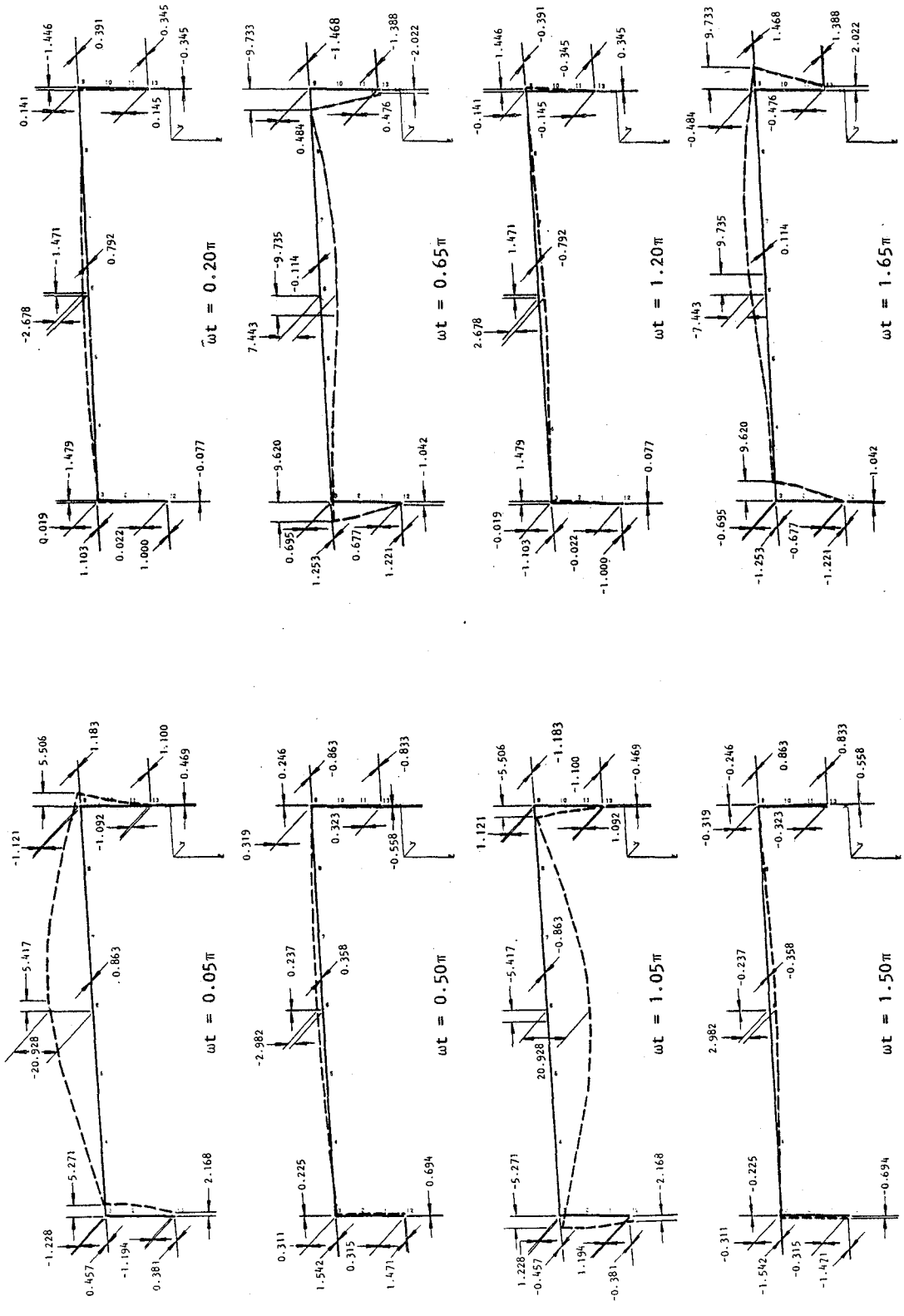

(a) R_{L_y} = 0.401 (b) R_{L_y} = 0.423

FIGURE 4-22. DEFORMED SHAPES OF BRIDGE SUBJECTED TO INCIDENT SH-WAVES WITH θ_H = 45 DEG, θ_V = 45 DEG

- When $\theta_H = \theta_V = 45$ deg, the phasing of the foundation motions does not correspond to that observed for the $\theta_V = 0$ deg and $\theta_V = 90$ deg cases. Instead, this phasing is altered because of the change in apparent wavelength; i.e., the foundation motions are no longer either of equal phase or opposite phase (Table 4-5). As a result of the change in apparent wavelength, sidesway motions of the bridge and vertical displacements of the road deck occur simultaneously at excitation frequencies of $R_{L_y} = 0.401$ and 0.423; i.e., they are now coupled. This coupling is clearly indicated in the deformed shape plots provided in Figure 4-22 for $R_{L_y} = 0.401$ and 0.423. It causes only a minor reduction in the peak vertical displacement at the midspan of the road deck, and a significant reduction in the peak x-displacement (Table 4-5).

4.5.3.2 Other Response Characteristics when $\theta_H = \theta_V = 45$ Deg

- The bridge response to the incident waves with $\theta_V = 45$ deg exhibits other characteristics that are similar to those described for the $\theta_V = 0$ deg case. For example, the curves defining the rotation of the foundation about the z-axis are similar for the two cases (Figs. 4-19d, 4-21d), except that the frequency of occurrence of each peak and valley is increased when $\theta_V = 45$ deg, because of the change in apparent wavelength. The same type of similarity exists for the curves defining the rotation of the road deck and the y-displacements of the bridge; i.e., the curves are similar for $\theta_V = 0$ deg and $\theta_V = 45$ deg except for a frequency shift due to the different apparent wavelength (Figs. 4-19c; 4-19d; 4-21c; 4-21d).

CHAPTER 5

REFERENCES

Abdel-Ghaffar, A.M. and Trifunac, M.D. (1977a) "Antiplane Dynamic Soil/Bridge/Soil Interaction for Incident Plane SH-Waves," *Proc. 6th World Conf. on Earthquake Eng. New Delhi, India, Jan 1977*, Vol. 4, pp 4-125 to 4-150.

----. (1977b) "Antiplane Dynamic Soil/Bridge Interaction for Incident Plane SH-Waves," *Earthq. Eng. & Struct. Dyn*, 5:2, Apr-Jun, pp 107-128.

Agbabian Assoc. (AA). (1972) *Dynamic Analysis of Bridge Structures Subject to Earthquake Loads*, R-7222-2432. El Segundo, CA: AA, Dec.

Bathe, K-J. and Wilson, E.L. (1972) "Large Eigenvalue Problems in Dynamic Analysis," *Proc. ASCE Eng. Mech. Div.* 98:6, Dec, pp 1471-1486.

----. (1973) "Eigensolution of Large Structural Systems with Small Bandwidth," *Proc. ASCE Eng. Mech. Div.* 99:3, Jun, pp 467-480.

----.; Wilson, R.L.; Peterson, V.E. (1974) *SAP IV, A Structural Analysis Program for Static and Dynamic Response of Linear Systems*, EERC-73-11, rev. 1. Berkeley, CA: Univ. of Calif. Earthquake Eng. Res. Center, Apr. (PB 221-967)

Bogdanoff, J.E. et al. (1965) "The Effect of Ground Transmission Time on the Response of Long Structures," *Bull. Seismol. Soc. Amer.* 55:3, Jun, pp 627-640.

Bullen, K.E. (1963) *An Introduction to the Theory of Seismology*. Cambridge, England: Cambridge Univ. Press.

Chopra, A.K. et al. (1969) "Earthquake Analysis of Earth Dams," *Proc. 4th World Conf. on Earthquake Eng. Santiago, Chile, Jan 1969*, Vol. 3, pp A5-55 to A5-72.

Clough, R.W. and Felippa, C.A. (1968) "A Refined Quadrilateral Element for Analysis of Plate Bending," *Proc. 2nd Conf. on Matrix Methods in Struct. Mech. Wright-Patterson AFB, OH, Oct 15-17*, pp 399-440. (AD 703 685)

Clough, R.W. and Penzien, J. (1975) *Dynamics of Structures*. New York: McGraw-Hill.

Dibaj, J. and Penzien, N. (1969) "Response of Earth Dams to Traveling Seismic Waves," *Proc. ASCE Soil Mech. Div.* 95:SM2, Mar, pp 541-560.

Ewing, W.M.; Jardetzky, W.S.; and Press, F. (1957) *Elastic Waves in Layered Media.* New York: McGraw-Hill.

Foss, J.W. (1977) "Communications Lifelines in Earthquakes," *Proc. on the Current State of Knowledge of Lifeline Earthquake Eng.* New York: TCLEE, Aug, pp 200-216.

Goto, H. et al. (1976) "Aseismic Displacement Requirements at Highway Bridge Girder Supports," *Proc. U.S.-Japan Seminar on Earthq. Eng. with Emphasis on Lifeline Systems, Tokyo, Japan, Nov.*, pp 105-118.

Goto Y. et al. (1973) "On the Earthquake Response of Submerged Tunnels," *Proc. 5th World Conf. on Earthquake Eng. Rome, Italy, Jun 1973.*

Hall, W.J. and Newmark, N.M. (1977) "Seismic Design Criteria for Pipelines and Facilities," *The Current State of Knowledge of Lifeline Earthquake Eng.* New York: Amer. Soc. of Civil Eng., pp 18-34.

Iguchi, M. (1977) "A Basic Study on the Behavior of Long Dimensional Size Buildings during Earthquakes," *Proc. 6th World Conf. on Earthquake Eng. New Delhi, India, Jan 1977,* Vol. 4, pp 4-37 to 4-42.

Isenberg, J. (1970) *Interaction between Soil and Nuclear Reactor Foundations during Earthquakes,* R-6915-1200. El Segundo, CA: Agbabian-Jacobsen Assoc., Jun.

Jennings, P.C. (1976) "Earthquake Problems of Networks and Systems," *Proc. U.S.-Japan Seminar on Earthq. Eng. with Emphasis on Lifeline Systems, Tokyo, Japan, Nov,* pp 5-14.

Johnson, J.A. (1977) "Possible Source Dependence of Ground Motion along a Pipeline," *Proc. 6th World Conf. on Earthquake Eng. New Delhi, India, Jan 1977,* Vol. 2, pp 2-57 to 2-62.

Johnson, N.E. and Galletly, R.D. (1972) "The Comparison of Response of a Highway Bridge to Uniform and Moving Ground Excitation," *Shock & Vibr. Bull.* 42:2, Jan, pp 75-85.

Kaldjian, M.J. (1973) "Foundation/Dam Interaction and Spatial Variation in Ground Motion," *Proc. 5th World Conf. on Earthquake Eng. Rome, Italy, Jun 1973.*

Kubo, K. (1973) "Behavior of Underground Waterpipes during Earthquakes," *Proc. 5th World Conf. on Earthquake Eng. Rome, Italy, Jun 1973.*

Lamb, H. (1904) "On the Propagation of Tremors over the Surface of an Elastic Solid," *Philosophical Trans. Royal Soc. London, Ser. A,* 203: pp 1-42.

Liu, S.C. and Fagel, L.W. (1971) "Earthquake Interaction by Fast Fourier Transform," *Proc. ASCE Eng. Mech. Div.* 97:EM4, Aug, pp 1223-1238.

Luco, J.E. (1977) Personal Communication to M.D. Trifunac, Apr.

----. and Wong, H.L. (1977) "Dynamic Response of Rectangular Foundations for Rayleigh Wave Excitations," *Proc. 6th World Conf. on Earthquake Eng. New Delhi, India, Jan 1977,* Vol. 4, pp 4-85 to 4-90.

Lysmer, J. (1975) *FLUSH, A Computer Program for Approximate 3-D Analysis of Soil/Structure Interaction Problems,* EERC-75-30. Berkeley, CA: Univ. of Calif. Earthquake Eng. Res. Center, Nov.

Masri, S.F. (1976) "Response of Beams to Propagating Boundary Excitation," *Earthq. Eng. & Struct. Dyn,* 4:5, Jul-Sep, pp 497-509.

----. and Weingarten, V. (1977) "Transient Response of Cooling Towers to Propagating Boundary Excitation," *Proc. 6th World Conf. on Earthquake Eng. New Delhi, India, Jan 1977,* Vol. 3, pp 3-257 to 3-262.

Matsushima, Y. (1977) "Stochastic Response of Structures due to Spatially Variant Earthquake Excitation," *Proc. 6th World Conf. on Earthquake Eng. New Delhi, India, Jan 1977,* pp 3-103 to 3-108.

Matthiesen, R.B. (1975) *Seismic Engineering Program - Proposed Program for FY76,* NSF-CA-114. Arlington, VA: U.S. Geol. Survey, Sep.

Miyajima, H. et al. (1976) "An Example of Seismic Design and Earthquake Response Measurement of Buried Pipelines," *Proc. U.S.-Japan Seminar on Earthq. Eng. with Emphasis on Lifeline Systems, Tokyo, Japan, Nov,* pp 177-196.

Nakano, H. (1930) "Some Problems Concerning the Propagations of the Disturbances in and on Semi-Infinite Elastic Solid," *Geophysical Magazine,* Vol. 2, pp 189-348.

Newmark, N.M. et al. (1977) "Comparison of Building Response and Free Field Motion in Earthquakes," *Proc. 6th World Conf. on Earthquake Eng. New Delhi, India, Jan 1977,* Vol. 3, pp 3-01 to 3-06.

Okamoto, S. (1973) *Introduction to Earthquake Engineering.* New York: Wiley.

Sakurai, A. and Takahashi, T. (1969) "Dynamic Stresses of Underground Pipe Lines during Earthquakes," *Proc. 4th World Conf. on Earthquake Eng. Santiago, Chile, Jan 1969,* Vol. 2, pp B4-81 to B4-96.

Scanlan, R.H. (1976) "Seismic Wave Effects on Soil-Structure Interaction," *Earthq. Eng. & Struct. Dyn.* 4:4, Apr-Jun, pp 379-388.

Tamura, C. et al. (1977) "Earthquake Observation along Measuring Lines on the Surface of Alluvial Soft Ground," *Proc. 6th World Conf. on Earthquake Eng. New Delhi, India, Jan 1977,* Vol. 2, pp 2-63 to 2-68.

Thau, S.A. (1967) "Radiation and Scattering from a Rigid Inclusion in an Elastic Medium," *Jnl of Appl. Mech.* Vol. 89, pp 509-511.

Toki, K. (1976) "Strain Amplitude by Body and Surface Waves in a Near Surface Ground," *Proc. U.S.-Japan Seminar on Earthq. Eng. with Emphasis on Lifeline Systems, Tokyo, Japan, Nov,* pp 15-28.

----. (1977) "Disintegration of Accelerograms into Surface and Body Waves," *Proc. 6th World Conf. on Earthquake Eng. New Delhi, India, Jan 1977,* Vol. 2, pp 2-209 to 2-214.

Tseng, W.S. and Penzien, J. (1975) "Seismic Analysis of Long Multiple-Span Highway Bridges," *Earthq. Eng. & Struct. Dyn,* 4:1, Jul-Sep pp 3-24.

Tsuchida, H. and Kurata, E. (1976) "Observed Earthquake Ground Displacements along a 2,500 Meter Line," *Proc. U.S.-Japan Seminar on Earthq. Eng. with Emphasis on Lifeline Systems, Tokyo, Japan, Nov,* pp 29-42.

Tsuchida, H. et al. (1977) "Observation of Earthquake Response of Ground with Horizontal and Vertical Seismometer Arrays," *Proc. 6th World Conf. on Earthquake Eng. New Delhi, India, Jan 1977,* Vol. 2, pp 2-173 to 2-178.

Udwadia, F.E. and Trifunac, M.D. (1974) "Variations of Strong Earthquake Ground Shaking in the Los Angeles Area," *Bull. Seismol. Soc. of Amer.* 64:5, Oct, pp 1429-1454.

Veletsos, A.S. et al. (1975) *Response of Structures to Propagating Ground Motions.* Houston, TX: Rice Univ., Apr.

Werner, S.D. (1976a) *Seismic Soil/Structure Interaction Guidelines,* SAN/1011-111. El Segundo, CA: Agbabian Assoc., Apr.

----. (1976b) "Effects of Traveling Seismic Waves on Structure Response: A Research Program," *Proc. U.S.-Japan Seminar on Earthq. Eng. with Emphasis on Lifeline Systems, Tokyo, Japan, Nov,* pp 43-58.

Wilson, E.L. (1970) *SAP A General Structural Analysis Program,* SEL-R-70-20. Berkeley, CA: Univ. of Calif., Sep.

Wolf, J.E. (1977) "Seismic Response Due to Traveling Shear Wave Including Soil/Structure Interaction with Base-Mat Uplift," *Earthq. Eng. & Struct. Dyn,* (in press).

Wong, H.L. (1975) *Dynamic Soil/Structure Interaction,* EERL-75-01. Ph.D. dissertation. Pasadena, CA: Calif. Inst. of Tech., May.

----. (1977) "The Coupled Translations and Rotations Caused by the Weight Distribution of a Nearby Building," paper presented at *Symp. on Applications of Computer Methods in Eng. University of Southern California, Los Angeles, Aug 23-26.*

----. and Luco, J.E. (1977) "Dynamic Response of Rectangular Foundations to Obliquely Incident Seismic Waves," *Earthq. Eng. & Struct. Dyn.* (in press).

Wong, H.L. and Trifunac, M.D. (1974) "Surface Motion of a Semi-Elliptical Alluvial Valley for Incident Plane SH-Waves," *Bull. of Seismol. Soc. of Amer.* 64:5, Oct, pp 1389-1408.

----. (1977) "A Note on the Effects of Recording Site Conditions on Amplitudes of Strong Earthquake Ground Motion," *Proc. 6th World Conf. on Earthquake Eng. New Delhi, India, Jan 1977,* Vol. 2, pp 2-119 to 2-124.

APPENDIX A

COMPUTATION OF GREEN'S FUNCTIONS FOR AN ELASTIC HALF-SPACE--SUBPROGRAM *GREEN*

The purpose of this appendix is to provide some mathematical background regarding the use of Subprogram GREEN to compute Green's functions for an elastic half-space that were originally derived by Lamb (1904) and Nakano (1930). The manner in which the resulting Green's functions are used to compute foundation/soil impedance matrices and driving forces is described in Appendix B.

This appendix is organized into three main sections. The first provides basic definitions regarding the elements of the Green's function matrix for an elastic continuum. The second section briefly describes how the Green's functions for an elastic half-space are obtained, while the final section briefly outlines the numerical procedures used in the actual computation of these Green's functions in Subprogram GREEN.

A.1 BASIC DEFINITIONS

Consider a force vector {P}, defined as

$$\left\{P\right\} = \begin{Bmatrix} P_1 \\ P_2 \\ P_3 \end{Bmatrix} e^{i\omega t} = \underset{\sim}{P} \qquad \text{(A-1)}$$

acting along the surface of a linear elastic half-space (see Fig. A-1). In Equation A-1 P_1, P_2, and P_3 are the three components of force oriented along the coordinate axes at an arbitrary point on the surface defined by the vector $\{x_o\}$, where

$$\left\{x_o\right\} = \begin{Bmatrix} x_1^o \\ x_2^o \\ 0 \end{Bmatrix} = \underset{\sim}{x}_o \qquad \text{(A-2)}$$

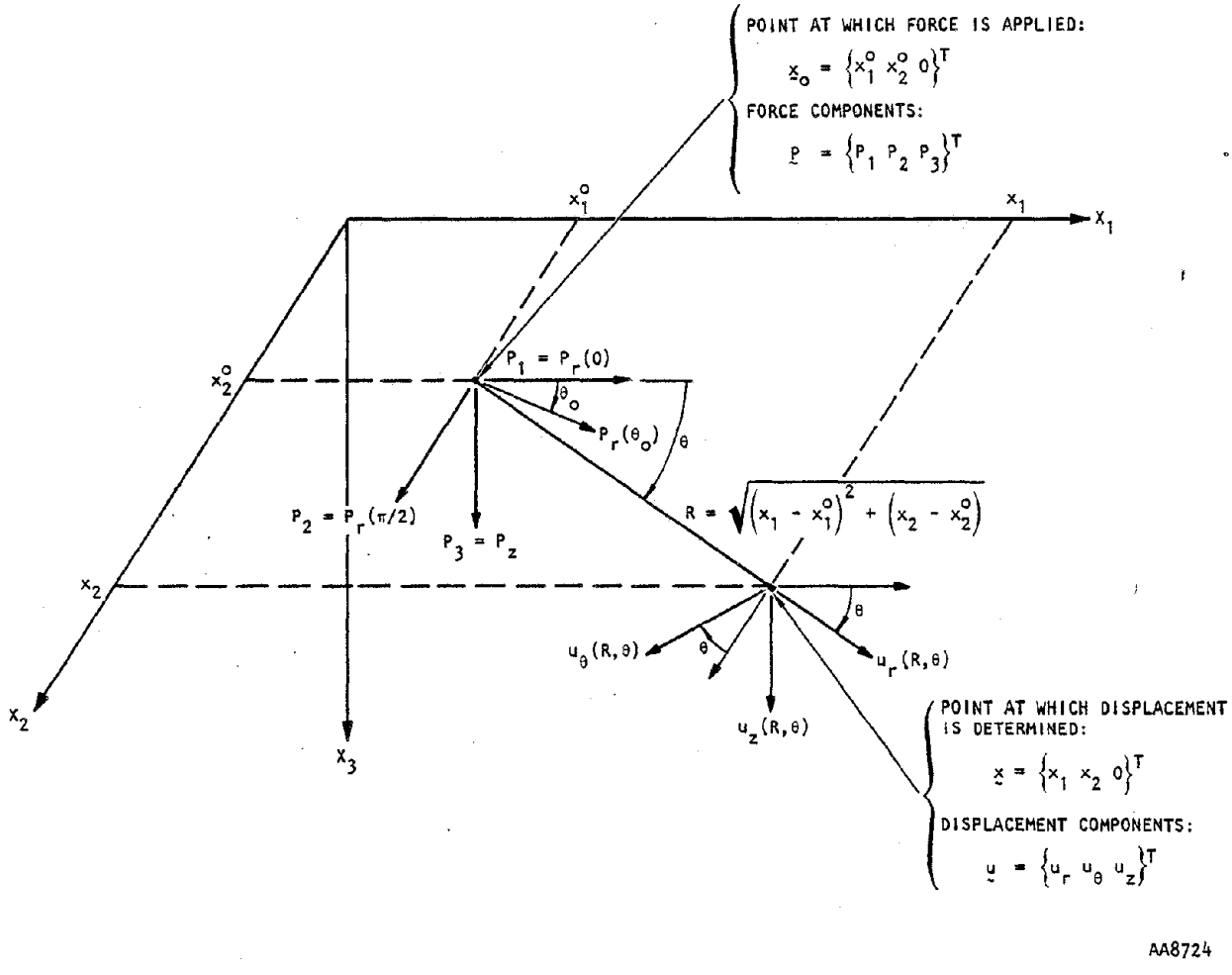

FIGURE A-1. NOTATION FOR DEVELOPMENT OF GREEN'S FUNCTIONS FOR A LINEAR ELASTIC SOIL MEDIUM

and the coordinate axes are shown in Figure A-1. The displacement vector {u} that results at another arbitrary point along the surface of the medium defined by {x}, where

$$\{x\} = \begin{Bmatrix} x_1 \\ x_2 \\ 0 \end{Bmatrix} = \underset{\sim}{x} \tag{A-3}$$

is computed as

$$\{u(\underset{\sim}{x})\} = \begin{Bmatrix} u_1 \\ u_2 \\ u_3 \end{Bmatrix} e^{i\omega t} = \left[G(\omega, \underset{\sim}{x} - \underset{\sim}{x}_o)\right] \{P(\underset{\sim}{x}_o)\} \tag{A-4}$$

where u_1, u_2, and u_3 are the three components of displacement. The matrix $[G(\omega, \underset{\sim}{x} - \underset{\sim}{x}_o)]$ is termed the Green's function matrix and is of order 3 x 3, i.e.,

$$\left[G(\omega, \underset{\sim}{x} - \underset{\sim}{x}_o)\right] = \begin{bmatrix} g_{11} & g_{12} & g_{13} \\ g_{21} & g_{22} & g_{23} \\ g_{31} & g_{32} & g_{33} \end{bmatrix} \tag{A-5}$$

In Equation A-5, $g_{\ell m}(\omega, \underset{\sim}{x} - \underset{\sim}{x}_o)$ relates the ℓth component of the displacement at $\underset{\sim}{x}$, u_ℓ, to the mth component of the force at $\underset{\sim}{x}_o$, P_m. Some properties of $g_{\ell m}$ are that

$$g_{21} = g_{12} \; ; \; g_{13} = -g_{31} \; ; \; g_{23} = -g_{32} \tag{A-6}$$

Equations A-5 and A-6 indicate that $[G(\omega, \underset{\sim}{x} - \underset{\sim}{x}_o)]$ has only six independent matrix elements. However, as shown subsequently, these six components can be specified by just four functions if the point load is considered in polar coordinates, as shown in Figure A-1. Therefore, in the remainder of this appendix, polar coordinates are employed.

For loads defined in polar coordinates, axis-symmetry and axis-asymmetry considerations require specification of only one horizontal load, $P_r(\theta_o)$, in addition to the vertical load P_z; i.e., all other horizontal loads can be represented by redefining the coordinate θ (Fig. A-1). Thus, without loss of generality, Equation A-4 can be expressed in polar coordinates as

$$\begin{Bmatrix} u_r(R,\theta) \\ u_\theta(R,\theta) \\ u_z(R,\theta) \end{Bmatrix} = \frac{1}{GR} \begin{bmatrix} f_{rr}\cos(\theta - \theta_o) & f_{rz} \\ f_{\theta r}\sin(\theta - \theta_o) & f_{\theta z} \\ f_{zr}\cos(\theta - \theta_o) & f_{zz} \end{bmatrix} \begin{Bmatrix} P_r(\theta_o) \\ P_z \end{Bmatrix} \qquad \text{(A-7)}$$

where

G = Shear modulus of elastic medium

$$R = |\underset{\sim}{x} - \underset{\sim}{x}_o| = \sqrt{(x_1 - x_1^o)^2 + (x_2 - x_2^o)^2}$$

$$\theta = \arg(\underset{\sim}{x} - \underset{\sim}{x}_o) = \tan^{-1}\left(\frac{x_2 - x_2^o}{x_1 - x_1^o}\right)$$

Equation A-7 holds for any linear elastic soil medium with an axis of symmetry about the z-axis. Therefore, a horizontally layered medium will also have Green's functions of the form indicated by Equation A-7.

A.2 GREEN'S FUNCTIONS FOR AN ELASTIC HALF-SPACE

A.2.1 GREEN'S FUNCTIONS IN POLAR COORDINATES

Consider now an elastic half-space with Poisson's ratio ν, shear modulus, G, and shear wave velocity, V_s. By rearranging the Green's functions (in polar coordinates) according to Equation A-7, the functions f_{rr}, $f_{\theta r}$, f_{zr}, f_{rz}, $f_{\theta z}$, and f_{zz} are dependent only on a dimensionless frequency parameter, a_o, defined as

$$a_o = \frac{\omega R}{V_s} \tag{A-8}$$

The resulting formulas are as follows:

$$f_{rr}(a_o) = \frac{a_o}{4\pi}\left[\int_0^\infty \frac{z\sqrt{z^2-1}\left\{J_2(a_o z) - J_o(a_o z)\right\}\,dz}{F(z)} + \int_0^\infty \frac{z}{\sqrt{z^2-1}}\left\{J_2(a_o z) + J_o(a_o z)\right\}\,dz\right] \tag{A-9}$$

$$f_{rz}(a_o) = \frac{a_o}{2\pi}\int_0^\infty \frac{z^2\left[(2z^2-1) - 2\sqrt{z^2-n^2}\sqrt{z^2-1}\right]J_1(a_o z)\,dz}{F(z)} \tag{A-10}$$

$$f_{\theta r}(a_o) = \frac{a_o}{4\pi}\left[\int_0^\infty \frac{z\sqrt{z^2-1}\left\{J_2(a_o z) + J_o(a_o z)\right\}\,dz}{F(z)} + \int_0^\infty \frac{z}{\sqrt{z^2-1}}\left\{J_2(a_o z) - J_o(a_o z)\right\}\,dz\right] \tag{A-11}$$

$$f_{\theta z}(a_o) = 0 \tag{A-12}$$

$$f_{zr}(a_o) = -f_{rz}(a_o) \tag{A-13}$$

$$f_{zz}(a_o) = -\frac{a_o}{2\pi}\int_0^{\infty} \frac{\sqrt{z^2 - n^2}\; z\, J_o(a_o z)\, dz}{F(z)} \tag{A-14}$$

where

$F(z)$ = Rayleigh determinant = $(2z^2 - 1)^2 - 4z^2\sqrt{(z^2 - n^2)(z^2 - 1)}$

$n = \frac{V_s}{V_p} = \sqrt{\frac{1 - 2\nu}{2(1 - \nu)}}$

V_s, V_p, ν = S-wave velocity, P-wave velocity, and Poisson's ratio, respectively, of the elastic half-space

J_o, J_1, J_2 = Bessel functions of order 0, 1, and 2, respectively

In Equations A-9 through A-14 it is observed that $f_{\theta z} = 0$ and $f_{zr} = -f_{rz}$; therefore, the total number of functions needed to define the Green's function matrix [G] in Equation A-7 is four. Furthermore, it is of interest for future reference to note the static limit of Equations A-9 through A-14, which corresponds to the limit of these expressions as a_o approaches zero. These are:

$$f_{rr}(a_o = 0) = \frac{1}{2\pi} \tag{A-15}$$

$$f_{rz}(0) = \frac{-n^2}{4\pi(1 - n^2)} \tag{A-16}$$

$$f_{\theta r}(0) = -\frac{-1}{4\pi(1 - n^2)} \tag{A-17}$$

$$f_{\theta z}(0) = 0 \tag{A-18}$$

$$f_{zr}(0) = -f_{rz}(0) \tag{A-19}$$

$$f_{zz}(0) = \frac{1}{4\pi(1 - n^2)} \tag{A-20}$$

A.2.2 GREEN'S FUNCTIONS IN CARTESIAN COORDINATES

The relationship of the displacements $\{u_1\ u_2\ u_3\}^T$ in Cartesian coordinates to those in polar coordinates $\{u_r\ u_\theta\ u_z\}^T$ can be expressed as

$$\begin{Bmatrix} u_1(\underset{\sim}{x}) \\ u_2(\underset{\sim}{x}) \\ u_3(\underset{\sim}{x}) \end{Bmatrix} = \begin{bmatrix} \cos\theta & -\sin\theta & 0 \\ \sin\theta & \cos\theta & 0 \\ 0 & 0 & 1 \end{bmatrix} \begin{Bmatrix} u_r(\underset{\sim}{x}) \\ u_\theta(\underset{\sim}{x}) \\ u_z(\underset{\sim}{x}) \end{Bmatrix} \tag{A-21}$$

Thus, by noting from Figure A-1 that

$$\begin{Bmatrix} P_1(\underset{\sim}{x}_o) \\ P_2(\underset{\sim}{x}_o) \\ P_3(\underset{\sim}{x}_o) \end{Bmatrix} = \begin{Bmatrix} P_r(0) \\ P_r(\pi/2) \\ P_z \end{Bmatrix} \tag{A-22}$$

one can relate $\{u_r\ u_\theta\ u_z\}^T$ at $\underset{\sim}{x}$ to $\{P_1\ P_2\ P_3\}^T$ at $\underset{\sim}{x}_o$ by combining Equations A-7 and A-22, i.e.,

$$\begin{Bmatrix} u_r(\underset{\sim}{x}) \\ u_\theta(\underset{\sim}{x}) \\ u_z(\underset{\sim}{x}) \end{Bmatrix} = \frac{1}{GR} \begin{bmatrix} f_{rr}\cos\theta & f_{rr}\cos(\theta - \frac{\pi}{2}) & f_{rz} \\ f_{\theta r}\sin\theta & f_{\theta r}\sin(\theta - \frac{\pi}{2}) & f_{\theta z} \\ f_{zr}\cos\theta & f_{zr}\cos(\theta - \frac{\pi}{2}) & f_{zz} \end{bmatrix} \begin{Bmatrix} P_1(\underset{\sim}{x}_o) \\ P_2(\underset{\sim}{x}_o) \\ P_3(\underset{\sim}{x}_o) \end{Bmatrix} \tag{A-23}$$

By substituting Equation A-23 into A-21, the quantities g_{ij}, as defined in Equation A-5, can be obtained as

$$\begin{bmatrix} g_{11} & g_{12} & g_{13} \\ g_{21} & g_{22} & g_{23} \\ g_{31} & g_{32} & g_{33} \end{bmatrix} = \frac{1}{GR} \begin{bmatrix} f_{rr}c^2 - f_{\theta r}s^2 & (f_{rr} + f_{\theta r})s\cdot c & f_{rz}c - f_{\theta z}s \\ (f_{rr} + f_{\theta r})s\cdot c & f_{rr}s^2 - f_{\theta r}c^2 & f_{rz}s + f_{\theta z}c \\ f_{zr}c & f_{zr}s & f_{zz} \end{bmatrix} \tag{A-24}$$

where c and s are shorthand notations for $\cos\theta$ and $\sin\theta$, respectively. In the above expression, the relationships defined in Equation A-6 between the off-diagonal g_{ij} elements are satisfied when Equations A-12 and A-13 are substituted into Equation A-24. Furthermore, a simplified form of Equation A-24 results if the expressions

$$\cos\theta = \frac{x_1 - x_1^o}{R} \tag{A-25}$$

$$\sin\theta = \frac{x_2 - x_2^o}{R} \tag{A-26}$$

are employed. This form is as follows:

$$g_{11} = \frac{1}{GR^3}\left\{(x_1 - x_1^o)^2 f_{rr} - (x_2 - x_2^o)^2 f_{\theta r}\right\} \tag{A-27}$$

$$g_{12} = \frac{1}{GR^3}(x_1 - x_1^o)(x_2 - x_2^o)(f_{rr} + f_{\theta r}) \tag{A-28}$$

$$g_{13} = \frac{1}{GR^2}(x_1 - x_1^o) f_{rz} \tag{A-29}$$

$$g_{22} = \frac{1}{GR^3}\left\{(x_2 - x_2^o)^2 f_{rr} - (x_1 - x_1^o) f_{\theta r}\right\} \quad \text{(A-30)}$$

$$g_{23} = \frac{1}{GR^2}(x_2 - x_2^o) f_{rz} \quad \text{(A-31)}$$

$$g_{33} = \frac{1}{GR} f_{zz} \quad \text{(A-32)}$$

With the above expressions, the values of g_{ij} can be calculated readily by interpolation if f_{rr}, $f_{\theta r}$, f_{rz}, and f_{zz} are tabulated as functions of a_o for a constant value of ν.

A.3 NUMERICAL EVALUATION OF GREEN'S FUNCTIONS FOR AN ELASTIC HALF-SPACE

The function of Subprogram GREEN is to numerically evaluate the parameters f_{rr}, f_{rz}, $f_{\theta r}$, and f_{zz} which were originally defined in Equations A-9, A-10, A-11, and A-14. The corresponding Green's functions are then obtained in Subprogram FOUND using Equations A-27 through A-32.

The numerical evaluation of these parameters involves expressing them in the form:

$$f_{rr} = \frac{a_o}{4\pi}(I_5 - I_6 + I_3 + I_4) \quad \text{(A-33)}$$

$$f_{rz} = \frac{a_o}{2\pi} I_2 \quad \text{(A-34)}$$

$$f_{\theta r} = \frac{a_o}{4\pi}(I_5 + I_6 + I_3 - I_4) \quad \text{(A-35)}$$

$$f_{zz} = -\frac{a_o}{2\pi} I_1 \quad \text{(A-36)}$$

where

$$I_1 = \int_0^\infty \frac{z\sqrt{z^2 - n^2}\, J_o(a_o z)\, dz}{F(z)} \tag{A-37}$$

$$I_2 = \int_0^\infty \frac{z^2\left[(2z^2 - 1) - 2\sqrt{z^2 - n^2}\sqrt{z^2 - 1}\right] J_1(a_o z)\, dz}{F(z)} \tag{A-38}$$

$$I_3 = \int_0^\infty \frac{z\, J_2(a_o z)\, dz}{\sqrt{z^2 - 1}} \tag{A-39}$$

$$I_4 = \int_0^\infty \frac{z}{\sqrt{z^2 - 1}} J_o(a_o z)\, dz \tag{A-40}$$

$$I_5 = \int_0^\infty \frac{z\sqrt{z^2 - 1}\, J_2(a_o z)\, dz}{F(z)} \tag{A-41}$$

$$I_6 = \int_0^\infty \frac{z\sqrt{z^2 - 1}\, J_o(a_o z)\, dz}{F(z)} \tag{A-42}$$

and

$$F(z) = \text{Rayleigh determinant}$$
$$= (2z^2 - 1)^2 - 4z^2\sqrt{(z^2 - n^2)(z^2 - 1)}$$

Therefore, it is seen that the determination of Green's functions for an elastic half-space essentially reduces to computing the functions I_1, I_2 ... I_6. The paragraphs that follow describe how this is carried out.

It is relatively simple to define the integrals I_3 and I_4. Using any standard set of integral tables, they can be expressed as follows

$$I_3 = \frac{1}{a_o}\left\{\left[\frac{2 \sin a_o}{a_o} - \cos a_o\right] + i\left[\sin a_o - \frac{2(1 - \cos a_o)}{a_o}\right]\right\} \quad \text{(A-43)}$$

$$I_4 = \frac{1}{a_o}\left[\cos a_o - i \sin a_o\right] \quad \text{(A-44)}$$

In this, it is noted that I_3 and I_4 are both imaginary because, in Equations A-39 and A-40, the integrand $z/\sqrt{z^2 - 1}$ is imaginary for $0 < z < 1$.

Unlike I_3 and I_4, which correspond to the horizontal SH-waves generated by the source, the integrands of I_1, I_2, I_5, and I_6 all contain the Rayleigh determinant $F(z)$. Because of the complexity of $F(z)$, these integrals must be evaluated numerically. Prior to the numerical integration, however, it is convenient to first transform the integrals by a contour integration path similar to that suggested by Ewing et al. (1957). This step is necessitated by the fact that $F(z) = 0$ at $z = s$. Having this singularity at $z = s$, the conventional numerical integration scheme would fail; however, by using contour integration, the residue of this singularity contributes the Rayleigh waves with the wave speed $V_R = V_s/s$, where V_s is the shear wave velocity. This results in the following integrals:

$$I_1 = -\frac{2}{\pi}\int_0^{\infty} \frac{\tau\sqrt{\tau^2+n^2}\,K_o(a_o\tau)\,d\tau}{(2\tau^2+1)^2 - 4\tau^2\sqrt{\tau^2+1}\,\sqrt{\tau^2+n^2}}$$

$$+ \; i\left\{-\pi H_o^{(2)}(a_o s)\,\frac{s\sqrt{s^2-n^2}}{F'(s)}\right.$$

$$+ \int_0^{n} \frac{k\sqrt{n^2-k^2}\,H_o^{(2)}(a_o k)\,dk}{(2k^2-1)^2 + 4k^2\sqrt{(1-k^2)(n^2-k^2)}}$$

$$\left. + \; 4\int_n^{1} \frac{k^3(k^2-n^2)\sqrt{1-k^2}\,H_o^{(2)}(a_o k)\,dk}{(2k^2-1)^4 + 16k^4(1-k^2)(k^2-n^2)}\right\} \qquad \text{(A-45)}$$

where $K_o(a_o\tau)$ is the Kelvin function and $H_o^{(2)}(a_o k)$ is the Hankel function of the second kind, both of which are of zeroth order. Similarly,

$$I_2 = i\left\{-\pi H_1^{(2)}(a_o s)\,\frac{s^2\left[(2s^2-1) - 2\sqrt{(s^2-n^2)(s^2-1)}\right]}{F'(s)}\right.$$

$$\left. + \; 2\int_n^{1} \frac{k^2(2k^2-1)\sqrt{(1-k^2)(k^2-n^2)}\,H_1^{(2)}(a_o k)\,dk}{(2k^2-1)^4 + 16k^4(1-k^2)(k^2-n^2)}\right\} \qquad \text{(A-46)}$$

$$I_5 = -4\int_n^1 \frac{\tau^2\sqrt{\tau^2 - n^2}\,(1 - \tau^2)\,J_2(a_o\tau)\,d\tau}{(2\tau^2 - 1)^4 + 16\tau^4(1 - \tau^2)(\tau^2 - n^2)}$$

$$+ 2\int_0^{(s-1)} E(x)\,dx + \int_{2s-1}^{\infty} \frac{\tau\sqrt{\tau^2 - 1}\,J_2(a_o\tau)\,d\tau}{F(\tau)}$$

$$+ i\left\{\int_0^n \frac{k\sqrt{1 - k^2}\,J_2(a_o k)\,dk}{F(k)}\right.$$

$$+ \int_n^1 \frac{k\sqrt{1 - k^2}\,(2k^2 - 1)^2\,J_2(a_o k)\,dk}{(2k^2 - 1)^4 + 16k^4(1 - k^2)(k^2 - n^2)}$$

$$\left. - \frac{\pi s\sqrt{s^2 - 1}\,J_2(a_o s)}{\left.\frac{dF(k)}{dk}\right|_{k=s}}\right\} \qquad \text{(A-47)}$$

where s is the root of the equation:

$$F(s) = (2s^2 - 1)^2 - 4s^2\sqrt{(s^2 - n^2)(s^2 - 1)} = 0$$

and

$$E(x) = \frac{1}{2}\left[\frac{(s + x)\sqrt{(s + x)^2 - 1}\,J_2\left(a_o(s + x)\right)}{F(x)}\right.$$

$$\left. + \frac{(s - x)\sqrt{(s - x)^2 - 1}\,J_2\left(a_o(s - x)\right)}{F(-x)}\right]$$

$$I_6 = -\frac{2}{\pi}\int_0^{\infty} \frac{\tau\sqrt{\tau^2+1}\,K_o(a_o\tau)\,d\tau}{(2\tau^2+1)^2 - 4\tau^2\sqrt{(\tau^2+1)(\tau^2+n^2)}}$$

$$+ \; i\left\{-\pi H_o^{(2)}(a_o s)\,\frac{s\sqrt{s^2-1}}{F'(s)}\right.$$

$$+ \int_0^{n} \frac{k\sqrt{1-k^2}\,H_o^{(2)}(a_o k)\,dk}{(2k^2-1)^2 + 4k^2\sqrt{(1-k^2)(n^2-k^2)}}$$

$$\left. + \int_n^{1} \frac{k\sqrt{1-k^2}(2k^2-1)^2\,H_o^{(2)}(a_o k)\,dk}{(2k^2-1)^4 + 16k^4(1-k^2)(k^2-n^2)}\right\} \qquad \text{(A-48)}$$

The significance of Equations A-45 through A-48 is that all singularities are now eliminated in the integrands for I_1, I_2, I_5, and I_6. Therefore, these integrals can be readily evaluated using standard numerical integration procedures. This numerical integration is carried out in Subprogram GREEN using Simpson's rule.

APPENDIX B

COMPUTATION OF FOUNDATION/SOIL INTERACTION EFFECTS--SUBPROGRAM *FOUND*

The purpose of this appendix is to describe the theory behind Subprogram FOUND--the method developed in this research program to represent foundation/soil interaction effects in the CASTI methodology. The theoretical basis for FOUND is an extension of earlier work by Wong (1975) and represents a technique for calculating impedance matrices and driving forces for a system of multiple, arbitrarily shaped, rigid, massless foundations on the surface of an elastic half-space.

This appendix is divided into four main sections. The first section provides the integral equations that relate contact stress to displacement. The second section describes how the foundation is discretized in this theoretical approach. The resulting development of the impedance matrix and driving forces for a single foundation on an elastic half-space is presented in the third section, and the final section contains a similar development for multiple foundations.

B.1 INTEGRAL EQUATION RELATING CONTACT STRESSES AND DISPLACEMENTS

To initiate this derivation, it is appropriate to briefly review the Green's function interrelationship between force and displacement that was already presented in Appendix A. Referring to Figure A-1 of that appendix, consider a harmonic point load defined as

$$\{P\} = \begin{Bmatrix} P_1 \\ P_2 \\ P_3 \end{Bmatrix} e^{i\omega t} \qquad \text{(B-1)}$$

that is acting on the free surface of a linear soil medium. The displacement vector

$$\{u\} = \begin{Bmatrix} u_1 \\ u_2 \\ u_3 \end{Bmatrix} e^{i\omega t} \tag{B-2}$$

corresponding to coordinates $\underset{\sim}{x} = \{x_1 \; x_2 \; 0\}^T$ and induced by the force $\{P\}$ applied at $\underset{\sim}{x}_o = \{x_1^o \; x_2^o \; 0\}^T$ can be computed using a Green's function matrix [G], as

$$\begin{Bmatrix} u_1 \\ u_2 \\ u_3 \end{Bmatrix} e^{i\omega t} = \left[G(\omega, \underset{\sim}{x} - \underset{\sim}{x}_o) \right] \begin{Bmatrix} P_1 \\ P_2 \\ P_3 \end{Bmatrix} e^{i\omega t} \tag{B-3}$$

The matrix elements of [G], denoted as $g_{\ell m}(\omega, \underset{\sim}{x} - \underset{\sim}{x}_o)$, relate the ℓ^{th} component of the displacement at $\underset{\sim}{x}$, $u_\ell(\underset{\sim}{x})$, to the m^{th} component of the point force at $\underset{\sim}{x}_o$, $P_m(\underset{\sim}{x}_o)$. A property of these elements is that

$$g_{21} = g_{12}; \qquad g_{13} = -g_{31}; \qquad g_{23} = -g_{32} \tag{B-4}$$

By superimposing many such point loads within an area A, the displacement at $\underset{\sim}{x}$ is

$$\{u(\underset{\sim}{x})\} = \iint_A [G(\omega, \underset{\sim}{x} - \underset{\sim}{x}_o)] \{T(\underset{\sim}{x}_o)\} \, dS_o \tag{B-5}$$

where $\{T(\underset{\sim}{x}_o)\}$ is a 3 x 1 vector that denotes the contact stress state at $\underset{\sim}{x}_o$. When the stress vector $\{T(\underset{\sim}{x}_o)\}$ is known, the displacement $\{u(x)\}$ can be obtained by direct integration over the area A. However, the current problem of determining impedance matrices and driving forces involves the specification of displacements of a rigid foundation. For this case, the integral equation (Eq. B-5) must be solved to determine the contact stresses $\{T(\underset{\sim}{x}_o)\}$ and the corresponding forces.

B.2 DISCRETIZATION OF FOUNDATION

A common procedure for obtaining the numerical solution of an integral equation is to transform the continuous integral formulation into a set of discrete algebraic equations that can be solved numerically. In this, the integral on the right-hand side of Equation B-5 is replaced by a sum over the yet unknown integrand, $[G]\{T\}$. The terms in this summation may be weighted in any manner, as required by the particular approximate integration procedure used.

Although the above approach can be applied to simple foundation shapes, it may not be appropriate for complicated shapes because of the lack of general numerical integration procedures for such cases. Therefore, an alternative approach is employed in which an irregular foundation area is partitioned into many small regular areas (e.g., rectangular) to simplify the numerical integration. This results in the following approximation to the integral in Equation B-5

$$\iint_A [G(\omega, \underset{\sim}{x} - \underset{\sim}{x}_o)]\{T(\underset{\sim}{x}_o)\}\, dS_o \cong \sum_{j=1}^{N} \iint_{A_j} [G(\omega, \underset{\sim}{x} - \underset{\sim}{x}_o)]\{T_j(\underset{\sim}{x}_o)\}\, dS_o \qquad (B\text{-}6)$$

where A_j is the area of the j^{th} subregion. The approximation in Equation B-6 arises from the fact that if rectangular subregions are employed, ΣA_j only approximates the area of an irregularly shaped foundation. This representation will be exact, however, for foundations that are either rectangular or of any other shape that can be decomposed exactly into rectangular subregions.

In the right side of Equation B-6, it is assumed that the contact stress vector $\{T_j(\underset{\sim}{x}_o)\}$ with A_j can be represented by a Taylor series expansion about a point $\underset{\sim}{x}_j$ within A_j as

$$\left\{T_j(\underset{\sim}{x}_o)\right\} = \left\{T_j(\underset{\sim}{x}_j)\right\} + \left\{\nabla T_j(\underset{\sim}{x}_j)\right\}^T\left\{\underset{\sim}{x}_o - \underset{\sim}{x}_j\right\} + \frac{1}{2!}\left\{\underset{\sim}{x}_o - \underset{\sim}{x}_j\right\}^T\left[H(\underset{\sim}{x}_j)\right]\left\{\underset{\sim}{x}_o - \underset{\sim}{x}_j\right\} + \ldots \quad \text{(B-7)}$$

where $\{\nabla T_j(\underset{\sim}{x}_j)\}$ and $[H(\underset{\sim}{x}_j)]$ involve first and second derivatives, respectively of $\underset{\sim}{T}_j(\underset{\sim}{x}_j)$. The values of the expansion coefficients $\{T_j(\underset{\sim}{x}_j)\}$, $\{\nabla T_j(\underset{\sim}{x}_j)\}$ and $[H(\underset{\sim}{x}_j)]$ are unknown and must be determined from compatibility conditions on the displacements of A_j, $\{u_j(\underset{\sim}{x}_o)\}$; this would result in simultaneous equations involving $\{T_j(\underset{\sim}{x}_j)\}$ and its derivatives.*

When employing this approach to obtain the stresses, a highly accurate representation of $\{T_j(\underset{\sim}{x}_o)\}$ over A_j, and thus $\{T(\underset{\sim}{x}_o)\}$ over A, can be obtained if A_j are taken to be small subregions of A and, in addition, if several terms of the expansion in Equation B-7 are used. However, a tradeoff between accuracy and numerical efficiency is often required, because the limiting factor for the numerical solution is the number of unknowns, i.e., the number of simultaneous equations that can be handled. For a large set of simultaneous equations, the computing cost can be prohibitive; also, numerical round-off errors may cause the solution to be unstable. Therefore, two alternative approaches present themselves: (1) to subdivide A into many small areas, A_j, and use a low-order Taylor series expansion of $\{T_j(\underset{\sim}{x}_o)\}$; or (2) to have fewer and larger areas A_j with a higher-order expansion of $\{T_j(\underset{\sim}{x}_o)\}$. In this application, the first alternative has been selected, in which the zeroth order of the expansion is used; i.e., $\{T_j(\underset{\sim}{x}_o)\}$ is assumed constant over A_j. This has been shown from past experience to result in

*This would be carried out by first substituting Equation B-7 into Equation B-6 and carrying out the integration over Aj, resulting in a discrete sum that is dependent on the Taylor series expansion coefficients. Then, by substituting into Equation B-5, expanding the displacements in a Taylor series, and prescribing these displacements and its derivatives, a set of simultaneous equations for the unknown stresses and stress derivatives would be obtained.

very good computational efficiency together with good accuracy and, in addition, it improves the approximation in Equation B-6 for arbitrarily shaped foundations. Furthermore, the assumption that $\{T_j(x_o)\}$ is constant within A_j is especially suitable for obtaining the foundation impedance matrix [K], since the elements of this matrix are proportional to the integral of the contact stress, i.e.,

$$K_{ij} \approx \int_A \int \{T(\underset{\sim}{x}_o)\} dS_o \tag{B-8}$$

As discussed subsequently, Equation B-8 represents a smoothing operation that eliminates the importance of the details in the distribution of $\{T(\underset{\sim}{x}_o)\}$.

B.3 DEVELOPMENT OF IMPEDANCE MATRIX AND DRIVING FORCES FOR A SINGLE RIGID FOUNDATION ON AN ELASTIC HALF-SPACE

B.3.1 GENERAL DISCUSSION

As noted in Subsection B.1, the determination of the foundation/soil impedance matrix and driving forces requires determination of the contact stresses induced along the surface of the foundation by certain prescribed displacements; i.e., in Equation B-5, $\{T(\underset{\sim}{x}_o)\}$ represents unknown contact stresses while $\{u(\underset{\sim}{x})\}$ represents the prescribed displacements. To determine these stresses, two assumptions have been employed thus far, namely that: (1) the foundation area, A_j, may be partitioned into N subregions, A_j, $j = 1, 2, \ldots, N$; and (2) the three components of contact stress vector $\{T(\underset{\sim}{x}_o)\}$ are equal to a constant $\{T_j\}$ within the subregion A_j.

Based on these assumptions, Equation B-5 can be rewritten (with the aid of Eq. B-6) as

$$\{u(\underset{\sim}{x})\} = \sum_{j=1}^{N} \left[\int_{A_j}\int G(\omega, \underset{\sim}{x} - \underset{\sim}{x}_o)\, dS_o\right]\{T_j\} = \sum_{j=1}^{N} [\phi(\underset{\sim}{x}, \underset{\sim}{x}_j)]\{T_j\}$$

$$= [\phi(\underset{\sim}{x}, \underset{\sim}{x}_1)]\{T_1\} + [\phi(x, x_2)]\{T_2\} + \ldots + [\phi(x, x_N)]\{T_N\} \tag{B-9}$$

where $[\phi(\underset{\sim}{x}, \underset{\sim}{x}_j)]$ is a 3 x 3 matrix defined as

$$[\phi(x, x_j)] = \left[\int_{A_j}\int G(\omega, \underset{\sim}{x} - \underset{\sim}{x}_o)\, dS_o\right] \tag{B-9a}$$

Physically, $[\phi(\underset{\sim}{x}, \underset{\sim}{x}_j)]$ defines the displacement vector $\{u(\underset{\sim}{x})\}$, at an arbitrary location $\underset{\sim}{x}$ that is induced by a unit value of the contact stress vector at the j^{th} subregion, $\{T_j\}$. To determine the N unknown stress vectors $\{T_j\}$ in Equation B-9, it is necessary to express $\{u(\underset{\sim}{x})\}$ in terms of displacements at N distinct points. For this purpose, it is assumed that $\{u(\underset{\sim}{x})\}$ can be adequately represented by specifying the displacements only at the centroids of the N subregions, A_j. Therefore, Equation B-9 can be expressed in the form

$$\{u_i\} = \begin{Bmatrix} u_1(\underset{\sim}{x}_i) \\ u_2(\underset{\sim}{x}_i) \\ u_3(\underset{\sim}{x}_i) \end{Bmatrix} = \sum_{j=1}^{N} [\phi_{ij}]\{T_j\} \tag{B-10}$$

where $[\phi_{ij}] = \left[\int_{A_j}\int G(\omega, \underset{\sim}{x}_i - \underset{\sim}{x}_o)\, dS_o\right]$

By writing Equation B-10 once for each of the N subregions in the foundation, the required N equations in terms of the N unknown stress vectors $\{T_j\}$ are provided. It now remains to define the compatibility equations that relate $\{u_i\}$ to the rigid-body motions of the foundation.

B.3.2 COMPATIBILITY RELATIONSHIPS

The displacements $\{u_i\}$ defined at the centroid, $\underset{\sim}{x}_i$, of each subregion, A_i, can be expressed as

$$\{u_i\} = \begin{Bmatrix} u_1(x_i) \\ u_2(x_i) \\ u_3(x_i) \end{Bmatrix} = \begin{Bmatrix} \Delta_1 - \theta_3 \cdot x_{2_i} \\ \Delta_2 + \theta_3 \cdot x_{1_i} \\ \Delta_3 + \theta_1 \cdot x_{2_i} - \theta_2 \cdot x_{1_i} \end{Bmatrix} \tag{B-11}$$

where

$\Delta_1, \Delta_2, \Delta_3$ = Rigid-body translation at origin of foundation coordinate system

$\theta_1, \theta_2, \theta_3$ = Rigid-body rotation about x_1, x_2, and x_3 axes of the foundations

The sign convention for these rigid-body motions is defined in Figure B-1. For simplicity, Equation B-11 can be written as

$$\{u_i\} = [H(\underset{\sim}{x}_i)]\{U\} \tag{B-12}$$

where

$$[H(\underset{\sim}{x}_i)] = \begin{bmatrix} 1 & 0 & 0 & 0 & 0 & -x_{2_i} \\ 0 & 1 & 0 & 0 & 0 & x_{1_i} \\ 0 & 0 & 1 & x_{2_i} & -x_{1_i} & 0 \end{bmatrix} \tag{B-12a}$$

$$\{U\} = \{\Delta_1 \ \Delta_2 \ \Delta_3 \ \theta_1 \ \theta_2 \ \theta_3\}^T \tag{B-12b}$$

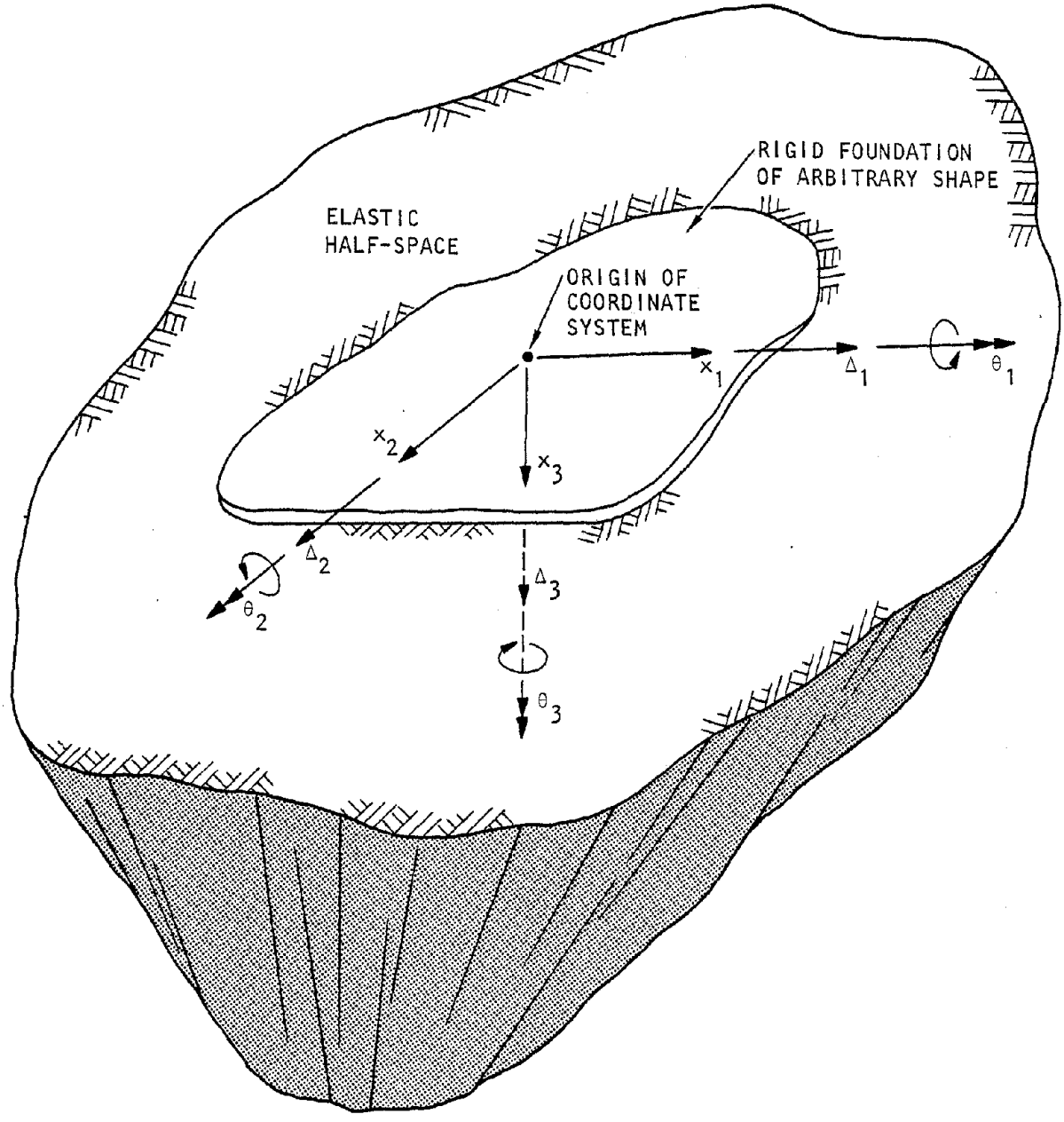

FIGURE B-1. SIGN CONVENTION FOR RIGID BODY MOTIONS OF FOUNDATION

These compatibility relationships, together with the results of the prior subsections, are all that is required to complete the derivation for the impedance matrix and the driving forces. In the subsection that follows, the remainder of this derivation is presented for a single foundation and, in Section B.4, the derivation is extended to consider multiple foundations.

B.3.3 DEVELOPMENT OF IMPEDANCE MATRIX AND DRIVING FORCE RELATIONSHIPS

To develop the impedance matrix and driving forces for a single foundation, the total displacement field at a point with coordinates $\underset{\sim}{x}$ (see Eq. B-2) is expressed as

$$\{u(\underset{\sim}{x})\} = \{u_{ff}(\underset{\sim}{x})\} + \{u_s(\underset{\sim}{x})\} \qquad \text{(B-13)}$$

where

$\{u_{ff}(\underset{\sim}{x})\}$ = Free-field displacement at location $\underset{\sim}{x}$

$\{u_s(\underset{\sim}{x})\}$ = Displacement caused by waves scattered from the rigid foundation

In Equation B-13, $\{u_{ff}(\underset{\sim}{x})\}$, the free-field motion, represents the motion caused by the incident seismic wave in the absence of all foundation elements. This vector also includes all scattered waves from any local geologic irregularities that might exist, although in the present application for an elastic half-space, no such irregularities are considered. The vector $\{u_s(\underset{\sim}{x})\}$, which represents the influence of the foundation on the displacement field, is defined by Equation B-9.

The determination of the impedance matrix and driving forces based on Equation B-13 employs the assumption described in Subsection B.3.1--namely, that the displacement field within the foundation $\{u(\underset{\sim}{x})\}$ can be expressed by specifying the displacements at the centroids of each of the

N subregions of the foundation. Therefore, Equation B-13 can be rewritten once for each subregion to form the expression

$$\begin{Bmatrix} \underset{\sim}{u}_1 \\ \underset{\sim}{u}_2 \\ \vdots \\ \underset{\sim}{u}_N \end{Bmatrix} = \begin{Bmatrix} \underset{\sim}{u}_{ff_1} \\ \underset{\sim}{u}_{ff_2} \\ \vdots \\ \underset{\sim}{u}_{ff_N} \end{Bmatrix} + \begin{Bmatrix} \underset{\sim}{u}_{s_1} \\ \underset{\sim}{u}_{s_2} \\ \vdots \\ \underset{\sim}{u}_{s_N} \end{Bmatrix} \tag{B-14}$$

where each bracketed vector shown in Equation B-14 is of order $3N \times 1$ and is itself comprised of N vectors of order 3×1 that denote the displacements at the centroids of each subregion, i.e.,

$\underset{\sim}{u}_i$ = Vector of total displacements

$\underset{\sim}{u}_{ff_i}$ = Vector of free-field displacements

and $\underset{\sim}{u}_{s_i}$ = Vector of displacements due to wave scattering

for the i^{th} subregion of the foundation.

In Equation B-14, the vector of free-field displacements, $\{\underset{\sim}{u}_{ff_i}\}$ is computed from the expression

$$\left\{u_{ff_i}\right\} = \left\{U_g\right\} e^{i\omega\left(t - \frac{x_i}{c}\cos\theta_H + \frac{y_i}{c}\sin\theta_H\right)} \tag{B-15}$$

where $\{U_g\}$ is the 3×1 complex amplitude vector of free-field motion at the origin of the coordinate system, x_i and y_i are the coordinates of the centroid of the i^{th} subregion, and c is the apparent velocity of the incident wave as observed on the free surface and along the direction of

propagation of the wave ($= V_s/\cos\theta_v$). The vectors $\underset{\sim}{u}_{s_i}$ and $\underset{\sim}{u}_i$ are defined using Equations B-10 and B-12, respectively. In particular, the displacement vector due to wave-scattering is defined as

$$\begin{Bmatrix} \underset{\sim}{u}_{s_1} \\ \underset{\sim}{u}_{s_2} \\ \vdots \\ \underset{\sim}{u}_{s_N} \end{Bmatrix} = [\Phi] \begin{Bmatrix} \underset{\sim}{T}_1 \\ \underset{\sim}{T}_2 \\ \vdots \\ \underset{\sim}{T}_N \end{Bmatrix} = [\Phi]\{T\} \tag{B-16}$$

where $\underset{\sim}{T}_j$ is the 3×1 contact stress vector for the j^{th} subregion, $[\Phi]$ is a $3N \times 3N$ matrix

$$[\Phi] = \begin{bmatrix} \underline{\phi}(\underset{\sim}{x}_1, \underset{\sim}{x}_1) & \underline{\phi}(\underset{\sim}{x}_1, \underset{\sim}{x}_2) & \cdots & \underline{\phi}(\underset{\sim}{x}_1, \underset{\sim}{x}_N) \\ \underline{\phi}(\underset{\sim}{x}_2, \underset{\sim}{x}_1) & \underline{\phi}(\underset{\sim}{x}_2, \underset{\sim}{x}_2) & \cdots & \underline{\phi}(\underset{\sim}{x}_2, \underset{\sim}{x}_N) \\ \vdots & \vdots & & \vdots \\ \underline{\phi}(\underset{\sim}{x}_N, \underset{\sim}{x}_1) & \underline{\phi}(\underset{\sim}{x}_2, \underset{\sim}{x}_N) & \cdots & \underline{\phi}(\underset{\sim}{x}_N, \underset{\sim}{x}_N) \end{bmatrix} \tag{B-16a}$$

and $\underline{\phi}(\underset{\sim}{x}_i, \underset{\sim}{x}_j)$ is a 3×3 matrix defined from Equation B-9a.* The total displacement vector for each subregion, is determined in terms of the rigid-body displacement vector for the foundation, {U}, from the following matrix equation

$$\begin{Bmatrix} \underset{\sim}{u}_1 \\ \underset{\sim}{u}_2 \\ \vdots \\ \underset{\sim}{u}_N \end{Bmatrix} = [\alpha]\{U\} \tag{B-17}$$

---

*In this notation, a partitioned matrix is underlaid by a dash; e.g., in Equation B-16a, $\underline{\phi}(\underset{\sim}{x}_i, \underset{\sim}{x}_j) = [\phi(\underset{\sim}{x}_i, \underset{\sim}{x}_j)]$.

where $\{U\}$ is the 6×1 vector of rigid-body displacements for the foundation (Eq. B-12b), and $[\alpha]$ is a $3N \times 6$ matrix that can be expressed in terms of N partitioned matrices, i.e.,

$$[\alpha] = \begin{bmatrix} \underline{\underline{H}}(\underset{\sim}{x}_1) \\ \underline{\underline{H}}(\underset{\sim}{x}_2) \\ \vdots \\ \underline{\underline{H}}(\underset{\sim}{x}_N) \end{bmatrix} \tag{B-17a}$$

In Equation B-17a, each partitioned matrix, $\underline{\underline{H}}(\underset{\sim}{x}_i)$, is of the order 3×6 and is defined for the i^{th} subregion in Equation B-12a.

Substituting Equations B-16 and B-17 into B-14, and rearranging, results in the following expression:

$$[\Phi]\{T\} = -\begin{Bmatrix} \underset{\sim}{u}_{ff_1} \\ \underset{\sim}{u}_{ff_2} \\ \vdots \\ \underset{\sim}{u}_{ff_N} \end{Bmatrix} + [\alpha]\{U\} \tag{B-18}$$

or, by inverting $[\Phi]$:

$$\{T\} = -[\Phi]^{-1}\begin{Bmatrix} \underset{\sim}{u}_{ff_1} \\ \underset{\sim}{u}_{ff_2} \\ \vdots \\ \underset{\sim}{u}_{ff_N} \end{Bmatrix} + [\Phi]^{-1}[\alpha]\{U\} \tag{B-18a}$$

Now $\{T\}$, the vector of contact stresses, can be decomposed into two parts, i.e.,

$$\{T\} = -\{T^D\} + \{T^R\} \tag{B-19}$$

where $\{T^D\}$ and $\{T^R\}$ are $3N \times 1$ vectors computed as:

$$\{T^D\} = [\Phi]^{-1} \begin{Bmatrix} \underset{\sim}{u}_{ff_1} \\ \underset{\sim}{u}_{ff_2} \\ \vdots \\ \underset{\sim}{u}_{ff_N} \end{Bmatrix} \tag{B-19a}$$

and

$$\{T^R\} = [\Phi]^{-1}[\alpha]\{U\} \tag{B-19b}$$

The vector $\{T^D\}$ corresponds to the vector of contact stresses generated in each subregion when the foundation is kept fixed while under the influence of the free-field seismic waves, $\underset{\sim}{u}_{ff_j}$ ($j = 1, \ldots N$). $\{T^R\}$ represents the contact stresses generated by the rigid-body motion of the foundation, $\{U\}$, in the absence of the incident seismic waves. The decomposition that is denoted in Equation B-19 was first suggested by Thau (1967) and has the advantage of providing a means for evaluating the state of stress along the soil/foundation interface in terms of the free-field motion and the rigid-body displacements of the foundation.

It now remains to compute the total foundation driving force vector $\{F^D\}$ and resisting force vector $\{F^R\}$; these result from summing the forces in each subregion that correspond to the contact stresses denoted in $\{T^d\}$ and $\{T^R\}$, respectively. For the j^{th} subregion, this summation is defined as

$$\{F\}_j = \begin{Bmatrix} F_1 \\ F_2 \\ F_3 \\ F_4 \\ F_5 \\ F_6 \end{Bmatrix}_j = A_j \begin{bmatrix} 1 & 0 & 0 \\ 0 & 1 & 0 \\ 0 & 0 & 1 \\ 0 & 0 & x_{2_j} \\ 0 & 0 & -x_{1_j} \\ -x_{2_j} & x_{1_j} & 0 \end{bmatrix} \begin{Bmatrix} T_1 \\ T_2 \\ T_3 \end{Bmatrix}_j \tag{B-20}$$

or

$$\{F_j\}_o = A_j[H(\underset{\sim}{x}_j)]^T\{T_j\} \tag{B-20a}$$

where A_j is the area of the j^{th} subregion and $[H(\underset{\sim}{x}_j)]$ is defined in Equation B-12a. The first three elements in the force vector (F_1, F_2, and F_3) correspond to the three force components induced by the j^{th} subregion contact stresses, while the last three elements (F_4, F_5, and F_6) correspond to the three moment components. Combining the effects from all of the subregions results in the following expression for the total foundation force vector

$$\{F\} = \sum_{j=1}^{N} A_j[H(x_j)]^T\{T_j\}$$

$$= [B]\{T\} \tag{B-21}$$

where [B] is a 6 x 3N matrix defined in partitioned matrix form as

$$[B] = \left[A_1 \underline{H}(\underset{\sim}{x}_1)^T \quad A_2 \underline{H}(\underset{\sim}{x}_2)^T \quad \cdots \quad A_N \underline{H}(\underset{\sim}{x}_N)^T \right] \tag{B-21a}$$

and each partitioned matrix $\underline{H}(\underset{\sim}{x}_j)^T$ is of order 6 x 3.

Now, premultiplying both sides of Equations B-19a and B-19b by [B] and using Equation B-21 results in the following expression for the total driving force vector $\{F^D\}$ and resisting force vector $\{F^R\}$

$$\{F^D\} = [B][\Phi]^{-1} \begin{Bmatrix} \underset{\sim}{u}_{ff_1} \\ \underset{\sim}{u}_{ff_2} \\ \vdots \\ \underset{\sim}{u}_{ff_N} \end{Bmatrix} \tag{B-22a}$$

$$\{F^R\} = [K_s]\{U\} \tag{B-22b}$$

where $[K_s]$, the 6 x 6 foundation/soil impedance matrix, is defined as

$$[K_s] = [B][\Phi]^{-1}[\alpha] \tag{B-22c}$$

B.4 DEVELOPMENT OF IMPEDANCE MATRIX AND DRIVING FORCES FOR TWO RIGID FOUNDATIONS ON AN ELASTIC HALF-SPACE

This section describes how the theory developed in the previous sections of this appendix can be extended to represent interaction effects between more than one rigid foundation on an elastic half-space. This is, of course, more complicated than the single-foundation case since the impedance matrix and driving force for each foundation in the system is now influenced not only by its own wave-scattering characteristics and applied loads by the incident waves, but also by wave scattering from the adjacent foundations.

The remainder of this section illustrates the theory for a case involving two rigid foundations of arbitrary shape on an elastic half-space; this was done to simplify the mathematical development although the extension of the basic concepts presented here to consider more than two foundations will be obvious. Also, for this case, two different derivations are presented. The first represents a complete formulation that provides accurate representation of the foundation/soil system driving forces and impedance matrices; however, the computational effort for this approach, which involves several large matrix inversions, is substantial. The second derivation, which represents the approach used in Subprogram FOUND, employs simplifying assumptions that reduce the computational effort with no significant reduction in accuracy.

B.4.1 COMPLETE FORMULATION

For the case of two foundations, Equation B-13 can be written in partitioned matrix form as

$$\begin{Bmatrix} \underset{\sim}{u}_1 \\ \underset{\sim}{u}_2 \end{Bmatrix} = \begin{Bmatrix} \underset{\sim}{u}_{ff_1} \\ \underset{\sim}{u}_{ff_2} \end{Bmatrix} + \begin{bmatrix} \underline{\Phi}_{11} & \underline{\Phi}_{12} \\ \underline{\Phi}_{12}^T & \underline{\Phi}_{22} \end{bmatrix} \begin{Bmatrix} \underset{\sim}{T}_1 \\ \underset{\sim}{T}_2 \end{Bmatrix} \qquad \text{(B-23)}$$

On the left side of Equation B-23, $\{u_1\}$ and $\{u_2\}$ correspond to the vector of total displacements at the centroid of each subregion in Foundations 1 and 2, respectively. Since each foundation may be simulated using a different number of subregions, $\{u_1\}$ and $\{u_2\}$ may be of different order; i.e. $\{u_1\}$ will be of order $3N_1 \times 1$ and $\{u_2\}$ will be of order $3N_2 \times 1$, where N_1 and N_2 correspond to the number of subregions in Foundations 1 and 2, respectively.* Utilizing the foundation compatibility equations (Eq. B-12), these total displacements can be expressed as

$$\begin{Bmatrix} \underset{\sim}{u}_1 \\ \underset{\sim}{u}_2 \end{Bmatrix} = \begin{bmatrix} \underset{\sim}{\alpha}_1 & 0 \\ 0 & \underset{\sim}{\alpha}_2 \end{bmatrix} \begin{Bmatrix} \underset{\sim}{U}_1 \\ \underset{\sim}{U}_2 \end{Bmatrix} \qquad \text{(B-24)}$$

where, for the i^{th} foundation ($i = 1, 2$), $[\underset{\sim}{\alpha}_i]$ is a matrix of order $3N_i \times 6$ that relates the displacement field at the centroid of each subregion to the 6×1 vector of rigid body displacements and rotations for the entire foundation, $\{U_i\}$ (Eq. B-12, B-12a, B-12b).

On the right side of Equation B-23, $\{u_{ff}\}_1$ and $\{u_{ff}\}_2$ correspond to the vector of free-field displacements at the location of the centroid of each subregion in Foundations 1 and 2, respectively. The second term on the right side of this equation represents the effects of wave scattering from the two foundations on the total displacement field for each foundation. For example, $\{T_1\}$ and $\{T_2\}$ represent the contact stress vectors at the centroid of each subregion in the first and second foundations, respectively; as for the displacements, the stress vectors are of order $3N_1 \times 1$ and $3N_2 \times 1$ for the two foundations. Then

$$[\Phi_{ij}]\{T_j\}$$

*Throughout the derivations presented for two foundations in Sections B-4 and B-5, the subscripts "1" and "2" denote Foundations 1 and 2, respectively. The reader is reminded that this use of subscripts differs from that employed in the derivations for the single foundation case in which the numerical subscripts denoted the subregions within the single foundation.

represents the displacements at the centroid of each subregion of the i^{th} foundation induced by the stress vector at the centroid of each subregion of the j^{th} foundation. In this, $[\Phi_{11}]$ and $[\Phi_{22}]$ is identical to the matrix defined in Equation B-16a for the single foundation case; these are of order $3N_1 \times 3N_1$ and $3N_2 \times 3N_2$, respectively. The cross matrix $[\Phi_{12}]$ is of order $3N_1 \times 3N_2$ and can be expressed as a series of partitioned matrices, i.e.:

$$\left[\Phi_{12}\right] = \begin{bmatrix} \underline{\Phi}_{1,1} & \underline{\Phi}_{1,2} & \cdots & \underline{\Phi}_{1,N_2} \\ \underline{\Phi}_{2,1} & \underline{\Phi}_{2,2} & \cdots & \underline{\Phi}_{2,N_2} \\ \vdots & \vdots & & \vdots \\ \underline{\Phi}_{N_1,1} & \underline{\Phi}_{N_2,2} & \cdots & \underline{\Phi}_{N_1,N_2} \end{bmatrix} \tag{B-25}$$

where

$\underline{\Phi}_{m,n}$ = 3 x 3 matrix that defines the displacement vector in the m^{th} subregion of Foundation 1 caused by the stress vector in the n^{th} subregion of Foundation 2

or

$$\underline{\Phi}_{m,n} = \left[\iint_{A_{n_2}} G(\omega, \underset{\sim}{x}_{m_1} - \underset{\sim}{x}_{n_2})\, dS_o\right] = \left[\Phi\left(\underset{\sim}{x}_{m_1}, \underset{\sim}{x}_{n_2}\right)\right] \tag{B-25a}$$

With this as background, Equation B-23 can be written as

$$\begin{bmatrix} \underline{\alpha}_1 & 0 \\ 0 & \underline{\alpha}_2 \end{bmatrix} \begin{Bmatrix} \underset{\sim}{U}_1 \\ \underset{\sim}{U}_2 \end{Bmatrix} = \begin{Bmatrix} \underset{\sim}{u}_{ff_1} \\ \underset{\sim}{u}_{ff_2} \end{Bmatrix} + \begin{bmatrix} \underline{\Phi}_{11} & \underline{\Phi}_{12} \\ \underline{\Phi}_{12}^T & \underline{\Phi}_{22} \end{bmatrix} \begin{Bmatrix} \underset{\sim}{T}_1 \\ \underset{\sim}{T}_2 \end{Bmatrix} \tag{B-26}$$

From the lower set of matrix equations (for Foundation 2) it is seen that

$$\left\{T_2\right\} = [\Phi_{22}]^{-1}\Big[\underbrace{\left[\alpha_2\right]\left\{U_2\right\}}_{\substack{\text{Total displacement in Foundation 2 subregions}}} - \underbrace{\left\{u_{ff_2}\right\}}_{\substack{\text{Free-field dis-placement}}} - \underbrace{\left[\Phi_{12}^T\right]\left\{T_1\right\}}_{\substack{\text{Displacement due to scattered waves from Foundation 1}}}\Big] \tag{B-27}$$

Substituting Equation B-27 into the upper set of matrix equation in Equation B-26 (for Foundation 1) $\{T_1\}$, the vector of contact stresses in Foundation 1 is expressed as

$$\left\{T_1\right\} = \underbrace{-\left\{\underset{\sim}{T}_1^{D_1} - \underset{\sim}{T}_1^{D_2}\right\}}_{\text{Driving forces}} + \underbrace{\left\{\underset{\sim}{T}_1^{R_1} - \underset{\sim}{T}_1^{R_2}\right\}}_{\text{Resisting forces}} \tag{B-28}$$

where

$\left\{T_1^{D_i}\right\}$ = Vector of contact stresses generated at Foundation 1 when the Foundation i is kept fixed under the influence of the free-field seismic waves $\{u_{ff_i}\}(i = 1,2)$

$\left\{T_1^{R_i}\right\}$ = Vector of contact stresses generated at Foundation 1 by the rigid body motion of the i^{th} foundation $\{U_i\}$ in the absence of the incident seismic waves

and

$$\left\{T_1^{D_1}\right\} = \left[\bar{\Phi}_{11}\right]^{-1}\left\{u_{ff_1}\right\} \tag{B-29a}$$

$$\left\{T_1^{D_2}\right\} = \left[\bar{\Phi}_{12}\right]^{-1}\left\{u_{ff_2}\right\} \tag{B-29b}$$

$$\left\{T_1^{R_1}\right\} = \left[\bar{\Phi}_{11}\right]^{-1}\left[\alpha_1\right]\left\{U_1\right\} \tag{B-29c}$$

$$\left\{T_1^{R_2}\right\} = \left[\bar{\Phi}_{12}\right]^{-1}\left[\alpha_2\right]\left\{U_2\right\} \tag{B-29d}$$

where

$\left[\bar{\Phi}_{11}\right]$ = Modified compliance of Foundation 1, including influence of Foundation 2

$$= \left[\Phi_{11}\right] - \left[\Phi_{12}\right]\left[\Phi_{22}\right]^{-1}\left[\Phi_{12}\right]^{T} \quad \text{(B-29e)}$$

$\left[\bar{\Phi}_{11}\right]^{-1}$ = Modified impedance of Foundation 1, including influence of Foundation 2

$\left[\bar{\Phi}_{12}\right]^{-1}$ = Modified impedance representing coupling between Foundations 1 and 2

$$= \left[\bar{\Phi}_{11}\right]^{-1}\left[\Phi_{12}\right]\left[\Phi_{22}\right]^{-1} \quad \text{(B-29f)}$$

It is noted that $\left\{T_1^{D_1}\right\}$ and $\left\{T_1^{R_1}\right\}$ are of exactly the same form as for the single foundation case (see Eq. B-19a and B-19b), except that the compliances and impedances are now modified to include the influence of the adjacent foundation. For a system with N foundations, a total of N modified compliance matrices of the type shown in Equation B-29e must be formed; each matrix will contain N terms representing the coupling effects from each foundation. The inversion of these matrices, required to form the impedance matrix for each foundation, increases the computational effort and computer storage requirements as compared to the single foundation case. The simplified approach presented in the next subsection is directed toward reducing these computational and storage requirements.

To obtain the final expressions for the driving and resisting forces, the contact stress effects must be summed as indicated by Equations B-20, B-20a, and B-21 for the single foundation case; i.e., $\{F_1\}$, the 6 x 1 vector of resultant forces acting at the origin for Foundation 1, is expressed in terms of the $3N_1$ x 1 vector of contact stresses, $\{T_1\}$, as

$$\{F_1\} = [B_1]\{T_1\} \quad \text{(B-30)}$$

where $[B_1]$ corresponds to the matrix $[B]$, (Eq. B-21a), as defined for Foundation 1.

Incorporating Equations B-28 into B-26 and rearranging, it can be shown that

$$\left\{F_1\right\} = -\left\{\underset{\sim}{F}_1^{D_1} - \underset{\sim}{F}_1^{D_2}\right\} + \left[\underline{K}_{11} \quad \underline{K}_{12}\right]\left\{\begin{matrix}\underset{\sim}{U}_1 \\ \underset{\sim}{U}_2\end{matrix}\right\} \tag{B-31}$$

in which the driving forces are expressed as

$$\left\{F_1^{D_1}\right\} = \left[B_1\right]\left[\bar{\Phi}_{11}\right]^{-1}\left\{u_{ff_1}\right\} \tag{B-31a}$$

$$\left\{F_1^{D_2}\right\} = \left[B_1\right]\left[\bar{\Phi}_{12}\right]^{-1}\left\{u_{ff_2}\right\} \tag{B-31b}$$

and the elements of the impedance matrix are

$$\left[K_{11}\right] = \left[B_1\right]\left[\bar{\Phi}_{11}\right]^{-1}\left[\alpha_1\right] \tag{B-31c}$$

$$\left[K_{12}\right] = \left[B_1\right]\left[\bar{\Phi}_{12}\right]^{-1}\left[\alpha_2\right] \tag{B-31d}$$

In a similar manner, it can be shown that the total forces applied at Foundation 2 are expressed as

$$\left\{F_2\right\} = \left\{\underset{\sim}{F}_2^{D_2} - \underset{\sim}{F}_2^{D_1}\right\} + \left[\underline{K}_{21} \quad \underline{K}_{22}\right]\left\{\begin{matrix}\underset{\sim}{U}_1 \\ \underset{\sim}{U}_2\end{matrix}\right\} \tag{B-32}$$

where the driving forces are

$$\left\{F_2^{D_2}\right\} = \left[B_2\right]\left[\bar{\Phi}_{22}\right]^{-1}\left\{u_{ff_2}\right\} \tag{B-32a}$$

$$\left\{F_2^{D_1}\right\} = \left[B_2\right]\left[\bar{\Phi}_{21}\right]^{-1}\left\{u_{ff_1}\right\} \tag{B-32b}$$

and the elements of the impedance matrix are

$$\left[K_{21}\right] = \left[B_2\right]\left[\bar{\Phi}_{21}\right]^{-1}\left[\alpha_1\right] \tag{B-32c}$$

$$\left[K_{22}\right] = \left[B_2\right]\left[\bar{\Phi}_{22}\right]^{-1}\left[\alpha_2\right] \tag{B-32d}$$

In the above expressions

$$\left[\bar{\Phi}_{22}\right]^{-1} = \left[\Phi_{22}\right] - \left[\Phi_{12}\right]^T\left[\Phi_{11}\right]^{-1}\left[\Phi_{12}\right] \tag{B-33e}$$

$$\left[\bar{\Phi}_{21}\right]^{-1} = \left[\bar{\Phi}_{22}\right]^{-1}\left[\Phi_{12}\right]^T\left[\Phi_{11}\right]^{-1} \tag{B-33f}$$

B.4.2 SIMPLIFIED FORMULATION

B.4.2.1 Discussion of Assumptions

The approach described in the previous subsection develops compliances for each foundation in the system that include the influence of the adjacent foundations. The inverse of this compliance is used to compute driving and resisting force vectors for each foundation. As previously noted, this particular step involves computational effort and computer storage requirements that can be much greater than for the single foundation case. The simplified formulation described in this section reduces these computational and storage requirements with no noticeable loss in accuracy.

The simplified formulation presented in this subsection is based on the assumption that the compliance of a single foundation is unaffected by the presence of the adjacent foundations. This assumption is based on prior computations carried out by Wong (1977) in which static compliance and impedance matrices for a two-foundation/elastic half-space system were computed for numerous foundation spacings. The computations showed that the spacing

of the foundations did not significantly affect the compliance matrices but did have an important influence on the impedance matrix for each foundation.

The physical basis for the above assumption can be seen by first considering the definition of the impedance and compliance matrices for a system of N rigid foundations on an elastic soil medium. The impedance matrix for such a system has the form

$$\left[K\right] = \begin{bmatrix} \underline{K}_{11} & \underline{K}_{12} & \cdots & \underline{K}_{1N} \\ \underline{K}_{12}^{T} & \underline{K}_{22} & \cdots & \underline{K}_{2N} \\ \vdots & \vdots & & \vdots \\ \underline{K}_{1N}^{T} & \underline{K}_{2N}^{T} & \cdots & \underline{K}_{NN} \end{bmatrix} \tag{B-34a}$$

and the corresponding compliance matrix is

$$\left[C\right] = \left[K\right]^{-1} = \begin{bmatrix} \underline{C}_{11} & \underline{C}_{12} & \cdots & \underline{C}_{1N} \\ \underline{C}_{12}^{T} & \underline{C}_{22} & \cdots & \underline{C}_{2N} \\ \vdots & \vdots & & \vdots \\ \underline{C}_{1N}^{T} & \underline{C}_{2N}^{T} & \cdots & \underline{C}_{NN} \end{bmatrix} \tag{B-34b}$$

where $\underline{K}_{ij}$ and $\underline{C}_{ij}$ $(i,j = 1,N)$ correspond to 6 x 6 partitioned matrices. The m^{th} column of $\underline{K}_{ij}$ corresponds to the reaction forces caused at the base of the i^{th} foundation by a unit displacement of the m^{th} degree of freedom of the j^{th} foundation, with all other degrees of freedom of both foundations fixed. Similarly, the m^{th} column of $\underline{C}_{ij}$ represents the rigid body displacements of the i^{th} foundation caused by a unit force applied along the m^{th} degree of freedom of the j^{th} foundation, with all other external forces applied to both foundations set to zero.

With the above definitions in mind, one can apply a unit displacement to one of the degrees of freedom of the i^{th} foundation in the N foundation

system, fixing all other foundations and all other degrees of freedom of the i^{th} foundation. For this case, the fixed adjacent foundations will restrain the soil from deforming; the extent of this restraint will be significant for closely spaced foundations and will decrease with increasing foundation spacing. Therefore, the forces applied to the i^{th} foundation in order to result in the above-indicated unit displacement, which corresponds to elements of its impedance matrix, $\underline{K}_{ii}$, will be strongly dependent on the spacing of the adjacent foundations. However, if one instead applies a unit force along one of the degrees of freedom of the i^{th} foundation, with no other external forces applied to the other foundations or to the other degrees of freedom of the i^{th} foundation, the situation changes. For this case, the adjacent massless foundations, which are no longer restrained from displacing, will tend to "ride along" with the soil as it deforms due to the load applied at the i^{th} foundation. Therefore, the displacements of the i^{th} foundation caused by its applied load, which corresponds to elements of its compliance matrix, $[\underline{C}_{ii}]$, will not be significantly affected by the presence or spacing of the other foundations, and can be reasonably well represented by neglecting these adjacent foundation elements. However, the off-diagonal partitioned matrices $\underline{C}_{ij}$, where $i \neq j$ will depend significantly on the separation distance between foundations.

With this discussion as background, the following two subsections outline the basic approach used in Subprogram FOUND to compute the impedance matrix and driving forces for a system of several rigid foundations on an elastic half-space. For simplicity, the procedure is described for a two-foundation system; however, it can easily be extended to consider any number of additional foundations.

B.4.2.2 Impedance Matrix for Two Rigid Foundations on an Elastic Half-Space

The steps in the simplified procedure for developing the impedance matrix for a system of two rigid, massless foundations on an elastic half-space follow.

(a) For Foundation 1, apply a force vector $\{F_1\}$ defined as

$$\{F_1\} = \begin{Bmatrix} 1 \\ 0 \\ 0 \\ 0 \\ 0 \\ 0 \end{Bmatrix} \tag{B-35}$$

i.e., the first element of $\{F_1\}$ has a unit value, while the remaining elements are zero.

(b) Compute the corresponding 6 x 1 vector of rigid body displacements, $\{U_1\}$, as

$$\{U_1\} = [C_{11}]\{F_1\} \tag{B-36}$$

where $[C_{11}]$ is the compliance matrix for Foundation 1, neglecting the presence of all other foundations. It is noted that this compliance involves the use of the matrix $[\Phi_{11}]$, as defined in Equation B-16a for a single foundation. In contrast, the complete formulation outlined in Subsection B.4.1 utilized the matrix $[\bar{\Phi}_{11}]$, which included the additional influence of the adjacent foundations. The basic premise of this simplified approach is that this additional influence on the compliance of a given foundation is not significant.

(c) Compute the displacements in each subregion of Foundation 1, using Equation B-17, i.e.,

$$\{u_1\} = \begin{Bmatrix} \underset{\sim}{u}_1 \\ \underset{\sim}{u}_2 \\ \vdots \\ \underset{\sim}{u}_{N_1} \end{Bmatrix} = [\alpha_1]\{U_1\} \tag{B-37}$$

where $\{u_1\}$ is a $3N_1 \times 1$ vector of displacements for the N_1 subregions in Foundation 1. The matrix $[\alpha_1]$ interrelates the subregion displacements and the rigid body displacements and is defined in Equation B-17a.

(d) Use the array of displacements obtained in Step *c* to obtain the corresponding stress distribution as

$$\{T_1\} = [\Phi_{11}]^{-1}\{u_1\} = [\alpha_{11}]^{-1}[\alpha_1]\{U_1\} \tag{B-38}$$

where $\{T_1\}$ is a $3N_1 \times 1$ vector of contact stresses, in which the state of stress within each subregion is assumed constant.

(e) Compute the displacements in the Foundation 2 subregions that are induced by wave-scattering effects from the stress state $\{T_1\}$, using the expression

$$\{u_2\} = [\Phi_{21}]\{T_1\} \tag{B-39}$$

where $\{u_2\}$ is of order $3N_2 \times 1$ for the N_2 subregions of Foundation 2 and $[\Phi_{21}]$ is a $3N_2 \times 3N_1$ matrix that uses Green's functions to relate the subregion displacements in Foundation 2 to the subregion stresses in Foundation 1. (See Eq. B-25.)

(f) Determine the corresponding stresses induced at Foundation 2 as

$$\{T_2\} = [\Phi_{22}]^{-1}\{u_2\} \tag{B-40}$$

and sum these stresses, applied over the subregion areas, to obtain the resulting forces, i.e.,

$$\{F_2\} = [B_2][\Phi_{22}]^{-1}\{u_2\} \tag{B-41}$$

where $\{T_2\}$, $[\Phi_{22}]$, $[B_2]$, and $\{F_2\}$ are of order $3N_2 \times 1$, $3N_2 \times 3N_2$, $6 \times 3N_2$, and 6×1, respectively.

(g) Obtain the 6 x 1 vector of rigid body displacements of Foundation 2 induced by $\{F_2\}$ to be

$$\{U_2\} = [C_{22}]\{F_2\} \tag{B-42}$$

where $[C_{22}]$ is the 6 x 6 compliance matrix for Foundation 2.

(h) The Foundation 2 displacements $\{U_2\}$, which were induced by the Foundation 1 force vector $\{F_1\}$ defined in Step *a* (Eq. B-35), corresponds to the first column of the compliance matrix $[C_{21}]$. (See Eq. B-34b.) Obtain the remaining columns of this matrix by redefining $\{F_1\}$ in Step *a* to have a unit value for each of its remaining elements, i.e.,

$$\{F_1\} = \begin{Bmatrix} 0 \\ 1 \\ 0 \\ 0 \\ 0 \\ 0 \end{Bmatrix}, \quad \begin{Bmatrix} 0 \\ 0 \\ 1 \\ 0 \\ 0 \\ 0 \end{Bmatrix}, \quad \cdots\cdots \quad \begin{Bmatrix} 0 \\ 0 \\ 0 \\ 0 \\ 0 \\ 1 \end{Bmatrix} \tag{B-43}$$

With each of these vectors as starting points, define the remaining columns of $[C_{21}]$ by repeating Steps *b* through *h*.

(i) With $[C_{21}]$ obtained as indicated above, define the total system compliance matrix [C]. Invert this matrix to obtain the system impedance matrix.

B.4.2.3 Driving Forces for Two Rigid Foundations on an Elastic Half-Space

The driving forces for each foundation in a multiple-foundation system must include: (1) the influence of the incident-wave motions applied to that foundation when it is restrained from displacing and (2) the influence of the waves scattered from the other foundations when they are subjected to incident-wave motions but are restrained from displacing. The driving force component induced at each foundation by Item (1) above, i.e., by the incident wave motions acting on that foundation, is given by the expression previously derived for a single foundation (Eq. B-22a of Subsection B.3.3), i.e.,

$$\begin{Bmatrix} D_1 \\ F_1 \end{Bmatrix} = \left[B_1\right]\left[\Phi_{11}\right]^{-1}\left\{u_{ff_1}\right\} \tag{B-44}$$

where $[B_1]$ is of order $6 \times 3N_1$ and is defined by Equation B-21a; $[\Phi_{11}]$ is the $3N_1 \times 3N_1$ compliance matrix defined by Equation B-16a; and N_1 is the number of subregions in Foundation 1. The vector $\{u_{ff_1}\}$ corresponds to the $3N_1 \times 1$ vector of incident-wave displacements applied to the centroid of each subregion. It is noted that the form of Equation B-44 is identical to that defined in the complete solution for the two-foundation formulation (Eq. B-31a) except in that formulation, the matrix $[\Phi_{11}]^{-1}$ is replaced by $[\bar{\Phi}_{11}]^{-1}$, which includes the influence of the adjacent foundation.

It now remains to compute the forces at Foundation 1 due to the scattered waves from Foundation 2. The steps involved in computing these forces are as follows:

(a) Compute the contact-stress distribution at Foundation 2 when it is subjected to incident-wave motions at the centroid of each subregion, that are defined by the $3N_2 \times 1$ vector $\{u_{ff_2}\}$. These stresses are

$$\left\{T_2\right\} = \left[\Phi_{22}\right]^{-1}\left\{u_{ff_2}\right\} \tag{B-45}$$

(b) Determine the $3N_1 \times 1$ vector of displacements at the centroid of each subregion in Foundation 1 that are induced by the scattered waves corresponding to the stress field $\{T_2\}$.

$$\{u_1\} = [\Phi_{12}]\{T_2\} \tag{B-46}$$

where $[\Phi_{12}]$ is of order $3N_1 \times 3N_2$ and has been defined in Equation B-25.

(c) Compute the corresponding contact stresses at Foundation 1:

$$\{T_1\} = [\Phi_{11}]^{-1}\{u_1\} \tag{B-47}$$

and sum these forces to obtain the total 6×1 force vector induced by the scattered waves from Foundation 2:

$$\begin{Bmatrix} \\ F_1^{D_2} \\ \\ \end{Bmatrix} = [B_1]\{T_1\} \tag{B-48}$$

(d) Substitute Equations B-45 through B-47 into Equation B-48 to obtain the expression

$$\begin{Bmatrix} \\ F_1^{D_2} \\ \\ \end{Bmatrix} = [B_1][\Phi_{11}]^{-1}[\Phi_{12}][\Phi_{22}]^{-1}\{uff_2\} \tag{B-49}$$

Referring to Equations B-29f and B-31b, it is seen that like $\{F_1^{D_1}\}$, the above expression for $\{F_1^{D_2}\}$ is identical to that computed in the complete solution (Subsec. B.4.1) except for the different definition of $[\Phi_{11}]^{-1}$.

(e) In a similar manner, compute the driving forces acting on Foundation 2 from the expressions

$$\begin{Bmatrix} D_2 \\ F_2 \end{Bmatrix} = \left[B_2\right]\left[\Phi_{22}\right]^{-1}\left\{u_{ff_2}\right\} \tag{B-50}$$

$$\begin{Bmatrix} D_1 \\ F_2 \end{Bmatrix} = \left[B_2\right]\left[\Phi_{22}\right]^{-1}\left[\Phi_{12}\right]\left[\Phi_{11}\right]^{-1}\left\{u_{ff_1}\right\} \tag{B-51}$$

which are analogous to Equations B-32a and B-32b.